

**PRODUCTION, CHARACTERIZATION, AND MECHANICAL BEHAVIOR OF
CEMENTITIOUS MATERIALS INCORPORATING CARBON NANOFIBERS**

A Dissertation

by

ARDAVAN YAZDANBAKHSH

Submitted to the Office of Graduate Studies of
Texas A&M University
in partial fulfillment of the requirements for the degree of

DOCTOR OF PHILOSOPHY

August 2012

Major Subject: Civil Engineering

Production, Characterization, and Mechanical Behavior of Cementitious Materials
Incorporating Carbon Nanofibers
Copyright 2012 Ardavan Yazdanbakhsh

**PRODUCTION, CHARACTERIZATION, AND MECHANICAL BEHAVIOR OF
CEMENTITIOUS MATERIALS INCORPORATING CARBON NANOFIBERS**

A Dissertation

by

ARDAVAN YAZDANBAKHSI

Submitted to the Office of Graduate Studies of
Texas A&M University
in partial fulfillment of the requirements for the degree of

DOCTOR OF PHILOSOPHY

Approved by:

Chair of Committee,	Zachary Grasley
Committee Members,	Rashid Abu Al-Rub
	Ramesh Talreja
	Sivakumar Rathinam
Head of Department,	John Niedzwecki

August 2012

Major Subject: Civil Engineering

ABSTRACT

Production, Characterization, and Mechanical Behavior of Cementitious Materials

Incorporating Carbon Nanofibers. (August 2012)

Ardavan Yazdanbakhsh

B.S., Azad University, Tehran;

M.S., University of Sharjah

Chair of Advisory Committee: Dr. Zachary Grasley

Carbon nanotubes (CNTs) and carbon nanofibers (CNFs) have excellent properties (mechanical, electrical, magnetic, etc.), which can make them effective nanoreinforcements for improving the properties of materials. The incorporation of CNT/Fs in a wide variety of materials has been researched extensively in the past decade. However, the past study on the reinforcement of cementitious materials with these nanofilaments has been limited. The findings from those studies indicate that CNT/Fs did not significantly improve the mechanical properties of cementitious materials. Two major parameters influence the effectiveness of any discrete inclusion in composite material: The dispersion quality of the inclusions and the interfacial bond between the inclusions and matrix. The main focus of this dissertation is on the dispersion factor, and consists of three main tasks: First a novel thermodynamic-based method for dispersion quantification was developed. Second, a new method, incorporating the utilization of silica fume, was devised to improve and stabilize the dispersion of CNFs in cement paste. And third, the dispersion quantification method and mechanical testing were employed to measure, compare, and correlate the dispersion and mechanical properties of CNF-incorporated cement paste produced with the conventional and new methods. Finally, the main benefits, including the increase in strength and resistance to shrinkage cracking, obtained from the utilization of CNFs in cement paste will be presented.

The investigations and the corresponding results show that the novel dispersion quantification method can be implemented easily to perform a wide variety of tasks ranging from measuring dispersion of nanofilaments in composites using their optical/SEM micrographs as input, to measuring the effect of cement particle/clump size on the dispersion of nano inclusions in cement paste. It was found that cement particles do not affect the dispersion of nano inclusions in cement paste significantly while the dispersion of nano inclusions can notably degenerate if the cement particles are agglomerated. The novel dispersion quantification method shows that, the dispersion of CNFs in cement paste significantly improves by utilizing silica fume. However, it was found that the dispersion of silica fume particles is an important parameter and poorly dispersed silica fume cannot enhance the overall dispersion of nano inclusions in cementitious materials. Finally, the mechanical testing and experimentations showed that CNFs, in absence of moist curing, even if poorly dispersed, can provide important benefits in terms of strength and crack resistance.

I dedicate this work to my wonderful parents,
Zahra and Mohammad-Ali,
for their love and support.

ACKNOWLEDGEMENTS

I sincerely thank my advisor Dr. Zachary Grasley for his scientific and personal mentorship and for creating many opportunities for my progress. I am grateful for the effort and support he provided to me while I was applying for jobs, and for his understanding at difficult times.

I carried out mutual projects with the research group of Dr. Rashid Abu Al-Rub. I would like to thank him for that opportunity and his important comments during my research. Special thanks to Dr. Sivakumar Rathinam who made a significant contribution to designing an implementation method for the dispersion quantification approach developed in this study. Additionally, I would like to thank Dr. Ramesh Talreja for serving me with excellent technical instruction in the classroom and for providing technical feedback on my work. Many thanks to Dr. Salah Altoubat, my Master's advisor, with whom I first performed systematic research. Special thanks to Dr. Dan Zollinger for his help and mentorship in my job search.

I would like to thank few of the great people who influenced my life with their friendship, help, and sharing of their ideas and philosophy. My brother and lifelong friend Arash has greatly supported me in all aspects of my life. My dear friend Ehsan Fatemi encouraged and helped me to start my Master's studies in the United Arab Emirates. And finally, with my friend Khaled Haj Hamed, who shared with me his realistic perspective on life and people, I experienced the value of friendship with people from diverse backgrounds.

At the end, I thank my parents for devoting a big portion of their life to me and encouraging me to pursue higher education.

LIST OF ABBREVIATIONS AND TERMINOLOGY

α_i	Angle of rotation
ρ	Partial density of the inclusions
σ_{\max}	Maximum tensile stress in the lower fiber of the beam under loading
τ	Magnitude of the torque required to rotate the particle
b	Beam's width
cm	Cementitious material, including cement and pozzolanic materials such as fly ash or silica fume
CNF	Carbon nanofibers
CNT	Carbon nanotubes
CNF/T	Carbon nanofibers/tubes (Carbon nanofilaments)
d_{ik}	Distance between a particle at the initial position i and possible final position k
D^t	Dispersion
Dispersive work	The minimum amount of work required to move the particles in a domain so that they form a fully uniform dispersion. When assuming that the force required to move each particle is unity, dispersive work is the minimum total distance required to move the particles so that they form a uniform distribution.
F	Applied force
\mathbf{F}	Deformation gradient
FEA	Finite element analysis
f_{kj}	Force necessary to move a particle from initial position k to final position
\mathbf{I}	Identity tensor

j	The mass flux vector
nanoinclusion/ <i>c</i>	Nanoinclusions to cement mass ratio
R	The rigid rotation tensor
Resilience	Amount of energy absorbed by a material while being deformed in the elastic zone. (Also referred to as modulus of resilience.)
RVE	Representative volume element
RPS	Relative particle size
SEM	Scanning electron microscopy
Strain capacity	Maximum strain that a material undergoes before failure
TEM	Transmission electron microscopy
UV-vis	UV-visible spectroscopy
u	The displacement vector of the point in the body
U	The right stretch tensor
u₀	Reference displacement
v	Velocity
V	The left stretch tensor
<i>w/c</i>	Water to cement mass ratio
<i>w/cm</i>	Water to cementitious material mass ratio
w^a	Dispersive works related to the actual state of dispersion
w^{nu}	Dispersive works related to the fully non-uniform state of dispersion
W^t	Dispersive work for the domain of interest
W_{\max}^t	Work required to fully disperse the inclusions when they form the worst possible dispersion in the domain
W_i^r	The work required to rotate each particle <i>i</i>
X	The position of some point in the body in the initial state
x	The position of the same point in the body in the final state

TABLE OF CONTENTS

	Page
ABSTRACT	iii
DEDICATION	v
ACKNOWLEDGEMENTS	vi
LIST OF ABBREVIATIONS AND TERMINOLOGY	vii
LIST OF FIGURES.....	xii
LIST OF TABLES	xix
1 . INTRODUCTION.....	1
1.1. Problem statement	1
1.2. Scope of thesis.....	4
1.3. Performed tasks and thesis outline	6
2 . CARBON NANOFILAMENTS IN CEMENTITIOUS MATERIALS AND THE ISSUES OF DISPERSION	10
2.1. Carbon nanofilaments.....	11
2.2. Dispersion, bond, and mechanical properties.....	12
2.3. Qualitative and quantitative methods of measuring dispersion.....	15
2.4. Experimental	18
2.5. Materials and preparation of specimens.....	18
2.6. Observations and discussion	21
2.7. Geometric clustering: another potential cause for the poor dispersion of CNF/Ts in cement paste	30
2.8. Concluding remarks.....	34
3 . A NOVEL METHOD FOR DISPERSION QUANTIFICATION OF INCLUSIONS IN COMPOSITES.....	36
3.1. Introduction	37
3.2. Past efforts to define dispersion	40
3.2.1. Methods based on feature size	40
3.2.2. Methods based on contact area between features.....	40
3.2.3. Methods based on feature local concentrations (quadrat methods)	41
3.2.4. Methods based on microstructural parameters.....	41
3.3. A novel measure of dispersion	44
3.3.1. Fully uniform and fully non-uniform states of dispersion	44

3.3.2. Definition and formulation of a dispersion parameter	46
3.3.3. Calculation of dispersive work.....	47
3.4. Discussion: The novel method of dispersion quantification vs. the previously developed methods.....	48
3.5. Implementation example for composites.....	54
3.6. Concluding remarks.....	56
4 . IMPLEMENTATION OF THE NOVEL DISPERSION QUANTIFICATION METHOD USING CONTINUUM THEORY	57
4.1. Introduction	57
4.2. Definitions	58
4.3. Motion of inclusions.....	60
4.4. Use of continuum theory to determine dispersion parameter.....	63
4.5. Discrete system.....	66
4.6. Example applications	69
4.6.1. Method validation	69
4.6.2. Carbon nanofibers dispersed in aqueous solution.....	73
4.7. Conclusions	74
5 . THE THEORETICAL MAXIMUM ACHIEVABLE DISPERSION OF NANOINCLUSIONS IN CEMENT PASTE	76
5.1. Introduction	76
5.2. Simulation and analysis of the maximum theoretical dispersion of nanoinclusions in cement paste.....	80
5.2.1. Parameter selection	80
5.2.2. Methodology	83
5.3. Results and Discussion.....	85
5.4. Concluding Remarks	88
6 . UTILIZATION OF SILICA FUME TO STABILIZE THE DISPERSION OF CARBON NANOFILAMENTS IN CEMENT PASTE.....	89
6.1. Introduction	89
6.2. Dispersing carbon nanofilaments in cement paste using silica fume.....	91
6.3. Experiment	92
6.3.1. Materials and instruments	92
6.3.2. Mix design, production and observation of CNF-incorporated cement paste	93
6.4. Results and discussion.....	95
6.5. Concluding remarks.....	99

7 . THE EFFECT OF CARBON NANOFIBERS ON THE MECHANICAL PROPERTIES OF HARDENED CEMENT PASTE	100
7.1. Introduction	100
7.2. Experimental	104
7.2.1. Materials and Instruments	104
7.2.2. Mix proportions, preparation of specimens, and testing	105
7.2.3. Calculations	109
7.3. Results and discussion	110
7.4. Concluding remarks.....	116
8 . SUMMARY AND CONCLUSIONS.....	118
REFERENCES	122

LIST OF FIGURES

- Figure 1. (a) Engineered cementitious concrete displaying a ductile behavior under bending load. (b) The ductile behavior is a result of the formation of multiple cracks bridged by fibers. (Photos are from the Inhabitat and ConstructionLawToday websites)2
- Figure 2. Effect of CNF dispersion quality on the transparency of solutions. All three specimens have the same CNF/water ratio. In specimen (a), CNFs were added to only water and mixed by a hand stirrer, which resulted in poor dispersion and as a result high transparency. In the specimen (b), CNFs were added to a solution of water and surfactant and mixed by a hand stirrer; this resulted in a slightly better and darker dispersion. In specimen (c), CNFs were sonicated in a water-surfactant solution. This produced a good and very dark dispersion.17
- Figure 3. Schematic layout of a UV-vis spectroscopy device, used for quantifying the dispersion of particles in a transparent medium. From the portion of radiation received by the detectors, the absorption capacity of the particles and thus the uniformity of their distribution can be determined.18
- Figure 4. Effect of surfactants on the dispersion of CNFs: Optical microscopy image of the distribution of VGCF-Hs (a) in water-Pluronic F98 solution and (b) only in water. Both specimens were sonicated for 15 minutes.22
- Figure 5. Two types of poor dispersion of CNFs (VGCF-Hs) in water. (a) non-disentangled clumps of CNF due to insufficient sonication, and (b) rebundling of CNFs as a result of drying. Both specimens have the same composition with Pluronic F98 was used as surfactant.22
- Figure 6. A comparison between the distribution of CNFs in water and cement paste. Image (a) is an optical micrograph of the dispersion of VGCF-Hs in water-superplasticizer solution. The distribution is relatively uniform, but some of the smaller fibers are agglomerated. Figure (b) is an SEM Image of the hardened cement paste in a location with a relatively high concentration of CNFs. The paste was made with the dispersion in (a). The majority of larger fibers are separated. However this image does not represent the distribution of CNFs in the matrix; in several areas of the fractured surface, no or few fibers could be observed by SEM.23
- Figure 7. Effect of sonication on the dispersion of Pyrograph CNFs in aqueous media. In both specimens the proportions are the same and the fibers have been added to a water-superplasticizer solution. Specimen (a) was only had-shaken while specimen (b) was sonicated for 15 minutes.24

- Figure 8. Cryo-TEM images of some undesired features in the sonicated dispersion of Pyrograph shown in Figure 10-a. Image (a) shows an impurity in the shape of a curled thread, and image (b) is a longitudinal bundle of CNFs caused by parallel agglomeration of the fibers.25
- Figure 9. SEM image of a longitudinal bundle of Pyrograph CNFs in hardened cement paste. The bundle is very similar to those observed in the dispersion used to make the paste (Figure 7-b). The image also shows that the fibers are not covered by hydration products.26
- Figure 10. Cryo-TEM images of Pyrograph showing different diameters and lengths of the CNFs. These fibers have been sonicated in an aqueous solution for 15 minutes and their aspect ratios are noticeably smaller than those of non-sonicated fibers. This means that long period of ultrasonic processing can break and shorten many of the CNFs.26
- Figure 11. SEM images of a clump of Pyrograph CNFs in a cavity of hardened cement paste. Both images are taken from the same location, but image (b) has a higher magnification. Agglomerations of this size were barely seen in Optical microscopy and TEM imaging of the CNF dispersion used to produce this paste. This suggests that the CNFs tend to reaggregate during and after paste mixing.28
- Figure 12. SEM images of Pyrograph CNFs on the fractured surface of hardened cement paste. Image (a) shows the CNFs pulled out of the matrix. This paste was made by simply adding CNFs and water to cement prior to mixing without any ultrasonic processing. Image (b) is from the specimen made by adding well-dispersed CNT solution to cement. Two fibers have broken at the same level as the surface of the crack, which indicates that the fibers have not been pulled out. A reason for such fractures is probably that sonication roughen the surface and as a result enhances the fiber-matrix interfacial bond. This also means that the bond strength is controllable and can even reach a high enough value to prevent fiber slippage.29
- Figure 13. Type I portland cement particles. (a) Several particles are as large as 10 micrometer. (b) a particle can be seen at left which is over 100 micrometer. The cement was kept in an airtight container after purchasing fresh. The dimensions of the particles are much larger than the expected average size of cement grains. These large dimensions can be a cause of the poor dispersion of CNFs in paste.32
- Figure 14. (a) Type I portland cement ball-milled for 15 hours. The average size of the particles is smaller than one micrometer and therefore the surface area of the milled cement is significantly larger than the original cement.

- (b) Fractured surface of hardened cement paste made by ball-milled cement-CNF mix. The CNF/cement ratio is 1.0%. Although the w/c ratio in this paste is very high (0.80), and therefore the paste has been subject to significant shrinkage stresses, large cracks were not observed during scanning the surface by SEM. Multiple closely-spaced nanocracks indicates the role of a high content of CNFs in stress distribution.....33
- Figure 15. SEM images of the fractured surface of hardened cement paste incorporating CNF. CNFs are agglomerated and most of the fractured area does not contain CNFs.34
- Figure 16. Schematic presentation of carbon nanotubes (CNTs) in ceramic nanocomposites. (a) The areas between ceramic particles in which CNTs can be distributed are shown with lighter color. (b) When a low dosage of CNT is used to reinforce the ceramic, the distribution of CNTs is relatively uniform and similar to the case in which CNTs could be placed anywhere in the matrix with no limitation imposed by ceramic particles. (c) When the CNT dosage is high, the distribution uniformity becomes poor. The effect of the ceramic particles scales with the size of the particles. The poor distribution resulting from the relatively large size of a composite's constituents is referred to as geometry-dependent clustering or inhomogeneity.39
- Figure 17. (a) Fully uniform and (b) fully non-uniform states of dispersion for 137 circular particles with the diameter of 4 length-units in a domain with the side length of 100 length-units. In a fully uniform dispersion, the statistical distribution of the values of particles' nearest neighbors has the maximum mean and the minimum standard deviation. In a fully non-uniform dispersion, the distribution has the minimum mean and the minimum standard deviation. This forms a single close-pack agglomeration, which should be located as far as possible from the domain's centroid.45
- Figure 18. Different distributions of 137 small particles in a square two-dimensional domain. The diameter of the particles and the side length of the domain are 4 and 100 units respectively. In (a) the particles are randomly distributed in the domain. In (b) the particles are distributed randomly between some larger particles of different phase. The presence of the larger particles have degenerated the dispersion quality of the smaller particles. (c) is an example of poor dispersion resulting from excessive geometry-dependent inhomogeneity.50
- Figure 19. Results from the concentration standard deviation method [96] (a quadrat method) used for quantifying the dispersion of the three domains in Figure 18. The graph shows the standard deviation values when different

element sizes ranging from 1 to 100 were used. It can be clearly seen that the results are sensitive to element size and choosing different element sizes can lead to different judgments about dispersion quality.....	51
Figure 20. (a) The values of dispersive work calculated for the three cases of Figure 18 and for their corresponding ideally non-uniform dispersion (worst dispersion) shown in Figure 17b. (b) The values of dispersion for the three cases. It should be noted that the values of dispersion for the fully uniform and fully non-uniform states of dispersion are 1 and 0 respectively.....	52
Figure 21. (a,b) Two images of CNT reinforced Al coating (From. [119]). The images were converted to simplified representations (c) and (d) by replacing each filament with a disk located at the filament's centroid. (e) and (f) are the fully uniform and fully non-uniform dispersions corresponding to (c).....	55
Figure 22. Rigid body translation and rotation of an inclusion.....	60
Figure 23. Fully dispersed 1-D system of inclusions with discrete width of 0.1.....	68
Figure 24. Methodology for quantifying W^I by subtracting the work performed in destroying inclusions in the discrete system.....	68
Figure 25. (Same as Figure 18) Three different example dispersions consisting of an equal number of small circular inclusions in equally sized domains.	70
Figure 26. Meshes of varying fineness of the initial dispersion shown in Figure 25b, where concentration is shown in grayscale with darker indicating higher concentration.	70
Figure 27. Meshes (100 x 100 elements) of the initial, worst case, and single particle cases for the domain shown in Figure 25a. The spatial dimensions of the domain for the single particle case are determined by the ratio of the number of disks to the domain area (i.e. the concentration of inclusions).	71
Figure 28. Convergence of D^I with increasing mesh fineness for the three initial dispersions illustrated in Figure 25.....	71
Figure 29. Micrographs ($215 \times 270 \mu\text{m}$) showing visually apparent a.) poor, b.) average, and c.) good aqueous dispersions of carbon nanofibers. Using the methodology described in this paper in conjunction with commercially available finite element software, the calculated dispersion qualities for the images are: a.) 0.44, b.) 0.62, and c.) 0.85.	74

- Figure 30. (a) A schematic illustration for geometry dependent clustering of CNTs in cement paste. When the paste is fresh, CNTs cannot penetrate into the cement grains. After the paste is hydrated the locations previously occupied by cement grains remain unreinforced. (b) The ratios corresponding to particle size distribution of typical Type I portland cement and the ratios corresponding to volume occupied by the particles of each size. Approximately 95% of this typical cement volume is occupied by grains that are larger than 20 μm78
- Figure 31. (Same as Figure 16) Effect of inclusion concentration on geometry dependent clustering. The images are the schematic presentation of carbon nanotubes (CNTs) in a ceramic nanocomposite. (a) The areas between ceramic particles in which CNTs can be distributed are shown with lighter color. (b) When a low dosage of CNT is used to reinforce the ceramic, the distribution of CNTs is relatively uniform and similar to the case in which CNTs could be placed anywhere in the matrix with no limitation imposed by ceramic particles. (c) When the CNT dosage is high, the distribution uniformity is significantly degraded.79
- Figure 32. Measured (via laser diffraction) particle size distributions for the three cements of varying fineness commonly used in the construction industry (from Bentz [151]).....81
- Figure 33. Simulated 3-D RVE of cement paste made from a coarse cement with w/c of 0.35, where cement particles are randomly dispersed within the paste.....84
- Figure 34. (a) Discretized RVE of cement paste incorporating nanoinclusions with w/c of 0.4. (b) The same RVE a few time steps after the start of mass diffusion finite element analysis.....85
- Figure 35. Maximum values of nanoinclusion dispersion for cements of varying fineness with w/c of 0.40 and nanoinclusion/c of 0.5% (typical ratios for producing CNT reinforced cement paste). As expected, the dispersion corresponding to coarse cement is the lowest due to the higher effect of geometry dependent clustering. These results show that the negative effect of geometry dependent clustering on dispersion of CNTs in cement paste is minimal.86
- Figure 36. Calculated dispersion values for cement paste made from regular cement and with different parameters typically used for producing CNT reinforced cement paste. (a) Demonstrates the effect of w/c on dispersion for two different concentrations of nanoinclusions. (b) Shows the effect of nanoinclusion concentration on dispersion for regular and agglomerated cement with an average agglomeration size of 200 μm87

- Figure 37. Optical microscopy images of fresh control paste three hours after mixing, acquired by a 20x objective lens. The images show that the CNFs are poorly dispersed and highly agglomerated. The scale bar applies to all three images.96
- Figure 38. CNFs in the SF-3 mix three hours after mixing acquired by a 100x objective lens. The images show that the CNFs are well-dispersed. The scale bar applies to all three images.96
- Figure 39. SEM images of the fractured surface of hardened control paste, indicating the poor dispersion of CNFs. (a) shows that a large portion of the paste does not contain CNFs. In this image CNFs are agglomerated in two different locations of the fractured surface. (b) is a closer look at the CNF agglomeration at the right side of image (a).97
- Figure 40. SEM images of fractured surface of hardened silica fume paste SF-3, indicating the uniform dispersion of CNFs. The scale bar applies to both images.97
- Figure 41. Dispersion of CNFs in cement pastes with different concentrations of silica fume. The error bars indicate one standard deviation either side of the mean.98
- Figure 42. (a) PVC molds used for making hardened cement paste specimens. (b) Fresh cement paste cast in the molds..... 107
- Figure 43. Four-point bending setup for testing hardened cement paste beam specimens..... 108
- Figure 44. Stress vs. Strain curves for some of the beam specimens made from batch 2..... 110
- Figure 45. An image of the fracture surface of the first tested beam from batch 2. The beam broke at a large air void on the surface..... 111
- Figure 46. Cement paste from batch 6 ($w/c = 0.25$, without silica fume and CNF) in the molds 24 hours after casting. The beams were not cured during this period and formed shrinkage cracks, some of them as deep as the beams, dividing the beams into pieces before demolding. 114
- Figure 47. Cement paste ($w/c = 0.40$, with silica fume to cement ration of 20 wt%, and without CNF) in the molds 24 hours after casting. The beams were not moist cured during this period and formed multiple deep shrinkage cracks. All of the beams were divided into pieces before demolding and therefore none of them could be tested in bending. Batch 8 was made

with the same proportions but was casted and cured in a humidity chamber with $RH \approx 100\%$115

Figure 48. A beam made from Batch 9, 24 hours after casting and immediately after demolding. These beams have been produced in the same condition (no curing) and with the same mix proportions as those of the beams shown in115

Figure 49. Schematic illustration of the sensitivity of flexural strength to dispersion...117

LIST OF TABLES

Table 1. The CNFs used in the experiment and the imaging methods used to study their dispersion.....	19
Table 2. Mixture proportions of the cement paste specimens.....	21
Table 3. Different values used for three different parameters investigated in this study; namely, w/c, nanoinclusion to cement mass ratio and cement fineness. The parameter combinations in each row were used to generate simulated cement paste RVEs for dispersion quantification.	82
Table 4. Mixture proportions for the control and silica fume mixes. The proportions are presented as mass ratios.....	94
Table 5. Mix proportion of the cement paste batches. *The difference between batch 5 and other batches containing CNFs is that in batch 5 CNFs were directly added, in form of dry powder, to cement paste in the mixer, while in the other batches CNFs were first dispersed in a water-superplasticizer solution using ultrasonic processing.	106
Table 6. Mechanical properties of the tested beams.	112

1. INTRODUCTION

1.1. Problem statement

Portland cement concrete is the most widely used material in the world after water. Amongst the important reasons are the economic and widespread availability of its constituents. However, concrete has important shortcomings: It is weak in tension and prone to cracking. The weakness in tension is typically overcome by using steel bars, yet full prevention of cracking is very hard to achieve. Not only do cracks have a negative impact on strength, they can significantly reduce the durability of concrete. The cracks increase the permeability of concrete and allow the penetration of gases and liquids that exist in the concrete's surrounding environment, which causes a gradual deterioration of both concrete and reinforcements.

Combating crack formation in concrete is a major topic in concrete science [1]. Cracking can be mitigated by different means from structural and mixture design to addition of continuous and discrete fibers such as reinforcement bars and synthetic fibers. In the past, it has been shown that the utilization of macro- and micro-fibers in concrete increases the number of cracks but at the same time decreases the crack opening width and the spacing between the cracks [2-4]. Concrete is inherently brittle and undergoes fracture, rather than plastic deformation, under an increasing load. Concrete can be designed in such a way that it "behaves similar to" a ductile material when the choices of mixture properties, fiber mechanical properties and fiber-matrix interfacial bond are optimized for this purpose (Figure 1a). In fact, this kind of concrete, usually referred to as "engineered cementitious concrete" (ECC), develops numerous brittle fractures while

This dissertation follows the style of *Composites Part A*.

loading (Figure 1b). However, the fibers bridge the formed macro cracks and control their propagation. In fiber reinforced cementitious materials such as ECC, formation of new cracks or increasing the crack length requires less energy than increasing the width of existing cracks because of the optimized interfacial bond between fibers and matrix that absorb high amounts of energy during the pull-out process. As a result, the large strain capacity of ECC is contributed by sequential development of multiple cracks, instead of continuous increase of crack opening [5]. The more numerous the cracks, the less their average width will be. At least theoretically, this width can reach down to nano or atomic scale. In that case, the cracks are so small that they can neither be regarded as damage nor affect permeability.

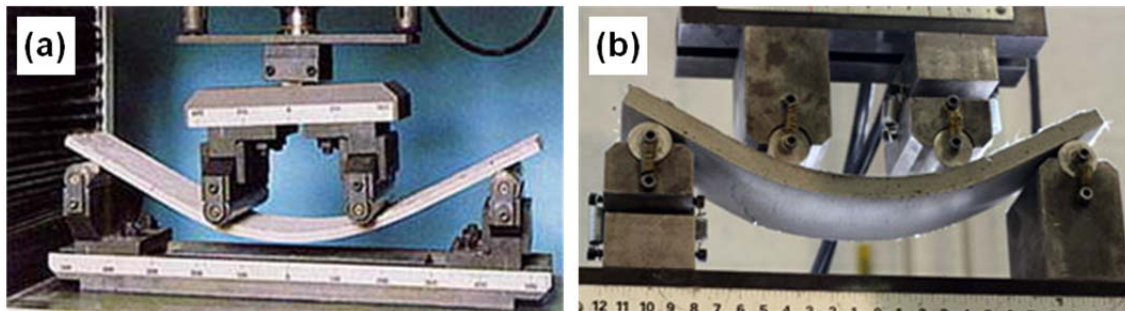


Figure 1. (a) Engineered cementitious concrete displaying a ductile behavior under bending load. (b) The ductile behavior is a result of the formation of multiple cracks bridged by fibers. (Photos are from the Inhabitat and ConstructionLawToday websites)

Studies by Wu and Li show that several parameters affect the formation of multiple cracks in ECC, amongst which are fiber length, diameter, volume fraction, elastic modulus, etc. [6]. The study shows that reducing the fiber diameter increases the number of cracks. Therefore, CNT/Fs, due to their very small diameters (ranging from 1 nm to 200 nm) have the potential for creating a concrete with high resistance to fracture and low permeability. Moreover, CNT/Fs have excellent mechanical properties such as very

high strength and Young's modulus. Therefore, they can improve such properties of concrete through a proper mixture design and engineered filament-matrix interfacial bond.

When the incorporation of CNT/Fs in cementitious materials is concerned, the first and foremost issue is the dispersion of these filaments. They tend to highly attract each other due to van der Waals forces and form clumps. Several methods have been developed to disagglomerate nano filaments and keep them separated from each other in different types of nanocomposites. However, most of those methods cannot be used effectively in cementitious materials reinforced with CNT/Fs. For example, one common method is to first disperse CNT/Fs in an aqueous solution by means of surfactants and ultrasonic processing and then mix the resulted dispersion with the rest of components. However, most of the surfactants that can be used to effectively to disagglomerate CNT/Fs in water have a negative impact on the chemical reaction (known as hydration) that occurs between water and cement resulting in a strong and high-quality concrete. The preliminary research for this thesis shows that such surfactants results in the entrapment of a significant amount of air in cement paste, significant delay in setting of the fresh cement paste and immature hydration that results in a weak material [7].

When a method is developed to improve the dispersion of inclusions (such as CNT/Fs) in a composite, it is important to quantify this improvement. Although qualitative methods of comparison between different states of dispersion (such as visual observation of the materials cross-sectional images and the individual judgment on dispersion qualities) is always helpful, a quantification method can measure "how much" the state of dispersion has improved. In the past century, many dispersion quantification methods have been developed [8]. However, most of these methods are fundamentally different in the interpretation of the concept of dispersion and what they actually measure as "dispersion". Furthermore, most of these methods have been often developed independently and within different disciplines of science such as materials engineering,

biology, ecology, and even astronomy. The lack of a consistent definition of dispersion and a universally accepted robust and practical dispersion quantification method is perceived and required to be addressed.

In the field of cement and concrete research, there have been few studies about the relationship between the physical properties of a cementitious nanocomposite (such as dispersion and nano inclusion concentration) and the mechanical behavior/properties of the cementitious materials. In light of the fact that most of the practical design models and codes, particularly in civil engineering and concrete structures, are fully or semi empirical (not to mention that the fully analytical models require to be validated with experimental data), it is important to augment the existing small database of the CNT/F-incorporated cementitious materials and determine the relationships between the major parameters (such as dispersion, interfacial bond, CNT/F dosage, etc.) and the mechanical behavior and properties of the nanocomposite.

1.2. Scope of thesis

The research on CNT/F-incorporated cementitious nanocomposites is new and its initiation dates back to slightly more than a decade ago. With the production methods that exist today, addition of CNT/Fs to cementitious materials does not cause significant improvement in material properties (particularly mechanical properties). As can be concluded from the previous section, there are numerous issues to be tackled to develop a useful and serviceable material. Amongst these issues are the dispersion quality of the nanofilaments, the limited maximum dosage of the nanofilaments in the cementitious materials (high dosage results in a poor dispersion of nanofilaments in the matrix), optimizing the filament-matrix interfacial bond properties, and the development of a practical production method. Furthermore, in the future, when the science and practice of CNT/F-incorporated cementitious nanocomposite is sufficiently advanced so that parameters such as dispersion, bond, maximum dosage, etc can be

improved/manipulated, mechanics of composites, micro- and nano-mechanics can and must be used to optimize the properties required for the nanocomposite assigned task.

The focus of this research is on production methods, enhancing dispersion, quantifying dispersion, and investigating the improvement in mechanical properties resulted from enhancing the production method, mix design, and dispersion. The study does not explore neither the methods of manipulating filament-matrix interfacial bond nor the micro/nano-mechanics of CNT/F-reinforced nanocomposites. The cementitious material investigated in this project was cement paste. Cement paste is the basic component and the adhesive agent of all cementitious materials (e.g. in cement mortar and concrete, sand particles and aggregates are glued to each other by cement paste). The first step in improving any cementitious material is improving its adhesive. Therefore, cement paste was the target material of the research. The investigations were mainly performed on incorporating CNFs rather than CNTs. The reason is that CNFs are usually more dispersible. Furthermore, CNFs can be observed by means of optical microscopy. As will be seen throughout this study, optical microscopy was invaluable for observing, quantifying, and understanding the dispersion of CNFs in cement paste. However, as the investigations of this thesis indicate, the presented dispersion- enhancement method can also enhance the dispersion of CNTs in cement paste.

The primary objectives of this research project are summarized below:

- design a production method that results in a significant improvement of CNF dispersion in cement paste, as compared to the dispersion achieved by available production methods.
- develop a practical, reliable, and bias-free dispersion quantification method that produces easily interpretable results.

- implement the novel dispersion quantification method to compare the dispersion of CNFs in cement pastes made with common traditional methods and the paste made with the new method.
- produce beam specimens of hardened cement paste and perform flexural bending test to observe the effect of CNFs and their state of dispersion in mechanical behavior and properties (such as flexural strength and modulus of elasticity) of hardened cement paste

1.3. Performed tasks and thesis outline

The tasks performed for this dissertation are as follows:

Task 1. Literature review

A thorough literature review was carried out at the beginning of the project about the past investigations on incorporating nano inclusions to cementitious materials, surface treatment of different inclusions for optimizing the interfacial matrix-inclusion bond, and also the mechanics that dictates the constitutive properties of such nanocomposites. These studies lead us to the selection of carbon nanofilaments as the inclusions for enhancing the properties of cementitious materials. In this dissertation, the literature review will not be presented in a separate chapter; it will be distributed throughout all the chapters of the dissertation. Each chapter will present a stage of the project that incorporates one or more tasks.

Task 2. Preliminary research on the incorporation of carbon nanofilaments in cementitious materials

Several, but not many, studies about the incorporation of CNF/Ts in cementitious materials were found. Some of them consisted of mechanical testing of CNF/T-incorporated cementitious materials, often reporting a minor improvement in mechanical properties due to the use of CNF/Ts. All of the studies emphasized that

dispersing carbon nano inclusions in cementitious matrices was a major obstacle and presented different approaches for alleviating this issue. Some of the most practical and effective methods amongst those were selected, implemented, and improved. However, it was found that none of the methods could result in a sufficient dispersion of CNF/Ts in cementitious matrices. During this stage of research, dispersion qualification methods including optical microscopy and scanning electron microscopy (SEM) were utilized to evaluate the quality of CNF/Ts dispersion in cement paste.

Task 3. Development of a method for improving and stabilizing the dispersion of CNF/Ts

As mentioned earlier and will be shown in section 2, the available methods for dispersing CNF/Ts in cement paste are not sufficiently effective. In this project many efforts were made and several new ideas were generated and explored to develop a practical and effective method for dispersing. One of those ideas led to an effective method that will be presented in section 6 and its effectiveness will be examined qualitatively, quantitatively, and also by means of mechanical testing investigations.

Task 4. Development of a dispersion quantification method

When a method for improving the dispersion of CNF/Ts in cementitious composites is developed, it is possible to discern the improvement by microscopic observation of CNF/Ts in the cementitious matrix. However, it is important to determine “how much” two states of dispersion are different. For this purpose, a quantification method is required that can be input by the micrographs of nanocomposite or the location of individual nanofilaments in a domain, and returns values as output, which can characterize the dispersion of nanofilaments. This dissertation reviews the major dispersion quantification methods developed in the past and discuss their shortcomings. A novel bias-free method that was developed

in this project will be presented and used throughout the dissertation to compare different states of CNF/T dispersion and investigate the relationship between dispersion and mechanical properties.

Task 5. Mechanical testing of CNF-reinforced hardened cement paste

There are few investigations in which specimens of CNF/T-reinforced cementitious materials have been mechanically tested to measure their mechanical properties. Sometimes, the reported results vary significantly from one investigation to the other. For example, some investigators have found that the use of CNF/Ts in cement paste reduces the compressive strength while another investigation reports the opposite. Such differences in results can have different reasons such as the variations in types of utilized fibers or the utilized procedures for dispersing CNF/Ts. In addition, the results are related to the size of tested specimens. Due to different reasons, particularly the high price of carbon nanofilaments in the past decade, typically very small specimens have been produced and tested. Testing small specimens, especially in a bending setup, can be problematic since the ratio of the size of inhomogeneous features, particularly air voids, to the dimensions of the cross-section of specimens are relatively high.

In this research project many beam specimens were produced and tested to investigate the effect of CNFs and the state of their dispersion on the mechanical properties (strength, stiffness, etc.) and behavior (crack formation) of hardened cement paste. The beam cross-sections were notably larger than those made in previous investigations.

Task 6. Development of design methodology for SRCC

In section 7, it will be shown that CNFs can significantly enhance the mechanical properties and crack resistance of cementitious materials. A practical design and production methodology is required in order to utilize CNF in cementitious

materials in industry. In section 2 and section 6, step-by-step methods are presented that details the methodology for the production of CNF incorporated cementitious materials.

The carbon nanofilaments experimented in this project were usually CNFs. The main reason is that CNFs are larger (diameter between 50 nm to 150 nm) than CNTs (diameter between 1 nm to 50 nm) and can be observed by optical microscopy and therefore, their dispersion in water and fresh cement paste can be studied with less effort. Although CNFs are easier to disperse compared to CNTs, as will be explained later, as long as CNTs can be uniformly dispersed in an aqueous solution (and this is possible through different methods of surface treatment), the method introduced in this dissertation (section 6) can be utilized to maintain and stabilize the dispersion of CNTs in cementitious materials as well.

2. CARBON NANOFILAMENTS IN CEMENTITIOUS MATERIALS AND THE ISSUES OF DISPERSION

Due to their excellent mechanical characteristics, carbon CNF/Ts are expected to enhance properties such as strength, ductility, and toughness in cementitious composites. However, such enhancements cannot be achieved unless the fibers are uniformly distributed in the composite and properly bonded to the matrix. CNF/Ts tend to agglomerate due to their high level of van der Waals interactions, and typically form a weak bond with hardened cement paste matrix. This chapter first presents a summary of the efforts made in the past to overcome these two problems. Some typical methods of qualitative measurement of the dispersion of CNF/Ts either in the hardened cement paste or the mix water are discussed. It should be noted that although both dispersion and bond are discussed in this chapter, the main focus of the research project is the issue of dispersion. The experiments presented here investigate the effect of surfactants on dispersion and their benefits and shortcomings when cementitious composites are concerned. It was shown that mixing cement and a well-dispersed water-surfactant-CNF solution may not result in a uniform distribution of CNFs in the paste or an optimal CNT-matrix interfacial bond. However, it was also found that the interfacial bond can reach to a level high enough to prevent fiber pullout.

In order to develop approaches of harnessing the outstanding properties of CNF/Ts and use them as reinforcement in cementitious materials, it is important to know the methods developed to solve the two major issues of dispersion and interfacial bond. The first objective of this chapter is to present a concise review of the research on dispersion and interfacial bond as reported in the literature. The second objective is to demonstrate, through experimental results, the difficulties associated with incorporating CNFs in cementitious materials. Research on reinforcing cementitious materials with CNF/Ts is relatively new and the number of investigations and experiments focused on this subject, especially with CNFs, is still very limited. CNFs, although weaker than CNTs, still have

very high tensile strength and modulus of elasticity. This chapter reports on experimental investigations that study the dispersibility of CNFs and some issues related to their interfacial bond with cementitious matrices.

2.1. Carbon nanofilaments

In the past decade there has been growing interest in CNTs for various composite applications owing to their remarkable physical properties. Mechanically, they exhibit elastic moduli of more than 1 TPa (1.5×10^8 psi)[9]. Their theoretical strength is 100 times that of steel, at only 1/6th the specific gravity[10]. Values as high as 60 GPa (8.7×10^6 psi) for ultimate strength and 6% for ultimate strain have been reported [11, 12]. Salvetat et al. reported an elastic strain capacity of 12%, which is 60 times higher than that of steel[9]. CNTs are also highly flexible, being capable of bending in circles or forming knots. Like macroscopic tubes, they can buckle or flatten under appropriate loadings[13]. Yakobson and Avouris summarize the mechanical behavior of CNTs[14]. The mentioned values have been obtained mostly through theoretical calculations and estimations. Due to their extremely small size (their diameter is usually less than 20 nm) it is very difficult to measure the mechanical properties of CNTs directly. CNFs on the other hand are relatively large; their diameter can be as large as 200 nm. Recently, Ozkan et al. succeeded in performing direct measurements on CNFs[15]. The CNFs that they investigated had a tensile strength between 2-5 GPa (2.9×10^5 - 7.3×10^5 psi) with an average modulus of elasticity of 300 GPa (4.4×10^7 psi).

Few studies have been carried out focusing on the effect of CNF/Ts on the mechanical properties of cementitious composites[16-21]. These studies have shown that CNF/Ts can improve properties such as tensile and compressive strength. Although CNF/Ts are still too expensive to be used in large concrete structures such as buildings, bridges and pavements, the accelerating advances in the methods of producing these nano reinforcements are leading us to promising futures for economical CNF/T-reinforced cementitious composites[22].

Two problems arise when using CNF/Ts to reinforce any kind of material. First, there is the question of dispersing them in the material; CNF/Ts attract each other with high magnitude due to van der Waal's forces. This results in the formation of agglomerations in the forms of entangled ropes and clumps which are very difficult to disentangle. Girifalco et al. showed that the cohesive energy between single-walled carbon nanotubes (SWCNTs) with a length of 100 nm to be about 2.9 keV[23]. The dispersion problem has been combated using methods like surface modification of the fibers, surfactants in combination with ultrasonic processing, and implanting or growing the fibers directly on non-hydrated cement grains.

The second problem limiting the effective use of CNF/Ts in cementitious materials is the difficulty in obtaining an optimal bond between the fibers and matrix due to the atomically smooth and nonreactive surface of these filaments[24]. Bonding is particularly an issue in cementitious composites as the interfacial bond between matrix and any type of straight fiber is relatively weak. If nanotubes are not completely dispersed and are assembled in bundles (ropes), there will be additional sliding inside the bundles[25]. Surface modification is the most common way of enhancing interfacial bond. The surface of CNF/Ts can be functionalized to chemically react with cement hydration products, thereby creating stronger interfacial bond[16]. This chapter is finalized by presenting an experimental program which incorporates CNFs and the use of surfactants and ultrasonic processing to enhance their dispersion in water and cement paste.

2.2. Dispersion, bond, and mechanical properties

Studies have shown that the wettability of CNTs in water is increased by the presence of polar impurities such as hydroxyl (-COH) or carboxyl (-COOH) end groups[26-28]. Additionally, the studies of Ebbesen et al. showed that the oxidation of CNTs cover their surface with carboxyl, carbonyl (-C=O), and hydroxyl groups, thereby improving their

ability to disperse in aqueous solutions[29]. Li et al. showed that these groups, as well as enhancing dispersion, react with calcium silicate hydrate (C-S-H) and calcium hydroxide (CH) and lead to a strong covalent force on the interface between the fibers and matrix[16]. One of the common methods of adding functionalized groups to the surface of CNTs is treating them with acid, typically a solution of H_2SO_4 and HNO_3 [30, 31]. In this method, CNTs are added to the acid solution and the oxidization is accelerated by using either reflux or sonication. In the sonication method, ultrasonic waves are transmitted from a probe into the liquid and produce alternate expansions and compressions. The pressure fluctuations give birth to microscopic bubbles (cavities), which expand during the negative pressure excursions and implode violently during the positive excursions. As the bubbles collapse, millions of shock waves, acoustic streaming, eddies and a combination of both pressure and temperature extremes are generated at the implosion sites. The cumulative amount of produced energy is extremely high and significantly accelerates chemical reactions and imposes dispersion[32].

The early experiments with acid treatment, perhaps due to procedure-related factors, did not show much improvement in mechanical properties of cementitious materials. Kowald used both acid treatment and sonication of CNTs in water and made cement paste specimen with CNT/cement mass ratios in the range of 0.5 to 5.0% [33]. The CNTs had diameters between 10 and 30 nm and lengths between 1 and 10 μm . Kowald tested the hardened specimens for compressive strength after 7, 14, and 28 days. Marginal improvements were observed in compressive strength and even a decrease in strength when the fiber dose was as high as 2.5% or more. Later, Li et al. performed a set of experiments with CNTs which had diameters and lengths at the ranges of 10-30 nm and 0.5-500 μm respectively[16]. The CNT/cement mass ratio was 0.5% and the ratio of water/cement/sand was 0.45:1:1.5. They did not apply sonication, but added methylcellulose (0.4% by mass of cement) to enhance dispersion. The bending and compression tests showed that the addition of acid treated CNTs increased the compressive and flexural strength by 19% and 25% respectively. The investigators later

used a similar method, combined with the sonication of CNTs in water prior to the mixing procedure, and produced cement paste with CNT/cement mass ratio of 0.5% [34]. The SEM images of fractured surfaces of hardened specimens showed that acid treatment enhanced both dispersion and bond. Untreated CNTs formed meshwork in the matrix while the treated CNTs were randomly distributed and covered by C–S–H.

The dispersion of CNF/Ts can also be enhanced by using surfactants. Dispersion of CNTs in liquid media is a well researched topic and many surfactants, combined with sonication, have shown to be effective[35]. The surfactants add charges or hydrophilic ends to the surface of CNTs while their bundles are exfoliated by sonication. Cwirzen et al. used CNTs (diameter 10 nm, length 2-4 μm) functionalized with carboxyl groups. They dispersed the CNTs in water by sonication while using polyacrylic acid polymers as surfactant. Using a mix containing only 0.045% of the CNTs, they observed a significant increase (as high as 50%) in compressive strength. Trettin and Kowald[17] briefly reported an experiment in which they used different types of polycarboxylate-based superplasticizers as surfactants to produce cementitious CNT-reinforced composites. The results of compressive and bending tests showed that the superplasticizers with longer lateral chains resulted in higher strength, which indicated better dispersion of CNTs and better interfacial bond between the fibers and matrix.

Another method to enhance dispersion of CNTs in cementitious composites is to distribute and attach the nanotubes to the surface of cement particles before hydration. Makar and Beaudoin dispersed CNTs (Single walled, diameter 1.4 nm) in ethanol by sonication, and then added cement to the liquid to form a slurry which was further sonicated for hours[36]. The slurry was then allowed to dry and ground to form a powder. The SEM images of the powder show that grains of cement powder have been well coated with CNT bundles. Maker et al. later made cement paste using CNT-coated cement produced with a similar method[37]. Through SEM imaging of the fractured surface of dry paste, they found that the distribution of the CNTs in the hydrated samples

is not the same as seen on the non-hydrated cement grains. CNT bundles were smaller in apparent diameter and more widely distributed in the hydrated matrix. The smallest bundles imaged had diameters less than 5 nm, suggesting that they were composed of only a few 1.4 nm diameter single walled CNTs. Nasibulin et al. have recently developed a method to grow CNF/Ts directly on the surface of cement particles[38]. They showed that the fibers were homogeneously dispersed in the paste made with the produced cement and intermingled with the products during the hydration process. Using this cement resulted in more than 100% increase in the compressive strength of hardened paste.

2.3. Qualitative and quantitative methods of measuring dispersion

Quantifying methods of dispersion were used frequently throughout this project. Some of the available commonly used methods are briefly explained in this section. Optical and scanning electron microscopy were predominantly utilized in this study to observe the dispersion of CNFs in cementitious matrices.

The most common way of evaluating the distribution of CNF/Ts in a composite is scanning electron microscopy (SEM). SEM is the only method that shows the actual distribution of both CNTs and CNFs in the hardened matrix, while the other common methods measure dispersion in the water used for producing cement paste. SEM is therefore utilized for the final validation of dispersion in the cementitious matrix. Images are normally taken from the fractured surface of a material in order to observe the CNF/Ts projecting out of the matrix. When the CNF/Ts are introduced to the paste by initially adding them to the mixing water, a uniform distribution of fibers in the matrix cannot be expected if they were not dispersed well in the water. Several methods are used to qualify or quantify dispersion in water. Three common methods, namely optical microscopy, Transmission Electron Microscopy (TEM) and UV-visible spectroscopy are briefly discussed below.

Although CNTs are too small to be seen by means of optical microscopy, if they are poorly dispersed, the agglomerations can be identified by this method. Since CNFs are larger than CNTs, the quality of their dispersion in water or in freshly mixed paste is easier to study by optical microscopy. Transmission electron microscopy (TEM) is used in order to observe the dispersion of CNF/Ts with much higher magnifications. In TEM, the image is formed from the interactions of electrons transmitted in the form of a beam through a very thin specimen (few hundreds of nanometers). Since the specimen should be solid, the dispersion is usually frozen rapidly and maintained at cryogenic temperatures, generally liquid nitrogen temperatures ($-196\text{ }^{\circ}\text{C}$; $-321\text{ }^{\circ}\text{F}$), in the form of amorphous ice.

Another common method of measuring dispersion in a transparent medium is ultraviolet-visible spectroscopy (UV-Vis). This method is based on the simple fact that the better CNF/Ts are dispersed in a liquid, the darker the dispersion is and therefore absorbs more light. Figure 2 shows three specimens of CNFs mixed in water. In the first specimen (Figure 2-a), CNFs were simply added to water and mixed by a hand-stirrer. In less than a minute after mixing, most of the CNFs settled down while a small portion floated at the top. In other words, there was no dispersion and the bulk liquid was completely transparent. In the second specimen (Figure 2-b), the CNFs were added and hand-mixed with a solution of water and surfactant. The CNFs were slightly dispersed and the specimen absorbed some light. Finally, in the third picture (Figure 2-c), the mixture of water, surfactant, and CNFs was sonicated for 10 minutes. This resulted in a good dispersion and the specimen absorbed a lot of light and was thus very dark.

The schematic layout of a UV-vis spectroscopy device is presented in Figure 3. In each step of measurement, the source sends radiation of a certain wavelength (in UV-visible range) through two specimens. One of the specimens is the dispersion of particles (CNF/Ts) in a liquid medium such as water or a water-surfactant solution, and the other specimen is only the liquid medium without any particle. Based on the strength of the

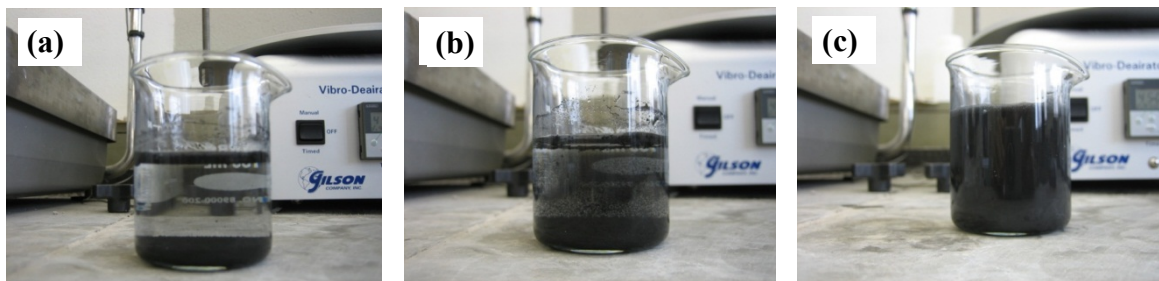


Figure 2. Effect of CNF dispersion quality on the transparency of solutions. All three specimens have the same CNF/water ratio. In specimen (a), CNFs were added to only water and mixed by a hand stirrer, which resulted in poor dispersion and as a result high transparency. In the specimen (b), CNFs were added to a solution of water and surfactant and mixed by a hand stirrer; this resulted in a slightly better and darker dispersion. In specimen (c), CNFs were sonicated in a water-surfactant solution. This produced a good and very dark dispersion.

radiation transmitted through the specimens and collected by the detectors, the portion of radiation absorbed by the particles is determined. CNF/Ts, if dispersed well, absorb the radiation of a specific range of wavelength depending on several parameters such as their size, length and shape. It has been shown that the wavelength range absorbed by some CNTs is between 200-350 nm, with an absorption peak at approximately 250 nm[39, 40]. UV-vis spectroscopy is quantitative, accurate and simple, and is a useful means for drawing comparisons between dispersions made from one type of CNF/T. However, UV-vis does not provide information about the bundle size and the distribution pattern of CNF/Ts, while optical microscopy, TEM, and SEM, despite being qualitative, are direct and visual measures of dispersion. In this research project optical microscopy, SEM, and occasionally TEM has been used to investigate the quality of dispersion. The next sections of this chapter present an experimentation program using these three methods.

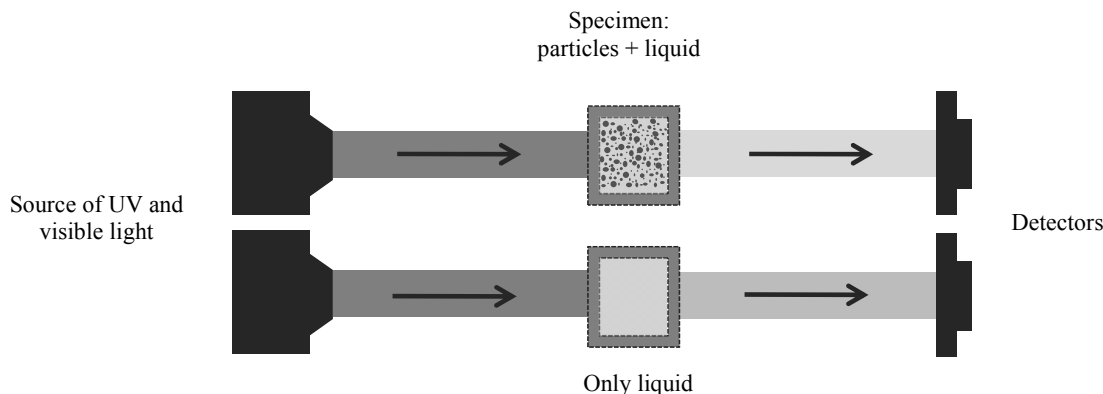


Figure 3. Schematic layout of a UV-vis spectroscopy device, used for quantifying the dispersion of particles in a transparent medium. From the portion of radiation received by the detectors, the absorption capacity of the particles and thus the uniformity of their distribution can be determined.

2.4. Experimental

The experimental investigations reported here aimed at studying the dispersibility of CNFs in aqueous solutions and cement paste, as well as characterizing the interfacial bond between CNFs and cement paste matrix. Solutions of CNFs in water was produced by different approaches and imaged by optical microscopy, and in one case with TEM. Subsequently, cement paste was made by either adding a CNF-water dispersion to cement or simply adding water to a dry mix of cement and CNFs. The fractured surface of hardened paste was imaged by SEM and some correlations and dissociation was found between the distribution of fibers in CNF-water dispersions, and in the paste specimens made from mixing the dispersions with cement. The SEM images of pulled-out and fractured CNFs were used to draw conclusions about the quality of interfacial bond between CNFs and cementitious matrix.

2.5. Materials and preparation of specimens

Two types of CNFs were investigated. Table 1 presents some information about dimension and surface area of the fibers as well as the methods used to study their

dispersion. The first type has an average diameter of 150 nm and length in the 10-20 μm range. The CNFs were provided by Showa Denko Group under the commercial name VGCF-H. The dispersion of the VGCF-H fibers in water was studied by optical microscopy, and their distribution in hardened cement paste was observed by SEM. The second type of CNF has a diameter between 60-150 nm and a length between 30-100 μm . The fibers were provided by Applied Science Company under the commercial name Pyrograph PR-24 (PS), referred to hereafter as Pyrograph. The Pyrograph fibers were studied using optical microscopy, SEM, and also TEM.

Table 1. The CNFs used in the experiment and the imaging methods used to study their dispersion.

Fiber Name	Producer	Avg. Diameter, nm	Avg. Length, μm	Sp. Surface Area, m^2/g	Optical Microscopy	TEM	SEM
VGCF-H	Showa Denko, Japan.	150	10-20	13	Yes	No	Yes
Pyrograph PR-24 (PS)	Applied Science, Ohio.	60-150	30-100	50-60	Yes	Yes	Yes

Most of the dispersions were made by **ultrasonically processing** the CNFs in a water-surfactant solution for 15 minutes. A Sonics & Materials (Vibra-Cell) model VC-505, 20 kHz liquid processor with a $\frac{1}{2}$ inch (12.5 mm) diameter titanium alloy probe was used at an amplitude setting of 50%. Two types of surfactants were used in this study. The first was a nonionic surfactant provided by BASF with the commercial name Pluronic F98. Moore et al. compared this surfactant with several other surfactants and found it effective for dispersing CNTs in water[35]. The second surfactant was a superplasticizer; a high range polycarboxylate-based water reducing admixture provided by W.R. Grace with the commercial name ADVA Cast 575. The surfactant/water and CNF/water mass ratios for all dispersion specimens were 1.71% and 1.14%, respectively. These proportions are the same as those used to make CNF-reinforced

cement paste specimens for SEM imaging. Each sample for optical microscopy was prepared by placing a small drop of dispersion on a glass slide and covering it with a thin slip. A Zeiss Axiophot microscope was used in the transmitted mode with a 40x dry objectives lens. For cryo-TEM, 5 μ L of diluted dispersion was added onto perforated carbon grids (2 μ m holes). Specimens were then plunge-frozen in liquid ethane at 100% relative humidity and transferred to a cryo-specimen holder that was maintained at -175 degrees Celsius throughout the length of the experiment. Observation was performed by an FEI Tecnai F20 transmission electron microscope.

Three CNF-reinforced hardened cement paste specimens were prepared for SEM observation. One of them contained VGCF-H CNFs and the other two contained Pyrograph CNFs. The mixture proportions of the specimens are shown in Table 2. In all specimens, the w/c ratio was 0.35 and CNF/c and surfactant/c mass ratios were 0.4% and 0.6% respectively. Ordinary Type I portland cement was used. Due to compatibility issues that will be discussed later, only the superplasticizer was used as surfactant. For specimens 1 and 2, the CNFs were sonicated and dispersed in the solution of water and superplasticizer for 15 minutes and then the dispersion was added to and mixed with cement. For specimen 3, water-superplasticizer solution was added to a dry mix of cement and CNFs. A small multi-speed planetary mixer was used for mixing paste with a method similar to that of ASTM C 305–06, but with a longer mixing time (total of 7 minutes) to enhance paste uniformity. For each batch after the mixing was completed, the paste was cast into small beam molds. All of the beams were demolded after 24 hours and then cured in lime saturated water. Three weeks after casting, the beams were broken, coated with 4 nm-thick Platinum/Palladium (80/20) layer to enhance surface conductivity while their fractured surfaces were observed by SEM. For SEM observation, the specimen made with VGCF-H was imaged by an FEI Quanta Q600FEG and the other specimens were imaged by a JEOL JSM-7500F.

Table 2. Mixture proportions of the cement paste specimens.

Batch No.	w/c	VGCF-H/c	Pyrograph/c, %	S.Plastiszer/c, %	Sonication
1	0.35	0.4	0	0.6	Yes
2	0.35	0	0.4	0.6	No
3	0.35	0	0.4	0.6	Yes

2.6. Observations and discussion

The effect of surfactants on the dispersion of CNFs in water is illustrated in Figure 4. Figure 4a shows VGCF-H fibers in water-Pluronic F98 solution after 15 minutes of sonication. They are well-dispersed and hardly any agglomeration can be seen. Figure 4b, on the other hand, shows a specimen made in the same condition but without any surfactant. The solution contains large clumps with only a small portion of CNFs floating individually in water. Figure 5 shows two types of poor dispersion of the CNFs in water. The first specimen (Figure 5a) has the same composition as the one shown in Figure 4a, but it was only sonicated for 15 seconds. Clumps of entangled fibers can be seen; the sonication period has not been long enough to disentangle them. A similar pattern of agglomerations could be observed when insufficient amount of surfactant was used, even when the dispersion was sonicated for 15 minutes. Figure 5b shows a different type of agglomeration; the CNFs are bundled longitudinally. This type of texture forms when the dispersion is drying due to evaporation or absorption of water by a dry media such as a piece of cloth. Figure 6a shows VGCF-Hs in water-superplasticizer solution after 15 minutes of sonication; the image shows that the superplasticizer is not as effective as Pluronic F98 in dispersing this type of CNF. The distribution of CNFs in a location on the fractured surface of hardened cement paste made with this dispersion is shown in Figure 6b. The fibers are mostly separated, however this image does not represent the whole area of the fractured surface; in many locations no or little fibers could be seen.

This suggests that a relatively uniform dispersion of CNFs in water does not guarantee a good dispersion in cement paste.

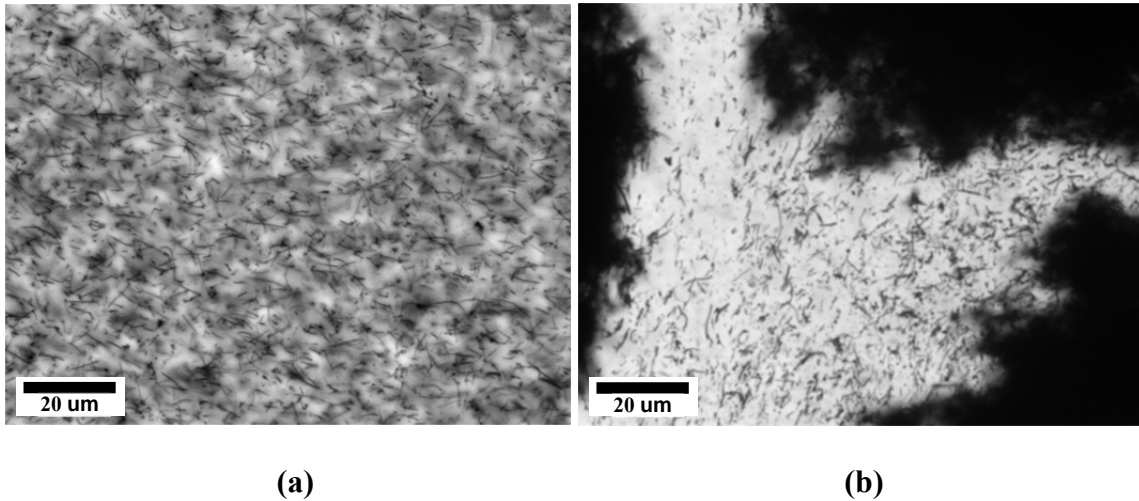


Figure 4. Effect of surfactants on the dispersion of CNFs: Optical microscopy image of the distribution of VGCF-Hs (a) in water-Pluronic F98 solution and (b) only in water. Both specimens were sonicated for 15 minutes.

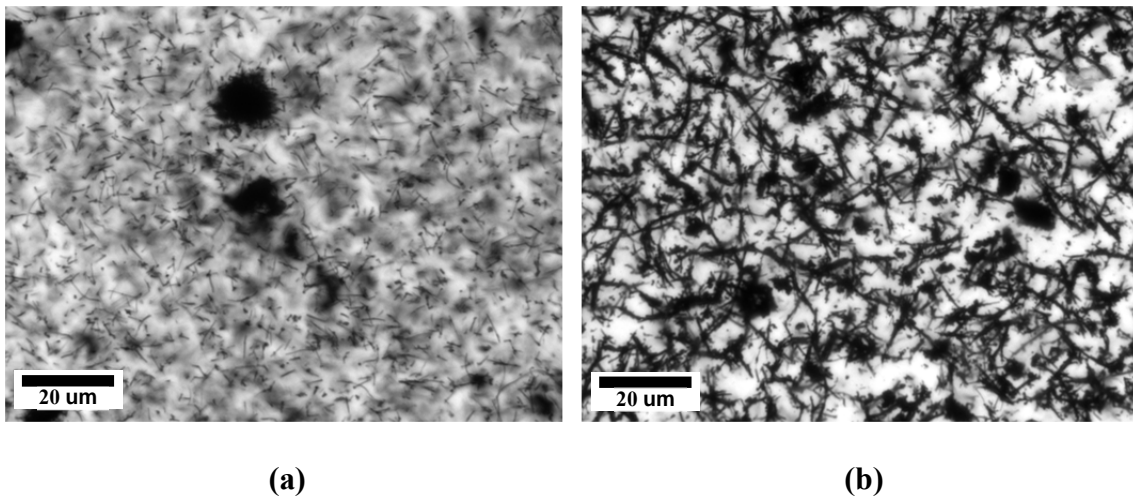


Figure 5. Two types of poor dispersion of CNFs (VGCF-Hs) in water. (a) non-disentangled clumps of CNF due to insufficient sonication, and (b) rebundling of CNFs as a result of drying. Both specimens have the same composition with Pluronic F98 was used as surfactant.

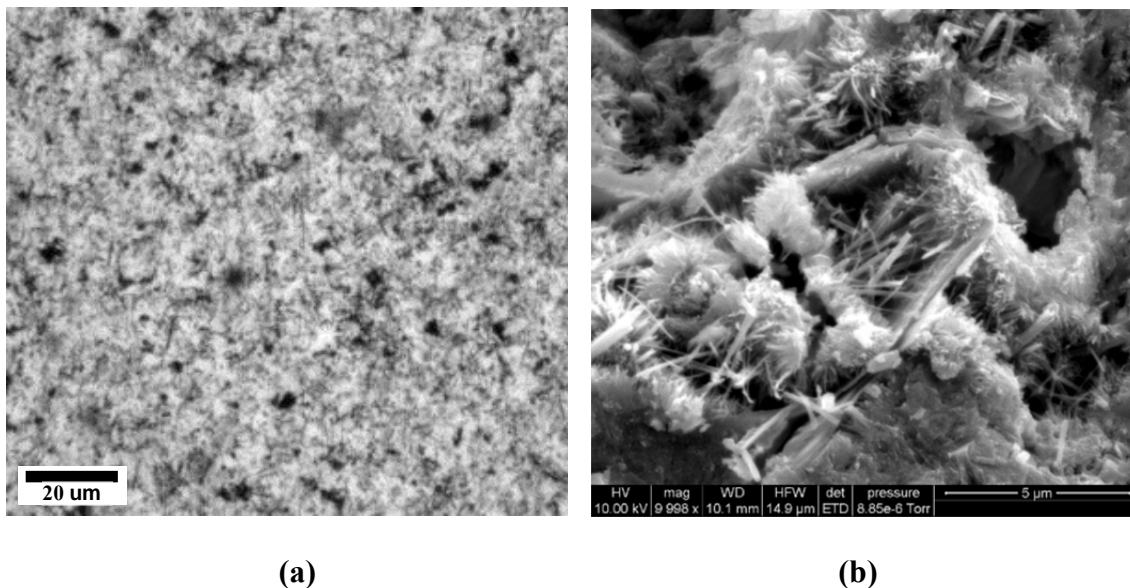


Figure 6. A comparison between the distribution of CNFs in water and cement paste. Image (a) is an optical micrograph of the dispersion of VGCF-Hs in water-superplasticizer solution. The distribution is relatively uniform, but some of the smaller fibers are agglomerated. Figure (b) is an SEM Image of the hardened cement paste in a location with a relatively high concentration of CNFs. The paste was made with the dispersion in (a). The majority of larger fibers are separated. However this image does not represent the distribution of CNFs in the matrix; in several areas of the fractured surface, no or few fibers could be observed by SEM.

The effect of ultrasonic processing on the dispersion of CNFs is illustrated in Figure 7; these are the optical microscopy images of the dispersion of Pyrograph in water-superplasticizer solution. Figure 7a shows the poor dispersion of CNFs in a superplasticizer-water solution that has been only hand-shaken for 7 minutes (the period of time used for mixing the cement paste specimens). In the sonicated mixture (Figure 7b), fibers seem to be well-dispersed. It should be mentioned that these fibers were more dispersible than VGCF-H and their distribution quality in water was almost the same with both Pluronic F98 and superplasticizer. However, some small and mostly round dark areas can be seen (Figure 7b). The dispersion was imaged by cryo-TEM in order to investigate the dark areas. Figure 8a shows a thread-like object which is curled and

packed. Such curled threads formed more than half of the dark areas in the dispersion. The nature of these objects is still unknown, but they may be impurities. Figure 8b shows a bundle of smaller CNFs that has not been disentangled despite sonication. These bundles formed the rest of dark areas in the dispersion. Figure 9 shows the SEM image of one of such bundles in the cement paste made with the CNT dispersion (specimen 3). TEM observations, however, showed that the CNFs were well dispersed in the solution and the portion of bundled fibers and impurities was small. The other fact revealed by the TEM images is that many of the CNFs in the dispersion were shorter than the minimum length specified by the manufacturer (Figure 10). The reason is probably, as also pointed out by Ozkan et al. who investigated the mechanical properties of a similar type of CNF[15], that some of the fibers break during sonication.

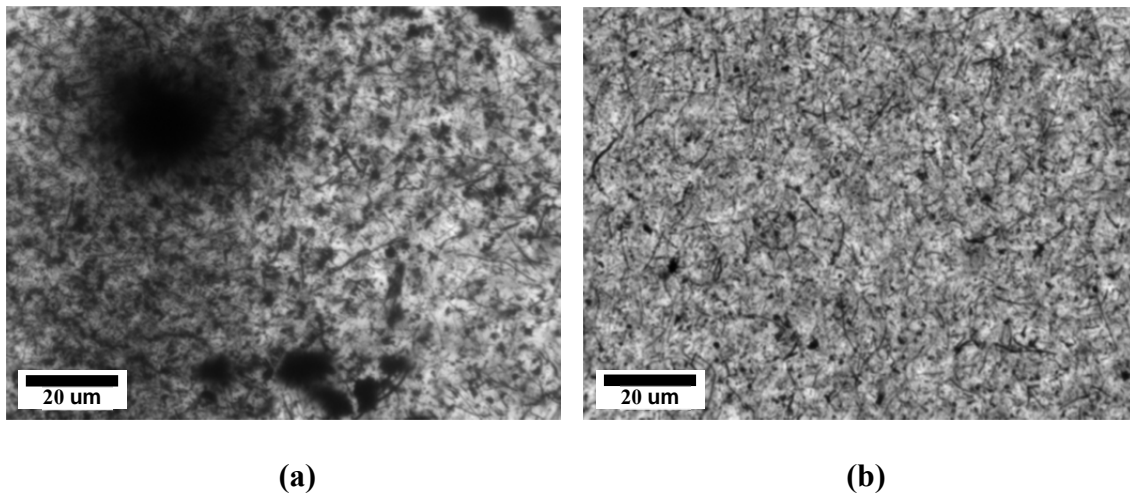


Figure 7. Effect of sonication on the dispersion of Pyrograph CNFs in aqueous media. In both specimens the proportions are the same and the fibers have been added to a water-superplasticizer solution. Specimen (a) was only had-shaken while specimen (b) was sonicated for 15 minutes.

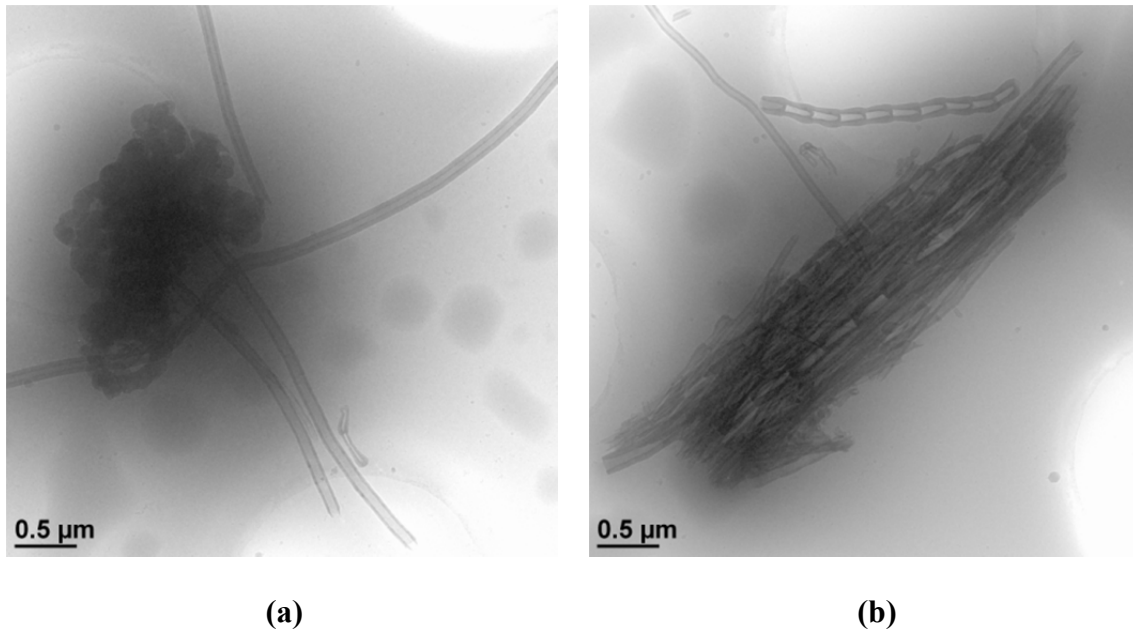


Figure 8. Cryo-TEM images of some undesired features in the sonicated dispersion of Pyrograph shown in Figure 10-a. Image (a) shows an impurity in the shape of a curled thread, and image (b) is a longitudinal bundle of CNFs caused by parallel agglomeration of the fibers.

The SEM study of the fractured surface of hardened cement paste made from the CNFs, either from their dispersion in water-superplasticizer solution or dry mix with cement, showed that these fibers did not have an overall uniform distribution in cement paste. During the paste surface scanning via SEM, many areas were observed that were not covered with CNFs. The SEM images related to Pyrograph (specimen 3) also revealed the presence of several agglomerations, although the CNFs were dispersed well in the solution prior to making the cement paste. One such agglomeration is shown in Figure 11. The underlying causes of reagglomeration of CNFs after adding the dispersion to cement can be explained through the effect of drying on dispersion. As mentioned earlier, initiation of drying of a CNF/T dispersion, and in general reduction in water/fiber ratio, results in bundling. When the dispersion is added to cement, the relatively large amount of cement adsorb the water rapidly. At this point the paste is still workable and fibers can move towards each other and form bundles.

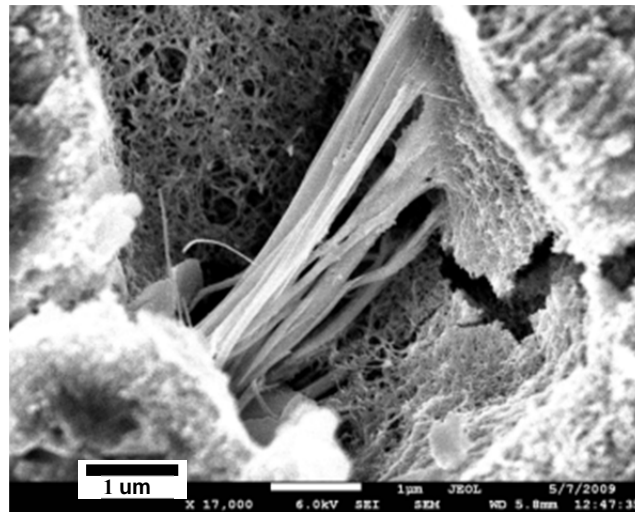
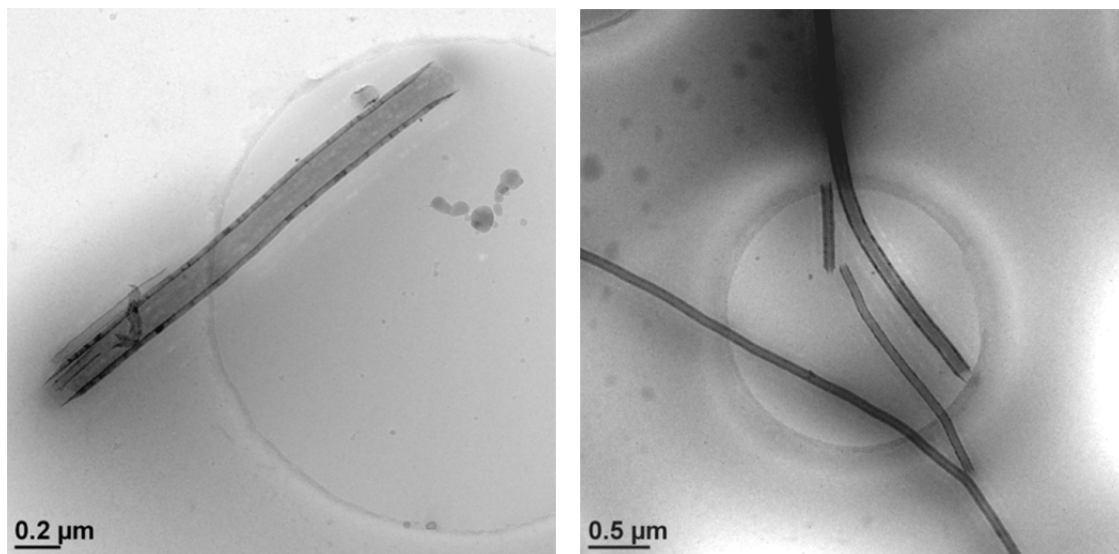


Figure 9. SEM image of a longitudinal bundle of Pyrograph CNFs in hardened cement paste. The bundle is very similar to those observed in the dispersion used to make the paste (Figure 7-b). The image also shows that the fibers are not covered by hydration products.



(a)

(b)

Figure 10. Cryo-TEM images of Pyrograph showing different diameters and lengths of the CNFs. These fibers have been sonicated in an aqueous solution for 15 minutes and their aspect ratios are noticeably smaller than those of non-sonicated fibers. This means that long period of ultrasonic processing can break and shorten many of the CNFs.

As mentioned earlier, Figure 11 shows a clump of CNFs within a pore in the hardened cement paste. These fibers are not covered by C-S-H or any hydration product, and they are not exposed by pull-out of the fibers during fracture. This is an indication of poor interfacial bond between the CNFs and matrix in several areas of the material with such cavities. In a CNF/T-reinforced composite the fibers are expected to be fully covered by and bonded to the matrix; otherwise, their presence is hardly beneficial. Bundling can limit the presence of hydration products in between the entangled fibers. This problem particularly exists in cementitious materials where the matrix components are large relative to the CNF/T size and the space between them. Kim et al. have shown that even polymeric composites resins do not infiltrate into agglomerates of CNTs[41]. However they, and later Li et al.[42], solved this problem by different methods of CNT surface modification including acid treatment. Figure 12 reveals another issue regarding CNF-cement matrix interfacial bond; this figure shows two different scenarios of what can happen to CNFs that bridge a crack. The image in Figure 12a is taken from the fractured surface of specimen 2 (in which CNFs were not sonicated in water). Several occurrences of fiber pullout are shown. The image in Figure 12b is taken from specimen 3 (in which CNFs were first sonicated in water-superplasticizer solution). In this image, two CNFs can be seen that are fractured at the same level as crack surface. This shows that the fibers did not get pulled out and the bond between the fibers and matrix was so strong that the CNTs broke when the crack propagated through them. The observations in Figure 12 indicate that it is possible to control the interfacial bond strength between CNFs and cementitious matrix, and this strength can be high enough to prevent pull-out. Additionally, although the occurrence of fiber pull-out and fracture was seen both in specimens 2 and 3, it is possible that sonication, due to the roughening of fiber surface, can improve the bond. More investigation is required to prove this hypothesis.

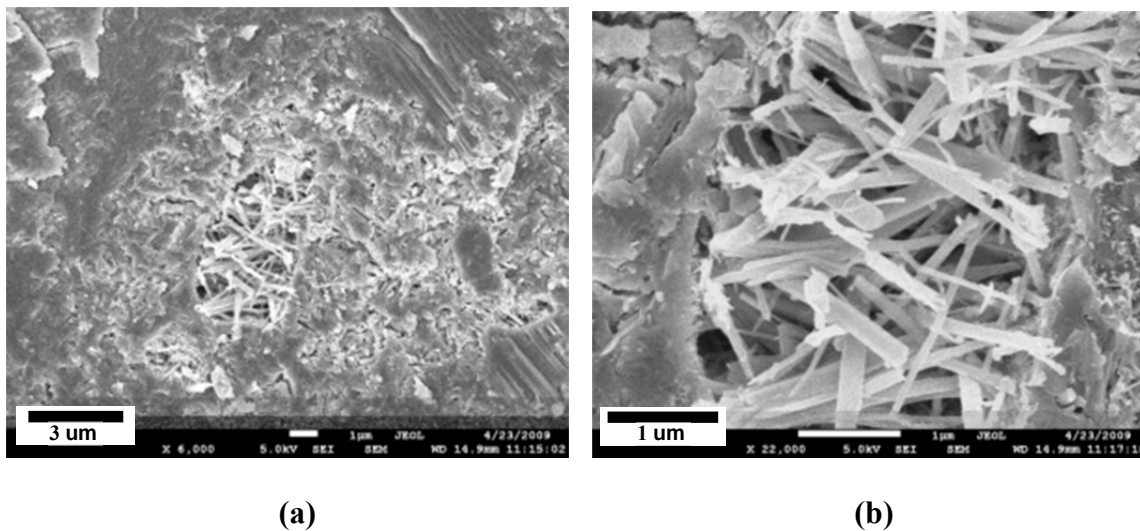


Figure 11. SEM images of a clump of Pyrograph CNFs in a cavity of hardened cement paste. Both images are taken from the same location, but image (b) has a higher magnification. Agglomerations of this size were barely seen in Optical microscopy and TEM imaging of the CNF dispersion used to produce this paste. This suggests that the CNFs tend to reaggregate during and after paste mixing.

As the experimental results showed, Pluronic F98 is more effective (compared to polycarboxylate-based superplasticizers) in disagglomeration of the CNFs in water. Stronger surfactants may prevent rebundling of the fibers during and after paste mixing. However, many of the effective surfactants are incompatible with cement hydration. For example, the experiments of the authors have shown that the addition of Pluronic F98 to cement paste increases the amount of entrapped air remarkably. Using Sodium Dodecylbenzene Sulfonate, which is an effective anionic surfactant, the cement paste entrapped air about 5 times more than is typical in plain cement paste. The paste also did not reach initial set until after 24 hours. Gum Arabic is a natural polymer that has shown to be an effective surfactant for dispersing CNTs in aqueous media[43]. However, it was observed by the authors that when some polycarboxylate-based superplasticizer was added to a dispersion produced by sonicating 1.0% mass of CNTs in a Gum Arabic-water solution (2.0% mass), the fibers reagglomerated and the dispersion turned into a gel-like material.

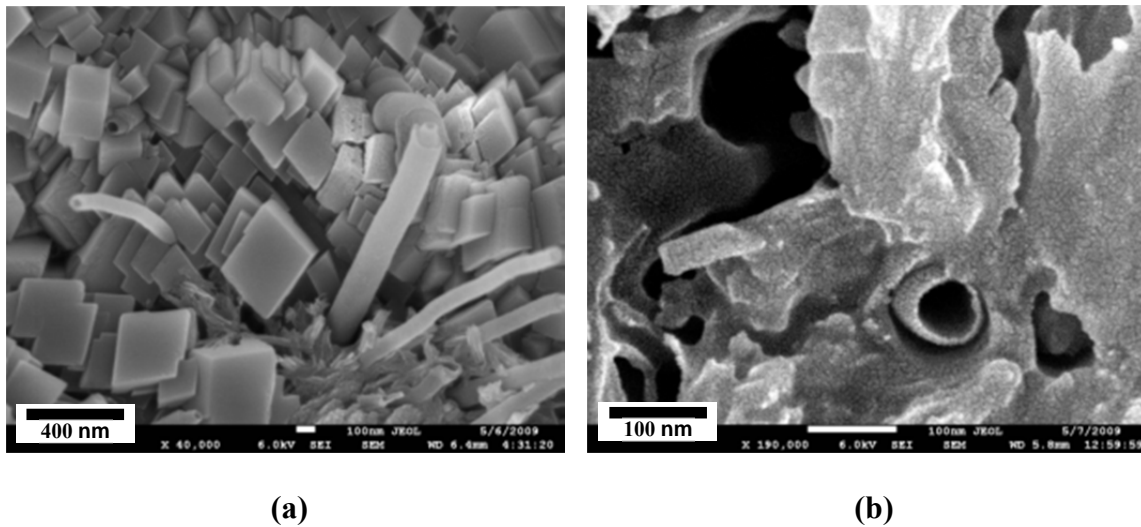


Figure 12. SEM images of Pyrograph CNFs on the fractured surface of hardened cement paste. Image (a) shows the CNFs pulled out of the matrix. This paste was made by simply adding CNFs and water to cement prior to mixing without any ultrasonic processing. Image (b) is from the specimen made by adding well-dispersed CNT solution to cement. Two fibers have broken at the same level as the surface of the crack, which indicates that the fibers have not been pulled out. A reason for such fractures is probably that sonication roughen the surface and as a result enhances the fiber-matrix interfacial bond. This also means that the bond strength is controllable and can even reach a high enough value to prevent fiber slippage.

There are stable CNT aqueous dispersions available in the market, like AquaCyl produced by Nanocyl Company, but they have some negatives effects on cement hydration. Cwirzen et al. found that Gum Arabic slowed down the hydration reactions and decreased the compressive strength of hardened cement paste[18]. All these findings show that a hydration-compatible surfactant may not always be the solution to the problem of producing cementitious composites with uniformly distributed and well-bonded CNF/Ts, and approaches such as surface functionalization and implantation on cement grains should be further investigated.

2.7. Geometric clustering: another potential cause for the poor dispersion of CNF/Ts in cement paste

The investigations of this chapter shown that the main reason for the poor dispersion of CNFs in cement paste was the reagglomeration of CNFs when the aqueous dispersion of CNF and superplasticizers was added to cement. In this section, geometric clustering, another possible cause for the poor dispersion of carbon nanofilaments in cement paste, which probably cannot be eliminated, is briefly discussed. This issue will be investigated thoroughly in section 5.

One of the least investigated causes of the poor dispersion of CNF/Ts in cement paste is the size of cement grains and is referred to as geometric clustering [7]. The average size of Type I portland cement is between 10-20 μm . Therefore, cement particles are very large compared to CNTs or even CNFs. The SEM observations show the geometry of typical cement particles (Figure 13). Many of the cement particles are as large as 10 μm and particles larger than 100 μm can be seen. These observations are in agreement with the measured cement particle size distribution by laser diffraction techniques [44]. Two parameters affect the role of cement particle size on the distribution of fibers in cement paste. The first parameter is the size of the fibers relative to cement particles. CNF/Ts are much smaller than macro-fibers and even micro-fibers, so uniform dispersion at a certain volume fraction requires much smaller spacing between fibers. Since CNF/Ts are much smaller than cement grains, the minimum consistent spacing between fibers is limited by the size of the cement grains. That is, the CNF/Ts cannot penetrate the cement grains and are thus separated by a larger than optimal spacing in the presence of large grains. By having larger than optimal spacing in certain regions of the material, smaller than optimal spacing between CNF/Ts occurs in other regions; the result is a greater potential for poor dispersion.

The second parameter dictating the role of cement particle size on CNF/T distribution is the distance between adjacent fibers given a uniform distribution of fibers in the matrix.

If this distance is larger than the average particle size, then cement grains do not disrupt uniform dispersion even if the grains are much larger than fibers. In order to make an approximate but reliable measurement of the distance between well-dispersed fibers, it was assumed that all fibers are aligned in one direction, that is, all the fibers are parallel. Based on TEM and SEM images of the CNFs, it was also assumed that the internal diameter of a CNF is 1.5 times of its wall thickness, and that the hollow part of CNF remains empty during and after paste mixing. With these assumptions, using CNFs with an average diameter of 100 nm in a paste with $w/c = 0.35$ and $CNF/c = 0.004$ (same as in the paste made in phase I), the distance between two adjacent CNFs would approximately be 5 μm . This means that if the average cement grain size was 4 μm , it would not have a negative effect on dispersion. However when the average size of cement particles is 10 μm or more, a uniform dispersion of CNFs with the mentioned mix design and fiber size is not possible. Moreover, when a higher dosage or fibers with smaller diameters are used, given a uniform distribution, the space between the fibers is reduced. For example, for the CNF/paste mass ratio of 1.0, the space between adjacent fibers would be 2.7 μm . As another example, if CNTs with an average diameter of 10 nm and CNT/c ratio of 0.5 is used, the space would be as small as 440 nm.

An experiment was carried out to find out whether it is possible to use fine-grain cement to produce CNF-cementitious composites. Figure 14a shows the SEM image of the cement produced by ball-milling the type I portland cement shown in Figure 13. The milled particles are very fine and their average diameter is less than 1 μm . When this cement was used to make a paste with $w/c = 0.35$, after adding water-superplasticizer solution to cement, mixing resulted in only a wet powder. The mix did not turn into a paste until the w/c and superplasticizer/cement ratios were increased to 0.52 and 0.03 respectively. The problem was more severe with the ball-milled cement-CNF mix; w/c and superplasticizer/cement ratios of 0.80 and 0.02 were used to achieve a paste mix. In both cases the paste was very viscous and had rapid exothermic heat output. However, despite the very high w/c ratio of the fibrous paste,

and as a result, the high magnitude of shrinkage stresses, the cracks were very fine and uniformly distributed throughout the fractured surface. This indicates the viability of CNFs in effective distribution of stress in cementitious composites (Figure 14b).

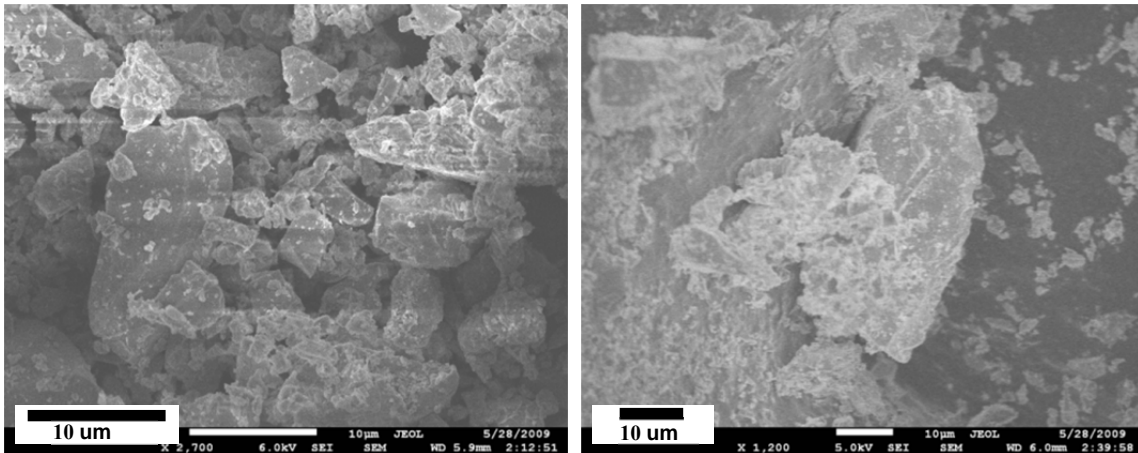


Figure 13. Type I portland cement particles. (a) Several particles are as large as 10 micrometer. (b) a particle can be seen at left which is over 100 micrometer. The cement was kept in an airtight container after purchasing fresh. The dimensions of the particles are much larger than the expected average size of cement grains. These large dimensions can be a cause of the poor dispersion of CNFs in paste.

A main reason for high demand of water by fine cement is that breaking cement grains into smaller particles increases the surface area of cement. Higher surface area results in more reactivity and also higher amount of water required to be adsorbed on the surface of cement particles to produce a workable paste. In general, the surface area of particles is inversely proportional to their dimension. In other words, if the particles of a given mass of cement are milled so that the nominal average diameter of the new particles is half of the original average particle diameter, the surface area becomes twice. Therefore, in the case of this experimental program, when the average size of the milled cement grains is less than one tenth of the size of original particles, the new surface area is over

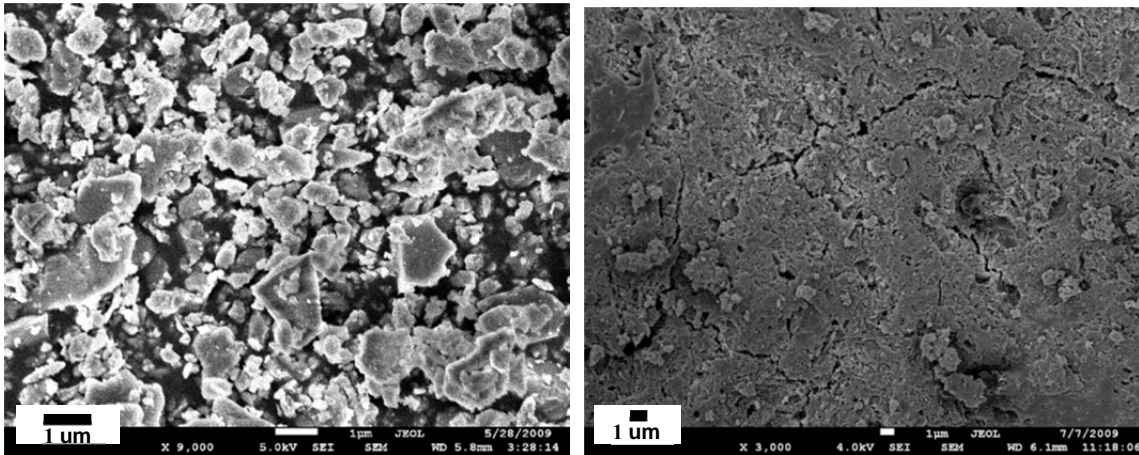


Figure 14. (a) Type I portland cement ball-milled for 15 hours. The average size of the particles is smaller than one micrometer and therefore the surface area of the milled cement is significantly larger than the original cement. (b) Fractured surface of hardened cement paste made by ball-milled cement-CNF mix. The CNF/cement ratio is 1.0%. Although the w/c ratio in this paste is very high (0.80), and therefore the paste has been subject to significant shrinkage stresses, large cracks were not observed during scanning the surface by SEM. Multiple closely-spaced nanocracks indicates the role of a high content of CNFs in stress distribution.

ten times greater, and therefore the required amount of adsorbed water and superplasticizer becomes significantly more. Using fine-grained cement has other disadvantages. Mehta has pointed out that using fine cement can have negative effects on durability [45]. The high amount of heat released during the hydration of fine cement can lead to thermal cracking. Also, finer cements generally produce more chemical and autogenous shrinkage [44]. As a result, milling cement or using very fine cement may not be a practical approach to enhance the dispersion of CNF/Ts in cementitious matrix. It should therefore be understood that CNF/Ts may not be able to be distributed uniformly in a cement paste above a certain volume fraction, depending on the particle size distribution of the cement. This fact should be taken into consideration when theoretically modeling and analyzing the behavior of CNF/T-reinforced cementitious composites.

Finally, the SEM observations of the fractured surface of hardened fibrous paste made with non-milled cement show that there are areas without any CNF with dimensions as large as hundreds of micrometers between the areas that contain CNFs (Figure 15). This is much larger than the size of the largest cement particle. Therefore the size of cement particles may not be the major reason for poor dispersion. The extent of the effect of geometric clustering on CNF/T dispersion in cement paste will be investigated in detail in section section 5.

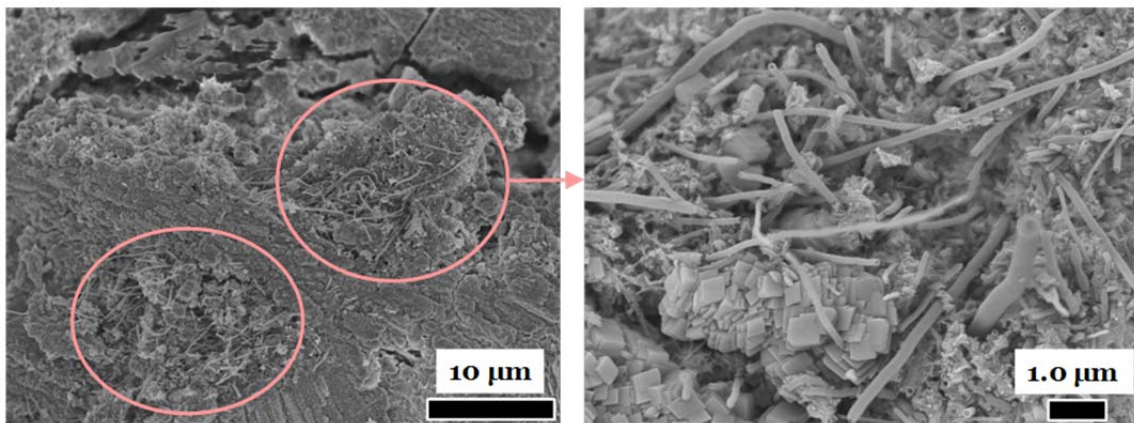


Figure 15. SEM images of the fractured surface of hardened cement paste incorporating CNF. CNFs are agglomerated and most of the fractured area does not contain CNFs.

2.8. Concluding remarks

A summary of the past investigations on the reinforcement of cementitious composites with CNTs was presented. Issues on dispersion, fiber-matrix interfacial bond, and surface functionalization were discussed. Studies focused on incorporating CNFs in cementitious composites are scarce. CNFs have much lower surface area compared to CNTs and are easier to disperse. An experimental program on two types of CNFs was presented. It was found that a polycarboxylate-based superplasticizer could properly

disperse a relatively high concentration (more than 1.0%) of one type of the fibers in water. However, the SEM images of hardened cement paste revealed the presence of bundles, clumps, and distribution non-uniformities. This suggests that some of the fibers reaggregate during and after paste mixing. This issue affect the quality of dispersion more severely than geometric clustering.

The SEM observations proved the possibility of the occurrence of both CNF pull-out and fracture, and therefore the controllability of CNF-cement matrix interfacial bond. The SEM images also showed that many of the agglomerated CNFs were not covered with or bonded to the matrix, since the paste had not infiltrated through them; this indicates the importance of examining additional approaches (such as fiber surface functionalization) to optimize both bond and dispersion. Seeking additional approaches to ensure dispersion and bond than surfactants is also important since more effective surfactants can negatively affect cement hydration. Moreover, more dispersible CNFs require less sonication, which would be another advantage since long period of sonication can break and shorten the fibers.

3. A NOVEL METHOD FOR DISPERSION QUANTIFICATION OF INCLUSIONS IN COMPOSITES

Dispersion quantification of inclusions in composites is useful and important. As an example, in this study the effect of geometric clustering on the dispersion of nanoinclusions in cement paste will be investigated (section 5). For this purpose, only a dispersion quantification method can determine “how much” geometric clustering affects dispersion. In addition, in this project a new method for enhancing the dispersion of CNF/Ts in cementitious materials will be presented. Again, a dispersion quantification method is required to measure “how much” the method is effective. This chapter will present a novel bias-free method of dispersion quantification after reviewing several major methods developed in the past and investigating their possible shortcomings. An approach, based on the continuum theory, for implementing the new method will be presented in section 4.

Distribution of constituents within a composite material dictates important constitutive properties and is therefore of interest for all multiphase materials including composites that incorporate nano-, micro-, and macro-inclusions. In the first part of this chapter, previously proposed methods for quantifying dispersion are reviewed and their applications and possible shortcomings are discussed. In the second part, a novel definition for dispersion is presented based on the thermodynamic concept of *work*; dispersion is measured based on the amount of work required to translate inclusions so they form the state of maximum uniformity. The method quantifies dispersion with a single parameter. Although multiple parameter methods can provide more information about the spatial distribution of inclusions, the new method is particularly useful when comparing overall dispersion quality of different domains. As an example, the dispersion of carbon nanotubes in an Al coating is quantified to demonstrate the robustness and practicality of the novel dispersion quantification method.

3.1. Introduction

Manufactured composite materials are ubiquitous in industries ranging from electronics to civil infrastructure, and include particulate (inclusions roughly spheroids) and filament (inclusions with high aspect ratio) reinforced materials. The constitutive properties of a composite are highly affected by the uniformity of distribution of inclusions (also referred to as *features*) in the material. For example, from the mechanical perspective, the distribution of inclusions has a strong influence on the local stress fields and therefore affects the durability and fracture characteristics of the composite material. Past research has studied the effect of inclusion distribution on mechanical properties and durability of a wide range of composites including polymeric [46-55], metallic [56-59], and cementitious [60-62]. A review of investigations focusing on nanocomposites can be found in the work of Sun et al. [63]. Many of these studies have used qualitative or semi-quantitative methods to quantify dispersion, such as the visual observation of micrographs obtained from scanning electron microscope (SEM) or transmission electron microscope (TEM) imaging, or the curves obtained from different spectroscopy devices.

Today, several kinds of nano inclusions such as carbon, metal, and silica nano particles or filaments are being used in a wide variety of materials to enhance their mechanical, electrical, optical, or catalytic properties. The use of carbon nanotubes (CNTs) or nano fibers (CNFs) in ceramics [64-67], cementitious materials [16-19, 34, 38], polymers [68], rubbers [69] and metals [70] are a few examples of such applications. Controlling the distribution of nano inclusions is a major challenge since very fine particles tend to highly attract each other, mostly due to van der Waal's forces and static charges, and form agglomerations. Numerous methods such as surface functionalization, ultrasonic and centrifuge processing are used to mitigate this problem [29, 35, 42, 71-75]. However, quantitative characterization of distribution uniformity remains one of the least investigated aspects of nano composite research.

Quantitative measurement of distribution uniformity is useful for three main reasons. First, qualitative methods such as visual observation of images of composites not only tend to suffer from subjective judgments, but also do not produce numerical values that can be used for systematic comparison of materials with the same components but different distribution of inclusions. Second, relatively little work has been done on establishing a constitutive link between the overall material response and the quality of dispersion [76-80]; a quantitative measure of dispersion uniformity is necessary for establishing such constitutive relationships. Third, a good quantitative method can be used to *predict* the best achievable distribution uniformity of inclusions given the size and volume fractions of the composite constituents. In general, when the host material (e.g. cement or ceramic) is in the form of finite sized impenetrable particles, increasing the concentration of inclusions can lower the uniformity of their distribution. In addition, the particles of the host material, especially when they are larger than the individual inclusions, can prevent the uniform distribution of the inclusions and cause geometry-dependent clustering/inhomogeneity [56].

Figure 16 presents schematic examples of CNTs in ceramics when CNTs are randomly distributed between ceramic particles. Figure 16a. shows ceramic particles during sintering while nano-inclusions can only penetrate into and reinforce the areas between ceramic particles. If the concentration of CNTs is low, the overall distribution of CNTs is close to random (Figure 16b.) However, when the concentration of CNTs is high, their overall distribution will be non-random and in the shape of the honeycomb network of boundaries between the ceramic particles (Figure 16c.) This non-uniformity would not occur if the ceramic particles were much smaller.

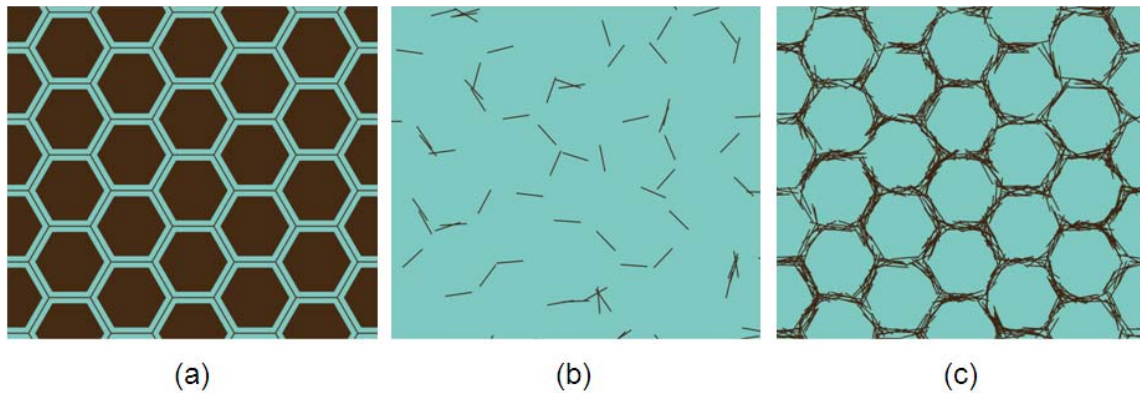


Figure 16. Schematic presentation of carbon nanotubes (CNTs) in ceramic nanocomposites. (a) The areas between ceramic particles in which CNTs can be distributed are shown with lighter color. (b) When a low dosage of CNT is used to reinforce the ceramic, the distribution of CNTs is relatively uniform and similar to the case in which CNTs could be placed anywhere in the matrix with no limitation imposed by ceramic particles. (c) When the CNT dosage is high, the distribution uniformity becomes poor. The effect of the ceramic particles scales with the size of the particles. The poor distribution resulting from the relatively large size of a composite's constituents is referred to as geometry-dependent clustering or inhomogeneity.

Geometry-dependent clustering is present in many composite materials. For example, in the production of some nano-composites, the host material is in the form of solid particles that are often larger than the nano inclusions. Examples of such materials are aluminum-CNT [81], ceramic-CNT [82], cementitious-CNT [7, 83] nanocomposites, and silica-latex films [84]. For materials of this type, it is important to quantify the maximum host particle size or nano-inclusion concentration that does not negatively affect the matrix uniformity.

Distribution uniformity can be divided into two aspects. The first aspect (referred to here as *dispersion*) is related to the spatial uniformity of the inclusions. The other aspect arises when the inclusions are filaments. In this case, the orientation of the filaments affects the constitutive properties of a composite as well. The past research on distribution uniformity has mostly focused on dispersion rather than orientation for two main reasons. First, filaments are only one of the several types of inclusions. Second, in many fibrous composites the filaments are intended to be randomly oriented; this is

usually achieved without any special effort and therefore the need to measure the orientation uniformity is unnecessary. Thus, the objective of this paper is to review past efforts to quantify dispersion and to subsequently introduce a novel definition and model for quantifying dispersion.

3.2. Past efforts to define dispersion

The quantitative characterization of dispersion has been treated to high degrees of mathematical sophistication for several decades (for references see [85-91]). Those efforts have set up the foundation for some of the methods that are well established in practical use today. Such methods have been developed in many fields of science including powder and mixing technology [92-98], microscopy and image analysis [99-101], ecology and biology [102-111], astronomy [89, 112, 113], computer science [114], chemical engineering and physics [115], and material and composite science [57, 59, 116-118]. More references for classic methods can be found in the work of Schwarz and Exner [99]. Dispersion quantification methods can be divided into four major categories as summarized below.

3.2.1. Methods based on feature size

These methods are usually used for materials such as ceramic and metallic composites which are made by dry mixing, and later, sintering/hot-pressing of impenetrable constituents [70]. Dispersion is quantified by relative particle size (RPS) ratio, which is defined as the ratio of the host particle size to reinforcement (inclusion) particle size [57, 59, 116]. RPS is a measure of geometry-dependent clustering. Higher RPS is expected to be an indication of higher clustering.

3.2.2. Methods based on contact area between features

These methods have been developed for composites with densely packed constituents of irregular shapes, for example concretes with high proportion of aggregates. Gurland [119], presented an aggregate dispersion quantification method based on the area of contact between the aggregates. In this method, which was also used later by Jang and

Chang [46] for toughened plastic reinforced with rubbery phases, the main measure of dispersion is the interface of separation, defined as:

$$dp = \frac{Sv(ab)}{Sv(aa) + Sv(ab)} = \frac{Sv(ab)}{Sv(total)} \quad (1)$$

where $Sv(ab)$ is the area of interface between the features and the matrix, and $Sv(aa)$ is the area of contact between contiguous features in a volume. The lower value of the separation interface is an indication of higher agglomeration and lower quality of dispersion.

3.2.3. *Methods based on feature local concentrations (quadrat methods)*

This category of dispersion quantification methods, here referred to as quadrat methods, define dispersion with the standard deviation/variance of the concentration of features among small quadrats (elements) with a characteristic size. The method can be implemented in different ways. For example, the domain can be discretized into elements and the feature concentration in each element be calculated, or a frame (quadrat) moves over the domain with a certain step size and the feature concentration within the slide be calculated in each step. Lower standard deviation of quadrat concentration is expected to indicate better dispersion. Quadrat methods have been used extensively in ecology to study the spatial distribution of species starting nearly a century ago [104, 105]. Variants of quadrat method are used in several applications due their simplicity and overall good judgment on dispersion when used carefully [92-98, 115].

3.2.4. *Methods based on microstructural parameters*

These methods are arguably the most researched and developed amongst other dispersion quantification methods. Major microstructural parameters are based on the distance between the features. When features are randomly scattered on a surface, the distances between them and their nearest neighbors have a Poisson distribution [100]. In fact, Poisson point processes are some of the most common mechanisms to produce

randomly dispersed features in spatial statistics [99, 100, 102, 109, 110, 120-123]. Clark and Evans presented an explicit expression for a dispersion measure R [103] according to

$$R = \frac{\bar{r}_A}{\bar{r}_E}, \quad (2)$$

where \bar{r}_A is the observed mean distance to nearest neighbor in the RVE under investigation and \bar{r}_E is the mean distance to nearest neighbor that would be expected if the individuals of that population were randomly distributed. Therefore, in a random distribution, $R = 1$. Under conditions of maximum possible aggregation, R is the nominal radius of the features since the features are closely packed. Considering the importance of the standard deviation of the distances between nearest neighbors, Schwarz and Exner defined the additional measure R' as

$$R' = \frac{\bar{s}_A}{\bar{s}_E}, \quad (3)$$

where \bar{s}_A is the variance of the distances to nearest neighbors in the RVE under investigation and \bar{s}_E is the variance of the distances to nearest neighbors in a random pattern. Therefore, in random sets $R \sim 1$ and $R' \sim 1$, in fully dispersed sets $R > 1$ and $R' \ll 1$, and in sets of clusters $R < 1$ and $R' > 1$.

Some other microstructural parameters have been defined using Voronoi polygons evolved from Dirichlet tessellation of domains [76, 77, 79, 80, 124, 125]. Dirichlet tessellation is defined as a subdivision of a domain, such that each feature in the domain has associated with it a polygonal region (Voronoi cell/polygon) that is closer to it than to any other feature. Dirichlet tessellation has been used to obtain the nearest neighbor distances and other microstructural parameters, including local area fraction (ratio of a feature's area to the associated Voronoi polygon) and the number of *near* neighbors

(number of the sides of the Voronoi polygon associated with a feature). The mean and standard deviation of these parameters, in addition to those of nearest neighbor values, have been used to characterize dispersion. These parameters have also been used within probability functions such as cumulative distribution and density functions. The cumulative distribution function $F(x)$ represents the probability that a parameter, e.g. the local area fraction or nearest neighbor distance, assumes a value smaller than or equal to x . The probability density function $f(x)$ refers to the probability of a parameter assuming a value x . The other function used for the characterization of spatial distribution is second order intensity function $K(r)$, defined as the number of points expected to lie within a distance r of an arbitrary point and divided by the number of points per unit area. Probabilistic analyses of dispersion have been implemented to analyze the micrographs of different composite materials. For example Akkaya et al. used some of the mentioned functions and microstructural parameters to quantify the dispersion of fibers in cementitious composites [61]. The judgment about the quality of dispersion is based on the visual comparison of the function curves of the domain under investigation and a reference domain of features, typically generated by Poisson's random point processes.

Some other methods of dispersion quantification based on microstructural parameters use stereology techniques known as intertrack measurements. In these methods, parallel lines are drawn on the image of a composite cross-section. The span between two adjacent particles on a line forms a track (free-path). Brian and Garry showed that for a random dispersion, track length distribution fits in a log-normal distribution function [101]. However, they did not quantify the deviation from the log-normal curve (which may be regarded as an indication for the poorness of dispersion). Another method of this type introduced by Luo and Koo is based on the assumption that if all of the inclusion particles are distributed at an equal free-path distance, the dispersion is perfect [117]. In this method, the actual frequency distribution of track lengths is represented with a probability distribution function of the same mean μ and standard deviation σ . The

probability function is usually lognormal, normal, or a combination of both. The dispersion is then quantified as the definite integral of this function on the interval $[(1-r) \cdot \mu, (1+r) \cdot \mu]$, where Luo and Koo used r values between 0.1 or 0.2. Recently, Tyson modified the method of Luo and Koo by considering both the free-path spacing and the agglomeration size in order to get a better quantitative measure of dispersion [126].

Bakshi et al. [118] introduced a quantification method specifically for the dispersion of CNTs in nanocomposites, for which they measured the nearest neighbor distances between CNT centroids. Their clustering parameter, CP is defined as

$$CP = \frac{NN_{5D}}{NN_{TOTAL}}, \quad (4)$$

where NN_{5D} is the sum of nearest neighbor distances that are less than five times of the CNTs' average diameter. NN_{TOTAL} is the sum of all the nearest neighbor distances. A lower value of CP indicates a more uniform dispersion.

3.3. A novel measure of dispersion

3.3.1. Fully uniform and fully non-uniform states of dispersion

An appealing measure of dispersion is intuitive, simple, and capable of quantifying dispersion for any kind of multiphase material. In addition, such a measure should not incorporate subjective parameters. The variety of available definitions for distribution uniformity (or dispersion) is in part due to the ambiguities arisen in perceiving the concept of a *good* dispersion. For example, in the RPS method, a good dispersion is regarded as one in which host particles are as small as possible, or in the stereology-based model of Brian and Garry [101], a good dispersion is considered as one in which inclusions are distributed randomly.

For the novel measure of dispersion to be defined in the following subsection, we define two limit cases: the fully non-uniform and the fully uniform dispersions. Dispersion can be defined based on where a distribution of interest stands between these extrema. There are a wide variety of definitions for a fully uniform dispersion. The reader is referred to the article by Poux et al. [95] for a summary of classic definitions. Almost all the definitions agree that in a full dispersion the inclusions are arranged in a regular repeating pattern, such as a lattice structure [127]. Based on this intuitive and visual understanding of a full dispersion, Figure 17a. shows the fully uniform state of dispersion for 137 particles with diameter of 4 length-units in a square domain with side length of 100 length-units.

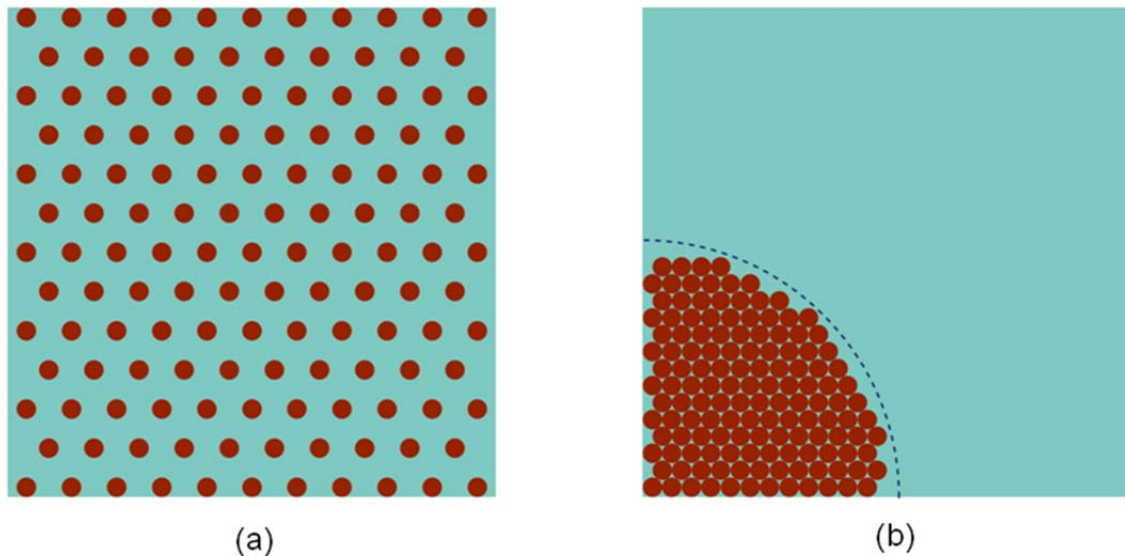


Figure 17. (a) Fully uniform and (b) fully non-uniform states of dispersion for 137 circular particles with the diameter of 4 length-units in a domain with the side length of 100 length-units. In a fully uniform dispersion, the statistical distribution of the values of particles' nearest neighbors has the maximum mean and the minimum standard deviation. In a fully non-uniform dispersion, the distribution has the minimum mean and the minimum standard deviation. This forms a single close-pack agglomeration, which should be located as far as possible from the domain's centroid.

A precise mathematical definition of full dispersion in agreement with Figure 17a. can be made based on nearest neighbor distances. In a full state of dispersion the statistical distribution of the distances between all inclusions and their corresponding nearest neighbors have the maximum mean and minimum standard deviation [100]. In a fully non-uniform state of dispersion, the statistical distribution of nearest neighbors have the minimum mean and minimum standard deviation, and the inclusions form a close-pack agglomeration located as far as possible from the domain centroid (Figure 17b). The latter condition is intuitively perceivable; if a domain consists of only one inclusion, it will be at the center of the domain in the best state of dispersion, and at the furthest corner in the worst state.

When inclusions have a distribution of sizes, the fully uniform state requires, the additional condition that the inclusions of each size (or size range) should be distributed in the domain as regularly as possible.

3.3.2. *Definition and formulation of a dispersion parameter*

Suppose there are a number of particles in a medium, like water. The more agglomerated these particles are, the more work is required to disagglomerate them and arrange them in the fully uniform state of dispersion (Figure 17a). Based on this idea, we define the concept of *dispersive work* as the minimum amount of work per volume (or area) of domain required to move inclusions so that they form a fully uniform dispersion.

Dispersion as a quantity should have a maximum value (e.g. 1) for the case in which particles already form a fully uniform pattern and no dispersive work is required to rearrange them (Figure 17a). It should also have a minimum value (e.g. 0) when the domain is in a state of fully non-uniform dispersion (Figure 17b). Dispersion, D^t , is then formulated as

$$D^t = 1 - \frac{w^a}{w^{nu}}, \quad (5)$$

where w^a and w^{nu} are the dispersive works related to the actual and fully non-uniform states of dispersion, respectively. Additionally,

$$w^j = \sum_{i=1}^n w_i^j, \quad (6)$$

where n is the number of inclusions in the domain and j is either a or nu . The work to move a particle in the domain is a function of the distance the particle must be moved and the magnitude of the force necessary to move it. As distance (i.e. the magnitude of displacement) and force can be defined in 1, 2, or 3 dimensions, the novel method for quantifying dispersion proposed in this paper is applicable in 1, 2, or 3 dimensions.

3.3.3. Calculation of dispersive work

There is a challenge to the direct calculation of dispersive work: if there are n inclusions in a domain of interest, there are $n!$ possible ways to move them to another predetermined state of dispersion. These alternatives should be compared to find the one in which the sum of distances moved by the inclusions is minimum. Unfortunately, $n!$ is normally a very large number even when n is as small as 10, which makes the computational load for the brute force measurement of dispersive work prohibitive. The problem of finding the dispersive work is a linear problem in the field of combinatorial optimization and is referred to as the bipartite weighted matching problem or the assignment problem [128, 129]. If the distances between each particle at the initial position i and possible final position k ($i, j, k \in [1 \dots n]$) are placed in matrix d_{ik} , the forces necessary to move each particle from initial position k to final position j are placed in a matrix f_{kj} , then an additional matrix x_{ij} may be constructed subject to the constraints

$$\begin{aligned}
\sum_i x_{ij} &= 1 \quad \forall i \\
\sum_j x_{ij} &= 1 \quad \forall j \\
x_{ij} &\in \{0,1\} \quad \forall i, j
\end{aligned} \tag{7}$$

The minimum total work expended by all particles is found by minimizing the linear system $x_{ij} d_{ik} f_{kj}$ (where the indices sum according to Einstein notation) by modifying x_{ij} within the constraints listed in Eq. (7). It should be noted that $x_{ij} = 1$ if the inclusion in location i is chosen to be moved to the location j , and $x_{ij} = 0$ otherwise. The inner product of $d_{ik} f_{kj}$ results in a matrix W_{ij} , which is the work performed in moving a particle from initial position i to final position j .

There are several algorithms available to solve the linear problem described above, including the Hungarian method developed in 1955 by Kuhn [130] and later optimized by Munkres [131]. The Hungarian method solves the assignment problem in $O(|n|^3)$ arithmetic operations, which makes it substantially faster than the brute force approach.

3.4. Discussion: The novel method of dispersion quantification vs. the previously developed methods

In this section, the methods reviewed earlier and their possible issues, which can be avoided when using the proposed work method, will be investigated. Artificially generated images of inclusion distributions will be used to support the discussion. Image generation was used instead of actual specimen images to produce patterns with distribution uniformities that are distinctly and intuitively different.

The RPS method is easy to use but its applicability is limited due to two major shortcomings. First, the RPS method does not take the effect of volume fraction of material constituents into consideration. For example, the method yields the same value for the case of CNT reinforced ceramics in Figure 16b. and Figure 16c. RPS may only provide an estimation of geometry-dependent clustering for certain feature concentrations. There have been few limited studies on the role of both RPS and constituent volume fractions on homogeneity and target properties of composites [132, 133], but to the knowledge of the authors these two measurement concepts have not been integrated to develop a quantification method for dispersion. The second issue is that the RPS method essentially defines dispersion based on the size of the inclusions and host particles and not their locations. In other words, the agglomeration of inclusions or host particles does not change the RPS ratio. As a result the method may only be useful when the host particles are uniformly distributed and the inclusions are uniformly distributed between the host particles.

The methods based on the contact area between features have limited application as well since the interface of separation cannot always be a measure of dispersion. For example, in both Figure 17a. and Figure 17b. the interface of separation is zero, but the states of dispersion are fully uniform and fully non-uniform respectively. Therefore, the method may only be useful when the concentration of features is high and their geometry is such that contact is possible¹.

¹ Two rigid spherical (or circular in 2-D) particles will always have a contact area of zero.

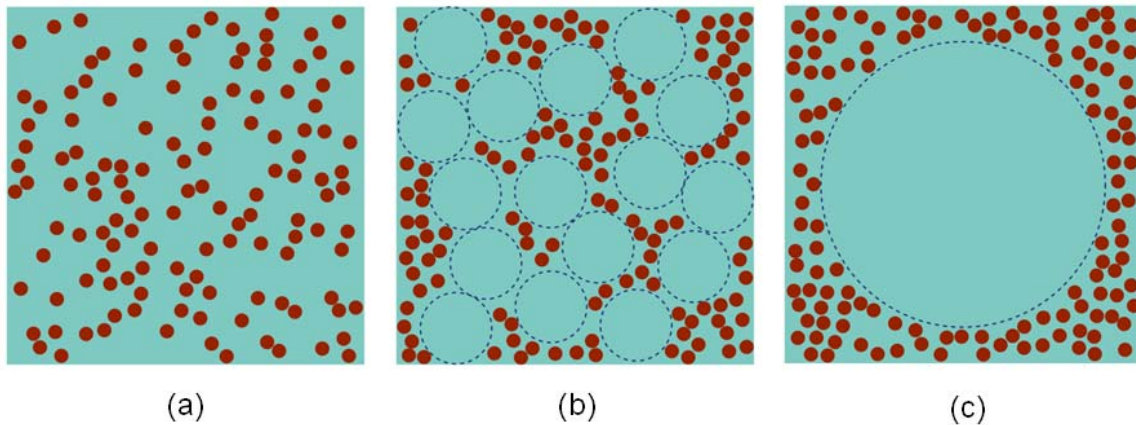


Figure 18. Different distributions of 137 small particles in a square two-dimensional domain. The diameter of the particles and the side length of the domain are 4 and 100 units respectively. In (a) the particles are randomly distributed in the domain. In (b) the particles are distributed randomly between some larger particles of different phase. The presence of the larger particles have degenerated the dispersion quality of the smaller particles. (c) is an example of poor dispersion resulting from excessive geometry-dependent inhomogeneity.

In quadrat methods, different choices of quadrat size can result in different judgments about dispersion quality. For example, the images in Figure 18 present three different states of dispersion for the small disks and domains of Figure 17. In Figure 18a. the disks are randomly distributed, while in Figure 18b. the distribution is degenerated by the presence of 16 larger circular regions representing the host material (geometry-dependent clustering). Figure 18c. shows an extreme situation in which the host material is in the form of a large circular region (with the same area as the sum of the areas of the 16 circular regions in the second case) and that the small disks are randomly distributed in the remaining area. The quadrat method was used for each of these images to quantify dispersion: a square slide (quadrat) scanned the domain surface with small steps (the step size used here was 1 length-unit in both x and y directions). In each step the concentration of small disks within the element (i.e. the area fraction of the disks within the slide area) was calculated, and the standard deviation of the concentrations calculated in all the steps was obtained as a measure of dispersion. Figure 19 presents the values of

this measure for element side length ranging from 1 to 100 length-units, and clearly shows the sensitivity of the method to element size. For example, although the particle distribution visually appears more uniform in case (b) compared to case (c), when the element is very small (side length between 1 and 9), the standard deviation of the better dispersion can be the same or even higher than the worst dispersion. In addition, while the method may be able to qualitatively rank the dispersion of the three sample systems when the element size is larger (between 10 and 50), it cannot quantitatively rank the systems. For example, according to this method, when the element size is 10, cases (b) and (c) are judged to have similar dispersion, but if the element size is 20, cases (a) and (b) are expected to have closer dispersion. Therefore, the method described does not converge on a unique, quantitative measure of dispersion as mesh size is either increased or decreased.

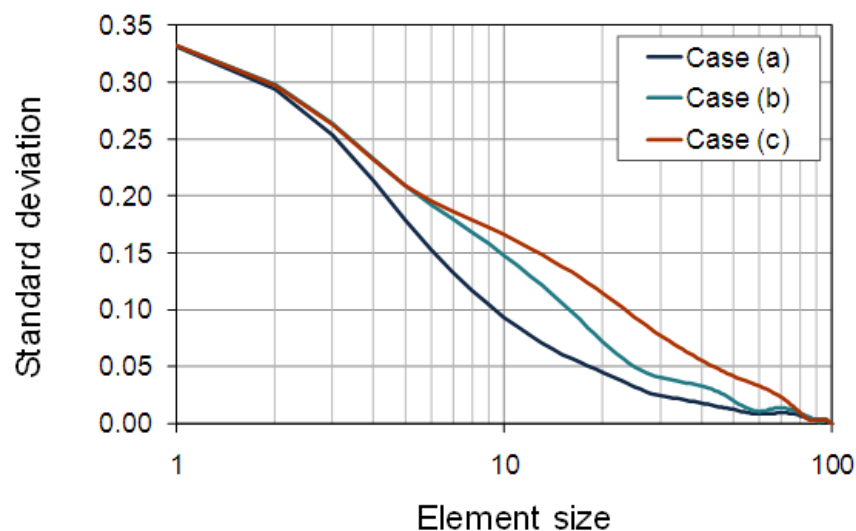


Figure 19. Results from the concentration standard deviation method [95] (a quadrat method) used for quantifying the dispersion of the three domains in Figure 18. The graph shows the standard deviation values when different element sizes ranging from 1 to 100 were used. It can be clearly seen that the results are sensitive to element size and choosing different element sizes can lead to different judgments about dispersion quality.

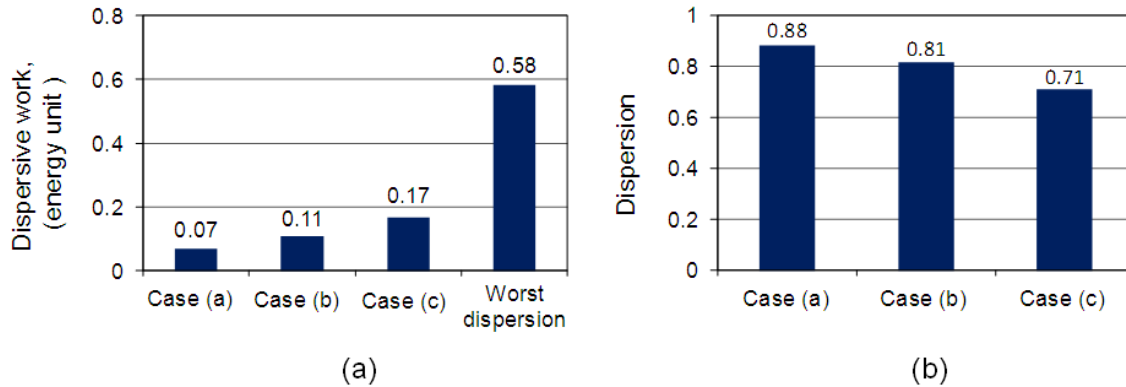


Figure 20. (a) The values of dispersive work calculated for the three cases of Figure 18 and for their corresponding ideally non-uniform dispersion (worst dispersion) shown in Figure 17b. (b) The values of dispersion for the three cases. It should be noted that the values of dispersion for the fully uniform and fully non-uniform states of dispersion are 1 and 0 respectively.

The majority of the methods based on microstructural parameters usually consist of more than one parameter (e.g. R , R' , etc.) for dispersion quantification. Multi-parameter models provide more information about the spatial distribution of features and are particularly useful when comparing different shapes and patterns of agglomerations. On the other hand, a single-parameter quantification model is attractive in the sense that the parameter value presents a bias-free judgment on the quality of dispersion. When comparing different domains to make a decision about which has an overall better quality of dispersion, the decision is prone to subjectivity when multi-parameter models are used.

The stereology method of Luo and Koo [117] is based on the assumption that if all the inclusion particles are distributed at an equal free-path distance, the dispersion is perfect. This assumption does not always hold; for example, if the domain consists of only one agglomeration in which particles are distributed at an equal free-path distance (like in Figure 17b.), the dispersion is judged as perfect. The other downside to the method is that there is not a clear criterion for selecting a value for r , and the selection of the log-normal distribution function may not be appropriate for every state of dispersion. For example, the distribution of free-path distances in Figure 17b. may be more appropriately fit by a bimodal distribution function.

The method of Bakshi et al. [118] is formulated for the case of CNT dispersion. The clustering parameter CP is based on the distances between CNT centroids which are less than or equal to five times the CNT diameter. It is not known yet if this parameter is appropriate for composites with inclusions of different size, geometry, or concentration. The constant five was chosen by Bakshi et al. based on experience and the geometry of CNTs under investigation.

The work method proposed in this paper has been devised in light of the discussed issues to be used as a robust tool in dispersion quantification and produce a dispersion score between the extremes of uniformity and agglomeration. A computer program implementing the Hungarian method was developed and used to measure the dispersive work for each of the examples in Figure 18; the force matrix was assumed to be

$f_{ij} = 1, \forall i, j$. The results, presented in Figure 20a, are as expected: intuitively better dispersions (such as Figure 18a.) require less work to achieve full dispersion. Using the values of dispersive work and Eq. (5), the dispersion value, d , was calculated and is presented in Figure 20b. It can be seen that the case of random distribution has the best dispersion (0.88) amongst the three cases. As mentioned earlier, the values of dispersion for the fully uniform and fully non-uniform states of dispersion are 1 and 0 respectively.

3.5. Implementation example for composites

In this section it is shown how the proposed method can be used to quantify the dispersion of inclusions in composites. The material used here is Al coating reinforced with CNTs. Figs. Figure 21a and Figure 21b show two SEM micrographs of the material from the work of Bakshi et. al [118]. It was found reasonable to assume that the CNTs are single-size since the size variation of the filaments is not very large; this assumption results in a remarkable reduction in computational effort. Each filament was regarded as a disk located at the filament's centroid (Figs. Figure 21c and Figure 21d), and the fully uniform and fully non-uniform dispersions were generated for each case (Figs. Figure 21e and Figure 21f). For each case, the area of the disks required to generate the worst dispersion was obtained using the filament area fractions in each SEM image reported by Bakshi et al. The dispersive work and dispersion were then calculated in the same way as for the model examples of Figure 18. The dispersion of Figs. Figure 21a and Figure 21b are 0.91 and 0.84 respectively, which indicates that the first RVE has a better dispersion than the second one. Although the difference in the quality of dispersion could be discerned by visual observation, the work method demonstrated this difference quantitatively.

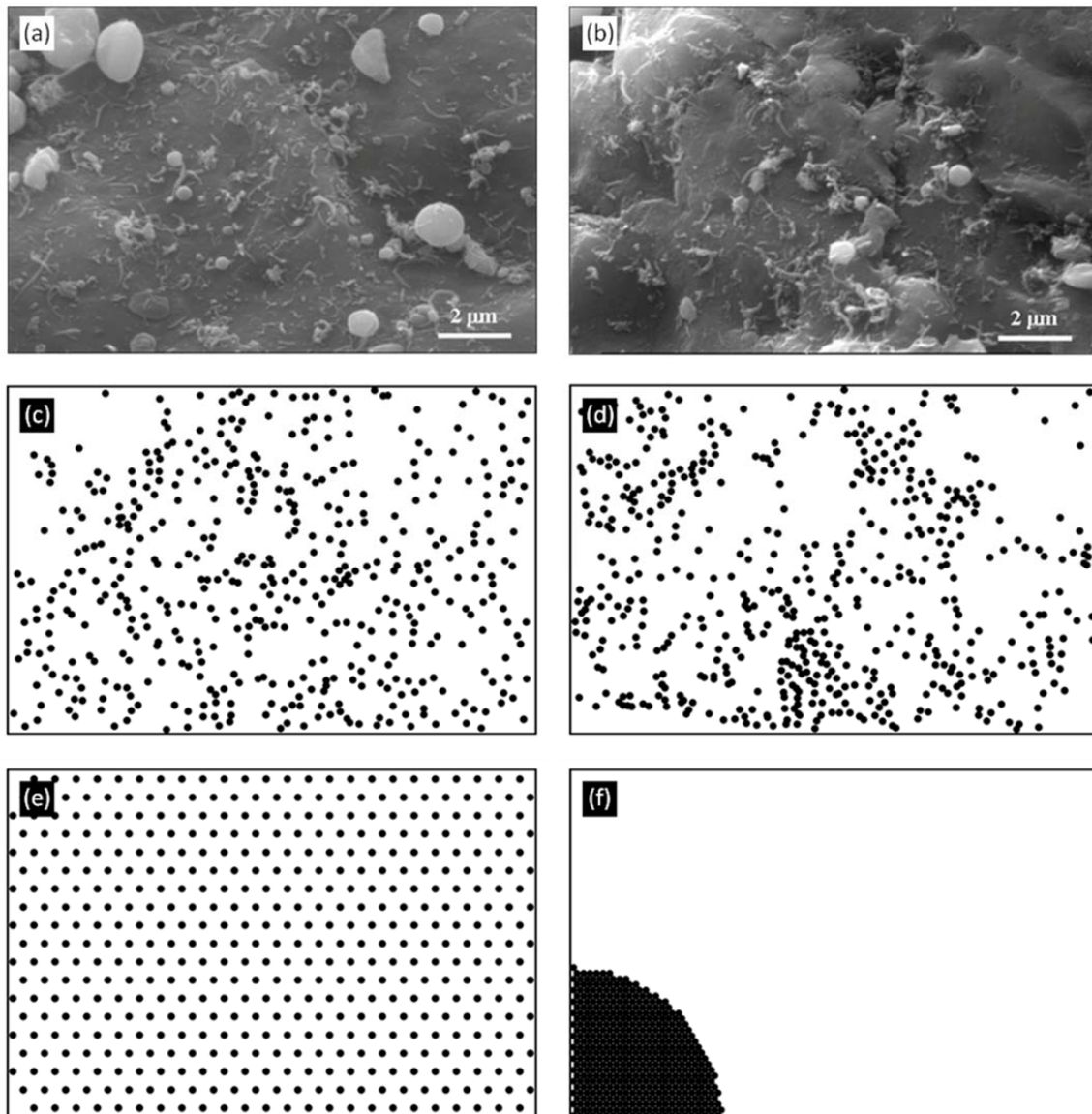


Figure 21. (a,b) Two images of CNT reinforced Al coating (From. [118]). The images were converted to simplified representations (c) and (d) by replacing each filament with a disk located at the filament's centroid. (e) and (f) are the fully uniform and fully non-uniform dispersions corresponding to (c).

3.6. Concluding remarks

In this chapter, several methods of quantifying the dispersion of inclusions in a composite were reviewed and their applications, advantages, and possible shortcomings were discussed. Some of the downsides to existing methods are rooted in the ambiguities related to the concept of dispersion; for example, in some cases dispersion quality is regarded as closeness to randomness and in other cases as the variation of concentrations in sample volume/areas. The ambiguities are mainly due to the fact that different methods have been developed to serve different and specific applications. In this paper, distribution uniformity was examined from a general, thermodynamic basis. An intuitive, simple, and robust measure of dispersion was presented based on the minimum amount of work necessary to create a fully uniform state of dispersion from an initial, partial state of dispersion. It was shown that this dispersion measure is readily implementable and may be used to characterize dispersion in a quantitative, bias-free manner.

4. IMPLEMENTATION OF THE NOVEL DISPERSION QUANTIFICATION METHOD USING CONTINUUM THEORY

A novel and robust method for quantifying the dispersion of discrete inclusions in a composite was introduced in the previous chapter. The method quantifies dispersion based on the minimum amount of work required to move the inclusions such that they are in a fully uniform state. As the new dispersion quantification method is founded on a physical thermodynamic framework, it is distinct from previously developed methods that have strictly a mathematical and statistical basis. However, implementation of the new method is computationally expensive for domains consisting of many inclusions. In this chapter, the novel dispersion quantification method is recast in terms of continuum mechanics and thermodynamics in order to make use of diffusion models, which makes possible the quantification of dispersion considering domains with many inclusions. To demonstrate the practicality of the new approach, the dispersion of carbon nanofibers in an aqueous solution is analyzed. It should be mentioned that the idea of using continuum mechanics and thermodynamics for implementing the work methods was produced by Zachary Grasley, who developed the derivations and formulations presented in this chapter.

4.1. Introduction

The question of how to effectively quantify the level of dispersion of rigid bodies (also in this work referred to as inclusions or features) in a continuous medium has been studied immensely over the last several decades. The interest in nanoparticle composites has driven an even greater interest in dispersion quantification since the composite constitutive properties (e.g. mechanical [74] and electrical properties [134]) are strongly influenced by the level of particle dispersion.

The novel dispersion quantification method presented in the previous chapter introduced a novel method of dispersion quantification that was shown to avoid many of the

limitations intrinsic to alternative methods [135]. The method is based on calculating the minimum total distance inclusions should move to reach a state of fully uniform dispersion. It was shown that the distance can be calculated using combinatorial optimization and linear programming. However, these methods become computationally prohibitive when the number of inclusions is high (over a few thousand considering current computational power). With the increasing application of nanoparticles and nanofibers, it is increasingly likely that domains with many thousand inclusions will need to be analyzed. In addition, in some micrographs it is impossible to distinguish individual particles, rendering the new method difficult to implement.

The objective of this paper is to illustrate how the novel dispersion method may be utilized in conjunction with continuum diffusion models in order to quantify the dispersion of a system of many particles (i.e. when $n \rightarrow \infty$) or a system where individual particles are difficult to distinguish. In order to make clear the appropriate use of diffusion models, the novel method will first be recast in terms of continuum mechanics and thermodynamics.

4.2. Definitions

The terms critical to the quantification effort will be defined in this section. As indicated in the introduction, there are several definitions of dispersion in the literature, which has led to the development of entirely different characterization models. As per Yazdanbakhsh et al. [135], the term “Distribution uniformity” is defined as a holistic term to encompass both “Dispersion” and “Orientation” of composites. Dispersion is meant to quantify translational uniformity and deals with the location of inclusion centroids while orientation is concerned with rotational uniformity and is mainly used for filament inclusions when their orientation is of interest.

In order to quantify dispersion, it is advantageous to fix a comparative measure; as such, we will define the state of fully uniform dispersion. In this paper, we define fully uniform dispersion via a thermodynamic, “maximum entropy” approach. For example,

in a system of gas molecules within a closed container, entropy is maximized when the time-mean spatial position of each molecule (inclusion) is such that the mean spacing between the neighbor inclusions is maximized and the standard deviation of the spacing between the neighbor inclusions is minimized. Similarly, for a system of identical inclusions in a state of fully uniform dispersion, the spacing between the adjacent inclusions will be uniform and maximum. Therefore, according to the novel method, the level of dispersion of a system of discrete rigid inclusions of uniform size and shape distributed within a domain can be quantified based on the minimum amount of work necessary to move each individual inclusion to a position such that the spacing between the mass centroids of the inclusions is uniform and maximum. This work is referred to as “dispersive work”.

The normalized level of dispersion may be calculated according to

$$D^t = 1 - \frac{W^t}{W_{\max}^t}, \quad D^t \in [0, 1], \quad (8)$$

where W^t is the dispersive work for the domain of interest and W_{\max}^t is the work required to fully disperse the inclusions when they form the worst possible dispersion in the domain (i.e. a system with minimum possible entropy). For example, if the representative volume element (RVE) is a cube, the state with minimum possible entropy is such that all inclusions within the RVE are tightly packed into one corner of the cube². Based on the definition for dispersion given in (8), we find that for any system $0 \leq D^t \leq 1$ with 0 being the worst possible dispersion and 1 being fully dispersed. The normalization performed in (8) allows the calculation of a dispersion measure that is not biased by domain size or concentration of inclusions.

² The particles must be packed into the corner rather than the center of the RVE because greater total work is required to displace the particles from the corner

In an analogous fashion as for dispersion, the level of orientation of a system of discrete rigid bodies distributed within a domain can be quantified by the minimum amount of work necessary to rotate each individual inclusion such that the longest axis of all inclusions are aligned in the same direction.³ For inclusions with nominal aspect ratio of unity, orientation has no meaning.

4.3. Motion of inclusions

The problem of quantifying the work necessary to translate and rotate rigid bodies requires quantification of particle displacements and rotation angles, and is thus a kinematical problem. As shown in Figure 22, we can treat the body motion as a deformation from some initial state to some final state.

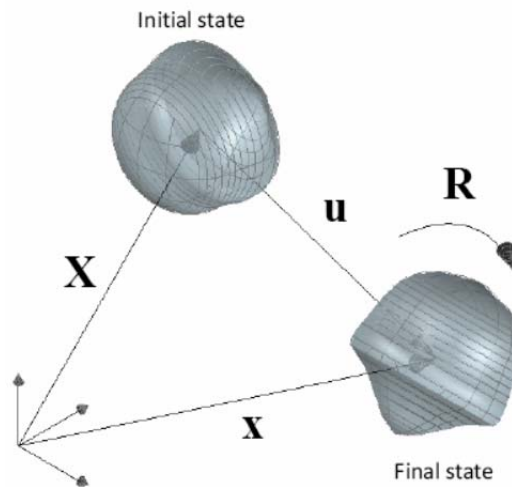


Figure 22. Rigid body translation and rotation of an inclusion.

The deformation $\mathbf{x} = \chi(\mathbf{X})$ is a mapping of a point in the body from an initial state to a final deformed state. If we let \mathbf{X} be the position of some point in the body in the initial state and \mathbf{x} be the position of the same point in the body in the final state, then

³ In domains with inclusions of high aspect ratios at high concentrations, full alignment may not be possible due to impingement. In such cases, complete uniform orientation may not be possible.

$$\mathbf{u} = \mathbf{x} - \mathbf{X} \quad (9)$$

is the displacement vector of the point in the body. The deformation gradient is defined as

$$\mathbf{F} = \frac{\partial \mathbf{x}}{\partial \mathbf{X}} = \nabla_{\mathbf{x}} \quad (10)$$

and can be decomposed as

$$\mathbf{F} = \mathbf{V}\mathbf{R} = \mathbf{R}\mathbf{U} \quad (11)$$

where \mathbf{V} is the left stretch tensor, \mathbf{U} is the right stretch tensor, and \mathbf{R} is the rigid rotation tensor. For the case of rigid body motion, the stretch tensors are equal to the identity tensor, \mathbf{I} , such that $\mathbf{F} = \mathbf{R}$. Therefore, $d\mathbf{x} = \mathbf{R}d\mathbf{X}$, which combined with (9) yields

$$\frac{\partial \mathbf{u}}{\partial \mathbf{X}} = \mathbf{R} - \mathbf{I} \quad (12)$$

Integration of (12) from a reference displacement (\mathbf{u}_0) and corresponding reference position (\mathbf{X}_0) results in

$$\mathbf{u}(\mathbf{X}) = \mathbf{u}_0 + \mathbf{R}(\mathbf{X} - \mathbf{X}_0) - (\mathbf{X} - \mathbf{X}_0) \quad (13)$$

which is the displacement of any point in the body as a function of the relation to the reference point. If the reference point is made to be the center of mass, then the displacement at the center of mass is simply $\mathbf{u} = \mathbf{u}_0$. The work performed in rigidly translating a body from the initial to final positions is

$$W_i^t = \mathbf{f}_i \cdot \mathbf{u}_i \quad (14)$$

where \mathbf{f}_i is the force vector applied to particle i in order to displace it, and \mathbf{u}_i is the displacement of particle i . The total translational work is the sum of the work performed in translating each particle such that

$$W^t = \sum_i \mathbf{f}_i \cdot \mathbf{u}_i \quad (15)$$

When orientation is of interest, the angle of rotation α_i of each particle i may be determined according to

$$\cos(\alpha_i) = \frac{1}{2}(\text{tr}(\mathbf{R}_i) - 1) \quad (16)$$

which is obtained by first orienting the reference bases such that the 3-direction is aligned with the axial vector of the rotation, then taking the trace of the rotation tensor. Since the trace operation is invariant, the expression in (16) holds for all bases. The work required to rotate each particle i is

$$W_i^r = \tau \alpha_i \quad (17)$$

where τ is the magnitude of the torque required to rotate the particle. Therefore, the total work of rotation, which is useful in quantifying degree of orientation of a system of discrete inclusions, is

$$W^r = \sum_i \tau_i \alpha_i \quad (18)$$

It should be mentioned that the novel approach can be used to perform tasks other than dispersion quantification, such as calculating the amount of energy required to put in a viscous media containing agglomerated inclusions in order to disagglomerate them and form a uniform dispersion. For example, if the domain in which the inclusions are located is a continuous fluid, then the force vector is quantifiable if one knows the

viscosity of the matrix; utilization of a realistic force vector means that the calculated dispersive work is directly proportional to the minimum amount of energy that must be input into the system (e.g. through sonication [136, 137]) to disperse the inclusions. In materials such as nanoparticulate composites where clumping is a problem due to strong van der Waal's forces (see e.g. [138]), the additional energy necessary to break the clumps could be accounted for by expressing the inter-feature attraction force \mathbf{f} as a nonlinear function of distance to neighboring inclusions. Finally, the additional energy necessary to be input into the system if the inclusions are compliant could easily be accounted for by modifying the above derivation to account for deformations where the stretch tensors $\mathbf{V} \neq \mathbf{I}$ and $\mathbf{U} \neq \mathbf{I}$.

4.4. Use of continuum theory to determine dispersion parameter

For the sake of brevity, in the remainder of the paper we will focus on the quantification of dispersion. In a domain with sparse, uniform inclusions, it is a simple matter to directly quantify the dispersive work. One may simply evaluate the initial positions of the inclusions, locate the nearest final position for each inclusion, and then calculate the distance each particle must move to quantify the work performed. However, in a system of many inclusions, such a process becomes tedious. It is not immediately obvious to which final position each inclusion should be moved in order to minimize the total work performed in moving the inclusions. If computational time were not an issue, one could simply calculate W' for every possible scenario ($n!$ total scenarios for n inclusions) and then take the minimum. Since the problem is in the class bipartite matching problems, one could also use a linear solving algorithm such as the Hungarian method [139] to reduce the computations to $O(n^3)$. However, as the number of inclusions in the system becomes large, even efficient algorithms such as the Hungarian method are too computationally expensive. One can reduce the size of the RVE, but only until the point where the RVE is still able to be considered “representative” of the domain as a whole. For situations that include geometry dependent clustering where the domain consists of

host particles surrounded by significantly smaller inclusions whose dispersion one wishes to quantify, the minimum size of the RVE is limited by the size of the host particles. As a result, even if the concentration of the inclusions is relatively low, there will still be a significant number of inclusions within the domain. An example of such a situation is the inclusion of carbon nanotubes in cement paste that consists of micrometer-sized host cement particles [137]. For such situations, an alternative means to calculate W^t is needed to quantify dispersion.

The computational challenges associated with quantifying dispersion of a domain of many inclusions can be handled by utilizing principles of continuum thermodynamics. When using the novel translational work minimization definition, the dispersion quantification problem can be viewed as analogous to the continuum diffusion problem. For example, consider a closed, vacuumed container. If a valve is opened such that a certain quantity of gas is released into one corner of the container, the gas will progressively diffuse throughout the container until the concentration field is uniform. Additionally, the gas will diffuse in such a way as to achieve the uniform, equilibrium condition with the least energy (work) expended as possible. In this way, the diffusing atoms or molecules are analogous to the inclusions in the domain of interest, and the initial condition in the diffusion problem is analogous to the initial, partially dispersed state.

When the diffusivity tensor \mathbf{D} does not vary with \mathbf{x} , the governing equation for the linear diffusion problem is the parabolic partial differential equation

$$\frac{\partial C(\mathbf{x}, t)}{\partial t} = \mathbf{D} \cdot \nabla^2 C(\mathbf{x}, t) \quad (19)$$

where \mathbf{x} is the spatial position in the domain, and t is the elapsed time. Eq. (19) expresses that the change in concentration with time of a certain point in a continuum is based on the difference between the concentration at the point and that of the average

value of the local surroundings (the Laplacian). Basing mass transport on the difference between the value at a point and the average value of the local surroundings results in the most efficient “flattening” of the concentration field [140], and thus is equivalent to minimizing the total distance traveled by inclusions in a discrete system.

For the dispersion problem, we consider a domain Ω that has Neumann boundary conditions such that the boundary flux is zero. Therefore, we can write

$$\begin{aligned} (\mathbf{D}\nabla C(\mathbf{x},t)) \cdot \mathbf{n} &= 0 & \forall \mathbf{x} \in \partial\Omega, t > 0, \\ C(\mathbf{x},t) &= C_i(\mathbf{x}) & \forall \mathbf{x} \in \Omega, t = 0 \end{aligned} \quad (20)$$

for boundary and initial conditions, where $C_i(\mathbf{x})$ is the initial concentration profile defined by the initial distribution of inclusions for which one wishes to quantify the dispersion and \mathbf{n} is the outward unit normal from the surface $\partial\Omega$. From (19) and (20), one can solve for the concentration field $C(\mathbf{x},t)$. The mass flux vector may be defined according to the relationship

$$\mathbf{j}(\mathbf{x},t) = \mathbf{D}\nabla C(\mathbf{x},t) = \rho(\mathbf{x},t)\mathbf{v}(\mathbf{x},t), \quad (21)$$

where ρ is the partial density of the inclusions and \mathbf{v} is the velocity of the dispersed phase. The velocity is defined as

$$\mathbf{v}(\mathbf{x},t) = \frac{d\mathbf{u}(\mathbf{x},t)}{dt}, \quad (22)$$

where \mathbf{u} is displacement of a particle at point \mathbf{x} . The displacement of a particle located at position \mathbf{x} over a time t may therefore be determined according to

$$\mathbf{u}(\mathbf{x},t) = \int_0^t \mathbf{v}(\mathbf{x},\tau) d\tau = \int_0^t \frac{1}{\rho(\mathbf{x},\tau)} \mathbf{j}(\mathbf{x},\tau) d\tau = \int_0^t \frac{\mathbf{D} \cdot \nabla C(\mathbf{x},\tau)}{\rho(\mathbf{x},\tau)} d\tau. \quad (23)$$

Using (23), the work necessary to move each particle may be determined according to (14). The total translational work performed by all particles may be determined according to

$$W^t(t) = \int_V \mathbf{f}(\mathbf{x}, t) \cdot \mathbf{u}(\mathbf{x}, t) dv \quad (24)$$

When $t \rightarrow \infty$, W^t is the total translational work necessary to move all inclusions from an initially undispersed state to a fully dispersed state, and is thus a measure of the level of dispersion of the inclusions in the initial configuration. The higher $W^t(t \rightarrow \infty)$, the poorer the initial dispersion, which may be quantified using (8).

4.5. Discrete system

Continuum theory is commonly used to describe physical systems that are actually discrete in nature. For example, diffusion of atoms or molecules is often modeled using continuum theory even though both atoms and molecules have a finite volume. The fact that a continuum is comprised of infinitesimally small particles (i.e. “points”) is not generally seen as problematic for representing discrete systems as long as the discrete particles are substantially smaller than the RVE and $n \rightarrow \infty$. Unfortunately, one cannot be assured these requirements will be met in dispersion studies. As $n \rightarrow 0$ or particle sizes approach that of the RVE, the continuum approximation leads to significant error since full dispersion is never completely achieved ($C(\mathbf{x}, t)$ asymptotically approaches $\langle C(\mathbf{x}, t) \rangle$ as $t \rightarrow \infty$). The reason $C(\mathbf{x}, t)$ asymptotically approaches the spatially average concentration $\langle C(\mathbf{x}, t) \rangle$ and will never actually reach the average is due to the fact that the inclusions in a continuum have no dimension and may therefore be further dispersed ad infinitum. In the real, discrete system, the inclusions have finite size such that at later times, continued dispersion only occurs by destruction of the discrete inclusions themselves and motion of progressively smaller and smaller chunks of the destroyed particles.

In order to account for the difference outlined above regarding continuum and discrete systems, it is necessary to quantify the work spent destroying inclusions. For example, consider the 1-D case. If $C^*(\mathbf{x}, t)$ is the normalized concentration of a discrete particle, an example fully dispersed domain is shown in Figure 23; any further dispersion of inclusions shown in Figure 23 would entail destruction of the inclusions. If we allow the dispersion (destruction) of inclusions shown in Figure 23 to proceed until a discrete time t_{large} , the work spent in destroying the inclusions (i.e. displacement of the destroyed particle chunks) would be $W^{t*}(t_{\text{large}})$. As illustrated in Figure 24, the work performed in dispersing discrete inclusions from a state of partial dispersion to the fully dispersed state (dispersive work) may be quantified according to

$$W^t = W^t(t_{\text{large}}) - W^{t*}(t_{\text{large}}), \quad (25)$$

which converges to the exact solution as $t_{\text{large}} \rightarrow \infty$. The work performed in destroying inclusions must also be considered when quantifying the dispersive work for the worst possible scenario for a given system. Therefore, the degree of dispersion in a discrete system can be determined using continuum theory according to

$$D^t = 1 - \frac{W^t(t_{\text{large}}) - W^{t*}(t_{\text{large}})}{W_{\text{max}}^t(t_{\text{large}}) - W^{t*}(t_{\text{large}})}, \quad D^t \in [0,1] \quad (26)$$

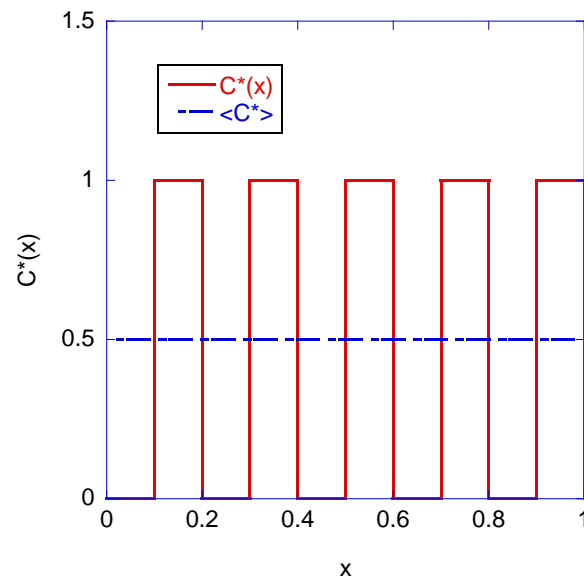


Figure 23. Fully dispersed 1-D system of inclusions with discrete width of 0.1.

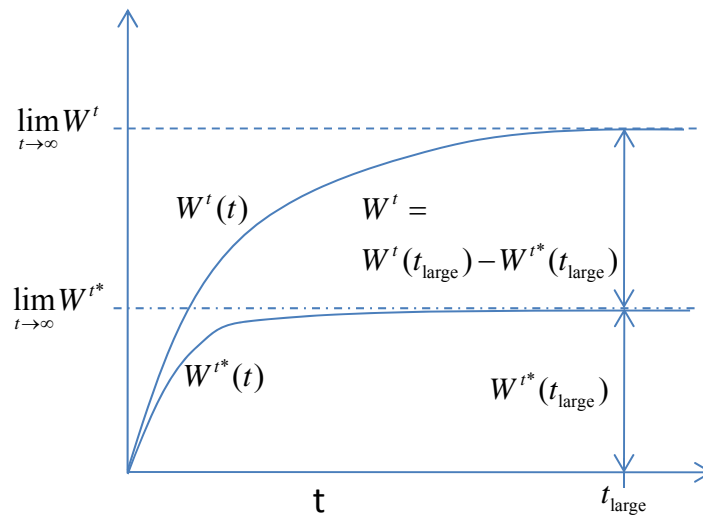


Figure 24. Methodology for quantifying W^t by subtracting the work performed in destroying inclusions in the discrete system.

4.6. Example applications

4.6.1. Method validation

In order to demonstrate the utility of the definition of dispersion and analogy to continuum diffusion modeling presented in this paper, a multi-dimensional finite difference code was written to determine dispersive work by solving (19) subject to the boundary and initial condition in (20). The code was written according the ADI method of Douglas and Gunn [141-143] for 1, 2, and 3 spatial dimensions; the Douglas and Gunn method is well described by [144], and is unconditionally stable.

Consider the 2-D initial discrete dispersions shown in Figure 25. Figure 25a is a random dispersion created with a random number generator, Figure 25b is a random dispersion encompassing 16 circular regions that have degenerated the dispersion (dashed lines), and Figure 25c is a random dispersion encompassing one large circular region that has degenerated the dispersion (dashed line). Each domain contains the same number of circular inclusions (137) with diameter of 4 units, while the dimensions of the domains in each case are 100 x 100 units. In order to evaluate the continuum modeling approach to calculating dispersion, the domains in Figure 25 were discretized in 2-D with varying levels of mesh fineness, as indicated in Figure 26. For each mesh, the finite difference approach was implemented by placing the nodes at the centroid of the appropriate elements. The total distance traveled by all inclusions in the system was calculated for the initial dispersion, the worst case dispersion, and for the destruction of a single particle (as shown in Figure 27) such that (26) could be used to calculate D^t . The calculated D^t for each mesh fineness for each domain in Figure 25 is plotted in Figure 28, which illustrates the convergence of the calculated D^t .

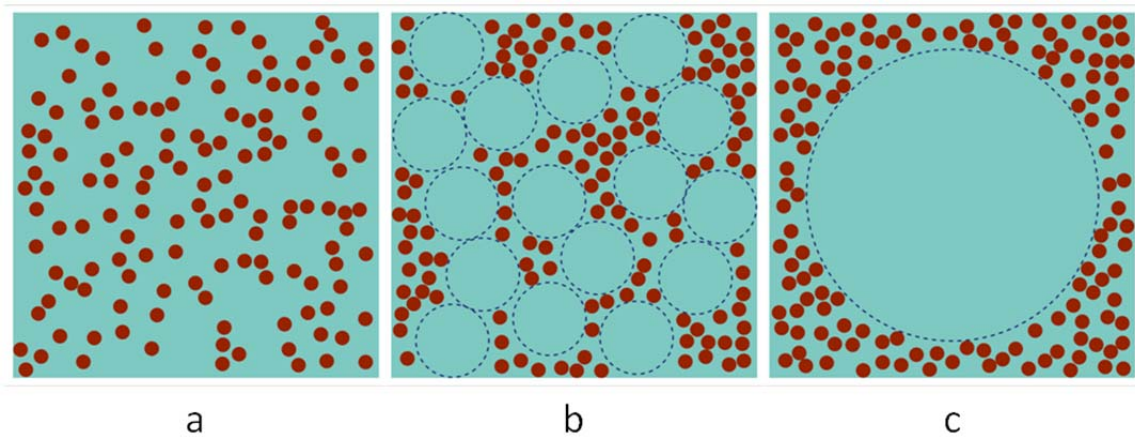


Figure 25. (Same as Figure 18) Three different example dispersions consisting of an equal number of small circular inclusions in equally sized domains.

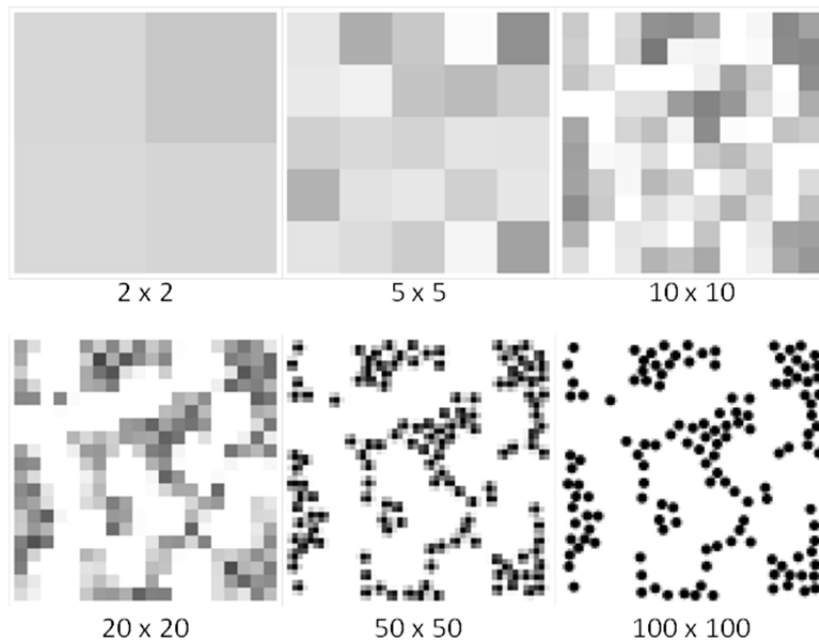


Figure 26. Meshes of varying fineness of the initial dispersion shown in Figure 25b, where concentration is shown in grayscale with darker indicating higher concentration.

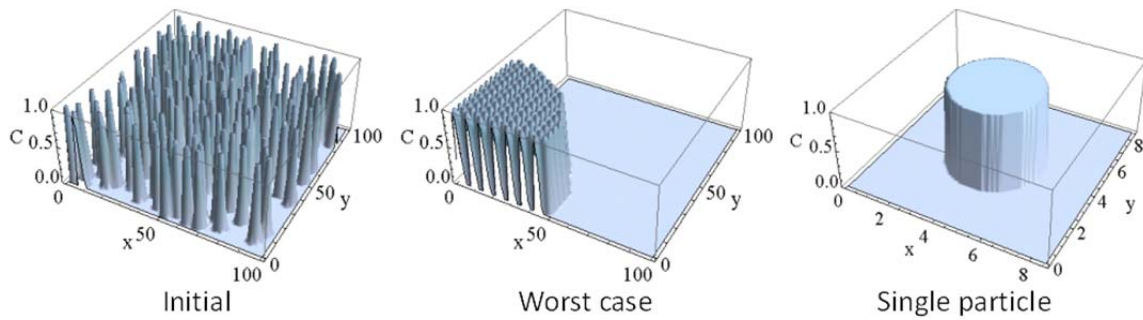


Figure 27. Meshes (100 x 100 elements) of the initial, worst case, and single particle cases for the domain shown in Figure 25a. The spatial dimensions of the domain for the single particle case are determined by the ratio of the number of disks to the domain area (i.e. the concentration of inclusions).

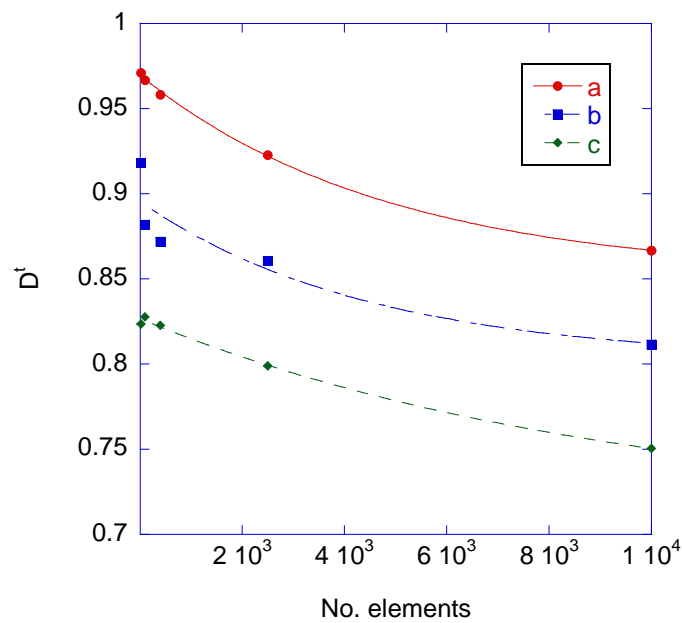


Figure 28. Convergence of D^I with increasing mesh fineness for the three initial dispersions illustrated in Figure 25.

To evaluate the validity of using the continuum approach, the dispersion of each image in Figure 25 was also calculated by treating each particle as discrete. The problem of finding the dispersive work of discrete inclusions is a linear problem in the field of

combinatorial optimization and is referred to as the bipartite weighted matching problem or simply the assignment problem [128, 129]. If the distances between each particle at the initial position i and possible final position k ($i, j, k \in [1 \dots n]$) are placed in matrix d_{ik} , the forces necessary to move each particle from initial position i to final position j are placed in f_{ij} , then an additional matrix y_{ij} may be constructed subject to the constraints

$$\begin{aligned} \sum_i y_{ij} &= 1 \quad \forall i, \\ \sum_j y_{ij} &= 1 \quad \forall j, \\ y_{ij} &\in \{0,1\} \quad \forall i, j. \end{aligned} \tag{27}$$

The minimum total distance traveled by all inclusions is found by minimizing the linear system $y_{ij}d_{ik}f_{kj}$ by modifying y_{ij} within the constraints listed in (7). It should be noted that $y_{ij} = 1$ if the inclusion in location i is chosen to be moved to the location j , and $y_{ij} = 0$ otherwise. The inner product $d_{ik}f_{kj}$ yields the work W_{ij} to move each particle from position i to final position j . Minimizing the linear system using the Hungarian algorithm [131, 139] one finds that for the three cases shown in Figure 25: **a**: $D^t = 0.88$; **b**: $D^t = 0.81$; and **c**: $D^t = 0.71$, where the relative ranking agrees with intuition.

Close inspection of Figure 28 shows that the calculated D^t using continuum modeling and finite difference for cases **a** and **b** converge closely to the values calculated for the discrete system as the mesh fineness increases. However, convergence of case **c** is slower (requiring finer mesh), which is attributed to the sharpness of the initial concentration gradient caused by the presence of the large circular region in the center of the domain [80].

As the mesh becomes coarser, the calculated D^t increases; this trend occurs because coarsening the mesh “flattens” the peaks in the initial concentration profile, which

reduces total flux from one element to another and thus the total distance traveled by all inclusions. Since the effect is more pronounced with respect to the initial dispersed condition than the worst case, D^t will always increase with mesh coarseness. The finite difference model for calculating D^t converges to the exact solution as the number of elements approaches infinity, the time step approaches zero, and the maximum time approaches infinity.

4.6.2. *Carbon nanofibers dispersed in aqueous solution*

In order to demonstrate the practicality of the novel dispersion quantification method presented in this paper, three micrographs of aqueous dispersions of carbon nanofibers with a broad range of visually apparent dispersion quality were selected for analysis (Figure 29). Each micrograph contains a large number of nanofibers, and each individual nanofiber is difficult to distinguish. To further illustrate the ability of available numerical techniques to be utilized to solve the dispersion analysis problem, commercially available finite element software was implemented in the analysis. The images were discretized (100 x 120 quadrilateral elements), and the average concentration of nanofibers in each element was determined using image analysis. Average nodal concentrations were determined through averaging of the concentrations of the nearest neighbor elements, and were assigned as an initial condition. The mass diffusion problem was solved utilizing 500 time steps for the actual image, the worst case for each image, and for the single particle destruction. The total distance (and thus total work) for each case was determined from the fluxes of each element, and the dispersion subsequently determined using (26). The calculated dispersion for the image with the worst visually apparent dispersion was 0.44, the calculated dispersion for the image with the average visually apparent dispersion was 0.62, and the calculated dispersion for the image with the good visually apparent dispersion was 0.85. Thus, the calculated dispersions agree well with intuition based on visual observation.

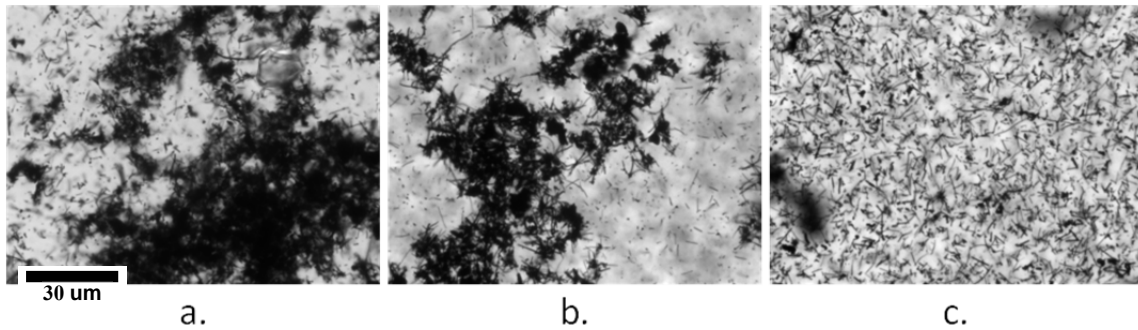


Figure 29. Micrographs ($215 \times 270 \mu\text{m}$) showing visually apparent a.) poor, b.) average, and c.) good aqueous dispersions of carbon nanofibers. Using the methodology described in this paper in conjunction with commercially available finite element software, the calculated dispersion qualities for the images are: a.) 0.44, b.) 0.62, and c.) 0.85.

4.7. Conclusions

The novel method for quantifying distribution uniformity of discrete inclusions in a domain is based on thermodynamic principles and avoids some of the inherent limitations of previously described methods for quantifying distribution uniformity described in the literature. In the new method, distribution uniformity is decomposed into translational work (dispersive work) and rotational work (orientational work). The use of continuum kinematics to describe the motion of the individual inclusions conveys the extensibility of the novel approach, which could easily be modified to account for any additional work required for dispersing compliant inclusions.

The calculation of dispersion was shown to be implementable using continuum theory for systems of many inclusions. The calculated dispersion for example systems showed that the results from the continuum approach implemented using a finite difference discretization converged to the solution obtained by tracking the translation of each discrete particle. The calculated dispersions of three example micrographs of carbon nanofibers dispersed in an aqueous solution demonstrated that the calculated dispersions using the novel technique discussed in this paper agree well with visual observation and intuition. Therefore, the method of quantifying dispersion presented in this work can be

implemented directly on systems of many inclusions, and is applicable to many fields of study ranging from ecology to materials science.

5. THE THEORETICAL MAXIMUM ACHIEVABLE DISPERSION OF NANOINCLUSIONS IN CEMENT PASTE

A major challenge of successfully incorporating nanometric inclusions (nanoinclusions), such as CNF/Ts, within cement paste is achieving a uniform distribution of the nanoinclusions, even if they are fully disagglomerated. Cement particles typically have a larger diameter than the average spacing between nanoinclusions when the nanoinclusions are fully dispersed, which means that the presence of cement particles degrades the theoretical maximum achievable dispersion of the nanoinclusions. To determine the significance of this effect, the novel thermodynamic-based dispersion quantification method presented in section 3 and section 4 was implemented to calculate the theoretical maximum achievable dispersion of nanoinclusions in cement paste. Three-dimensional simulations were performed for cement pastes with common values of water to cement ratio, nanoinclusion to cement ratio, and cement fineness. The results show that for cementitious nanocomposites simulated in this study, degradation of the maximum theoretical achievable dispersion of nanoinclusions due to the presence of cement particles is negligible as long as the cement particles are not agglomerated.

5.1. Introduction

Modification of cementitious materials at the nm length scale by addition of nanoinclusions (i.e. discrete particles with a characteristic size in the nm range) is a growing trend in cement and concrete research [145]. The incorporation of silica fume in concrete is probably the best example of the widespread use of nanoinclusions in the concrete construction industry [146]. In the past decade, the use of carbon nanotubes (CNTs) in cementitious materials has been studied by many investigators [7, 16-20, 83, 147, 148]. These filaments have extraordinary mechanical properties [7, 83] and their prices are decreasing rapidly [149]. CNTs are usually very difficult to disperse in an aqueous solution due to their low mass and strong van der Waal's attraction to each other, which often induces clumping. Despite the challenge of initiating and stabilizing

a well dispersed system of CNTs in the mix water of cementitious materials, it is expected that eventually a method will be developed to achieve this aim. Approaches may include surface modification of the filaments or using strong surfactants that do not negatively affect cement hydration. Unfortunately, even if nanoinclusions such as CNTs are able to be prevented from clumping and are well dispersed in the mix water, another problem known as geometry dependent clustering [56] would still prevent their uniform dispersion in cement paste. As schematically illustrated in Figure 30a, geometry-dependent clustering occurs when the host particles (e.g. cement grains) in a composite are much larger than the spacing between inclusions (e.g. CNTs). The presence of the large host particles degrades the maximum achievable dispersion of the inclusions by creating large contiguous volumes that are inaccessible to the inclusions. As an example, consider a cement paste with the mass ratios of $w/c = 0.35$ and $CNT/c = 0.005$. If the CNTs have a diameter of 10 nm and length of 1 μm the spacing between adjacent CNTs will be approximately 440 nm if they are uniformly dispersed [7]. This is much smaller than the average size of common portland cement grains (approximately 20 μm). Moreover, our laser diffraction analyses show that 95.5% of a typical cement volume is occupied by particles larger than 20 μm (Figure 30b). This means that when fine nanoinclusions such as CNTs are used, almost all of the volume of typical cement induces geometry dependent clustering of such nanoinclusions. Furthermore, in practice cement particles agglomerate before and during the production of paste. The size of cement clumps can be hundreds of micrometers, which causes increased geometry-dependent clustering.

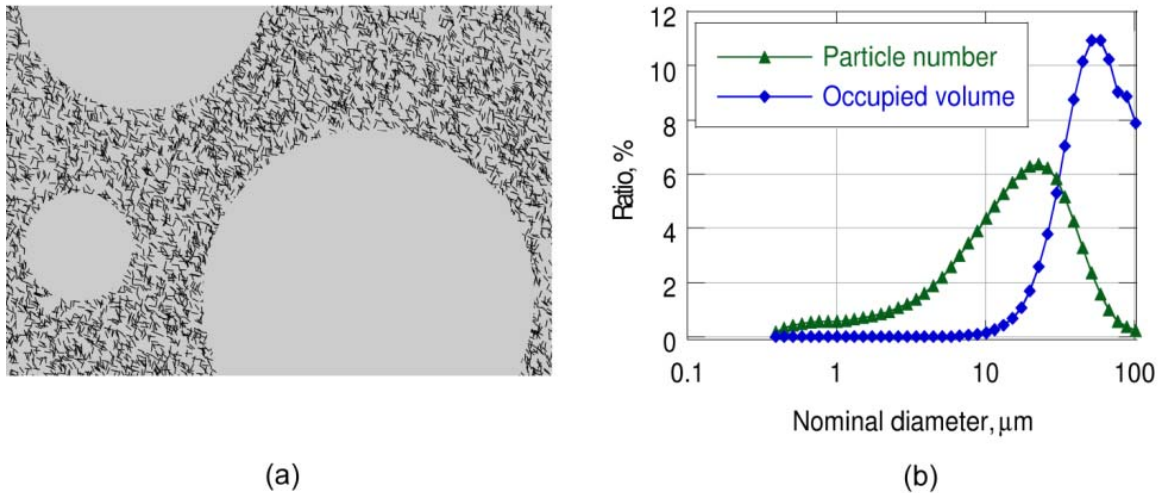


Figure 30. (a) A schematic illustration for geometry dependent clustering of CNTs in cement paste. When the paste is fresh, CNTs cannot penetrate into the cement grains. After the paste is hydrated the locations previously occupied by cement grains remain unreinforced. (b) The ratios corresponding to particle size distribution of typical Type I portland cement and the ratios corresponding to volume occupied by the particles of each size. Approximately 95% of this typical cement volume is occupied by grains that are larger than 20 μm .

As mentioned in section 3, the size of host particles is not the only parameter that affects dispersion due to geometry dependent clustering; the concentration of inclusions is as important. This importance is illustrated in Figure 31, which schematically presents a ceramic nanocomposite containing CNTs. Although the ceramic particles are larger than CNTs they do not notably affect the dispersion uniformity when the CNT concentration is low (Figure 31b). On the other hand, the geometry dependent clustering is significant when CNT concentration is high (Figure 31c). Constitutive properties of composites depend on the degree of dispersion uniformity. It is therefore important to know quantitatively to what extent the dispersion of nanoinclusions in cement paste is degraded by geometry dependent clustering. In other words, we wish to answer the question “What is the maximum theoretical achievable dispersion of nanoinclusions in typical cement paste?”

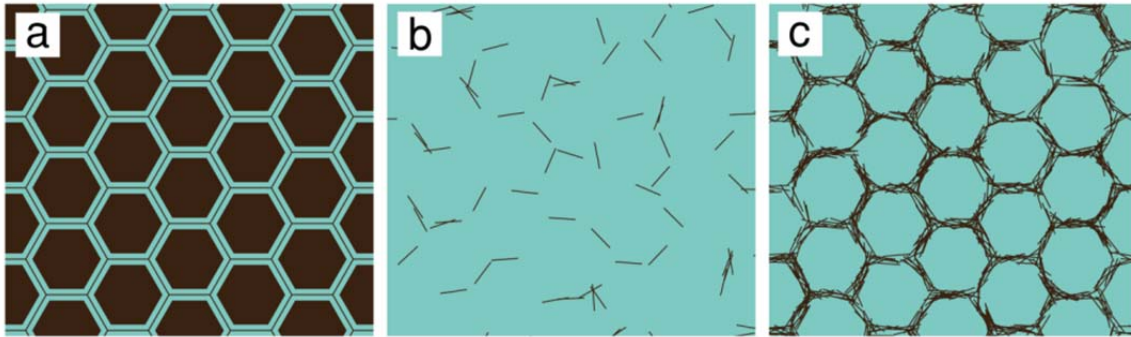


Figure 31. (Same as Figure 16) Effect of inclusion concentration on geometry dependent clustering. The images are the schematic presentation of carbon nanotubes (CNTs) in a ceramic nanocomposite. (a) The areas between ceramic particles in which CNTs can be distributed are shown with lighter color. (b) When a low dosage of CNT is used to reinforce the ceramic, the distribution of CNTs is relatively uniform and similar to the case in which CNTs could be placed anywhere in the matrix with no limitation imposed by ceramic particles. (c) When the CNT dosage is high, the distribution uniformity is significantly degraded.

The novel thermodynamics-based method of dispersion quantification (section 3 and section 4) is capable of handling an infinitely large number of particles with a moderate computational expense. This capability is very important and sometimes essential when measuring the dispersion of nano inclusions in cementitious materials; when dealing with cementitious nanocomposites the number of nanoinclusions in a representative volume element (RVE) can be significantly larger. For example, consider a CNT-reinforced cement paste with the typical proportions of $w/c = 0.4$ and $CNT/c = 0.005$ and CNTs with a diameter of 10 nm, length of 1 μm , and specific gravity of 1.4. Considering the fact that in typical cement there are grains as large as 100 μm , a cubic RVE with the side length of 500 μm ensures a reasonable representation of the composite material. Such an RVE contains approximately eight billion CNTs. For such a system, most traditional methods of dispersion quantification have a prohibitive computational expense.

The objective of this chapter is to utilize the novel dispersion quantification technique to predict the maximum theoretical achievable dispersion of nanoinclusions (such as CNTs) in cementitious nanocomposites considering geometry dependent clustering induced by the cement grains. For this purpose, RVEs of cement paste reinforced with nanoinclusions are simulated using commonly applied and researched w/c, CNT/c, and cement particle size distributions.

5.2. Simulation and analysis of the maximum theoretical dispersion of nanoinclusions in cement paste

For a nanoinclusion reinforced fresh cement paste made from a particular cement with the cement grains randomly dispersed, the maximum dispersion is achieved when the nanoinclusions are uniformly dispersed in the water that surround the cement grains. Evidently, the maximum achievable dispersion is not the fully uniform dispersion because of the geometry dependent clustering imposed by the presence of the (relatively) large cement particles. It should be noted that when the continuum diffusion method is used, the input for the analysis is the concentration of inclusions in each element in the discretized RVE rather than the location of individual inclusions. These concentrations can be readily calculated when the nanoinclusion to water ratio and the location and the size of each cement particle is known.

5.2.1. Parameter selection

Here, the main objective of the simulation and analysis is to observe the effect of geometry-dependent clustering on the dispersion of nanoinclusions in cement paste. Cement paste RVEs were generated with varying values of parameters such as w/c and nanoinclusion/c that are expected to have a strong influence on constitutive properties of the nanocomposite. Ranges for the parameters of interest were selected to match those commonly found in recent research on cementitious nanocomposites. For w/c, values of 0.35, 0.40, and 0.45 were considered. Three different cement particle size distributions were selected for analysis. These distributions were measured by Bentz for three types of

cement commonly used in the construction industry [150]. In this paper, the three types of cement are referred to as “fine”, “regular”, and “coarse” based on their particles size distribution as shown in Figure 32. As mentioned earlier, in practice cement particles typically agglomerate before or during concrete or cement paste production. In order to observe the effect of agglomerated cement on geometry dependent clustering, a cement paste made of clumped cement with an average agglomeration size of 200 was simulated.

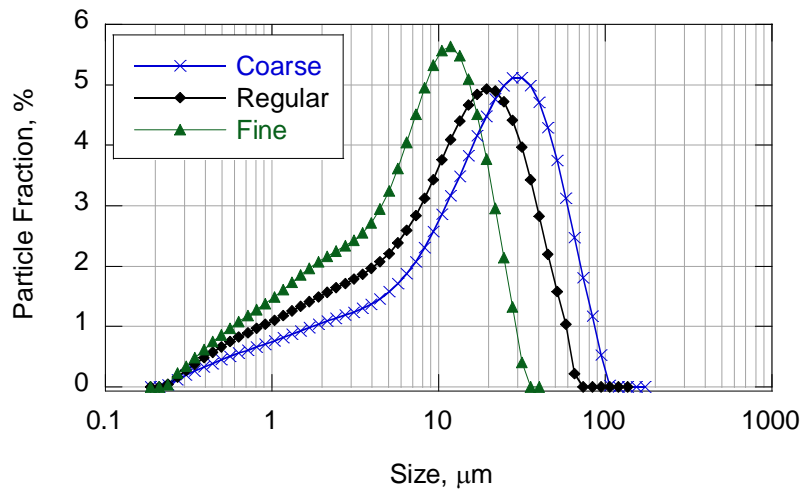


Figure 32. Measured (via laser diffraction) particle size distributions for the three cements of varying fineness commonly used in the construction industry (from Bentz [150]).

In current research on CNT - cement paste composites, CNT/c mass ratios below 1.0% are chosen since higher dosages of CNTs are very difficult to disperse even in the absence of geometry-induced clustering [7, 83, 147, 151-153]. Therefore, nanoinclusion/c of 0.3%, 0.5% and 0.7% were selected for this investigation. The combined parameter values for the domains generated and analyzed in this work are presented in Table 3. The specific gravity of the nanoinclusions was assumed to be 1.4 [154]. As it is possible in the future that new techniques will allow higher dosages of

nanoinclusions to be successfully dispersed, or new highly dispersible nanoinclusions as admixtures for cementitious materials will be developed, in addition to the mentioned dosages the very high nanoinclusion/c of 10.0% was also investigated. Cubic RVEs with side length of 500 μm were chosen. Our preliminary investigations show that this size is sufficiently large to be representative of any larger domain.

Table 3. Different values used for three different parameters investigated in this study; namely, w/c, nanoinclusion to cement mass ratio and cement fineness. The parameter combinations in each row were used to generate simulated cement paste RVEs for dispersion quantification.

w/c	Nanoinclusion/c, %	Cement fineness
0.40	0.5	Fine
0.40	0.5	regular
0.40	0.5	coarse
0.35	0.5	regular
0.40	0.5	regular
0.45	0.5	regular
0.35	10.0	regular
0.40	10.0	regular
0.45	10.0	regular
0.40	0.3	regular
0.40	0.5	regular
0.40	0.7	regular
0.40	0.3	agglomerated
0.40	0.5	agglomerated
0.40	0.7	agglomerated

5.2.2. Methodology

In order to quantify the effect of geometry-dependent clustering on the maximum theoretically achievable dispersion of nanoinclusions in cement paste, the first step is to generate a distribution of cement particles within a cubic domain. Since in practice cement paste is produced by blending water and cement in a mixer, the best expected dispersion of cement particles in water is achieved when cement grains are randomly distributed. A program was written (in *Mathematica*) to generate a spatially-random distribution of cement particles of a given particle size distribution in a cubic, three-dimensional domain. A simple algorithm typically used for random generation of impenetrable objects was applied [155]. In this algorithm, first the largest particle is placed in a random location in the domain. Then, the next largest particle is assigned with a random location in the domain. If a particle placement overlaps any previously placed particle, it is assigned a new random location. This process continues until the current particle does not overlap any previously placed particles. The same procedure is repeated for the rest of the particles until they are all placed in the domain.

For each cement and w/c, an RVE with a random distribution of cement particles was generated. Figure 33 shows such an RVE for the coarse cement and $w/c = 0.35$. A program was written to discretize the RVEs in order to determine the initial concentrations to assign as initial conditions for each element in the mass diffusion FEA. A mesh fineness of $50 \times 50 \times 50$ was chosen since our analysis showed that further convergence with finer meshes is negligible. The initial concentration value for each element was determined based on the nanoinclusion to water ratio (which can be obtained from the nanoinclusion/c and w/c) and the volume of cement grains located within each element. Figure 34a shows a discretized domain for the coarse cement and $w/c = 0.40$. Mass diffusion analysis was performed on the RVE using commercial FEA software (*Abaqus 6.8*). One thousand time steps were used for each analysis to achieve sufficient calculation accuracy. As can be seen in the discretized RVE (Figure 34a), the initial mass concentration of the elements located within cement particles is zero since

they contain no nanoinclusions. Similarly, the initial concentration of each element located fully within the aqueous part of the RVE is the same as the concentration of nanoinclusions in water. Figure 34b shows the same RVE after a few steps of the finite element analysis. In order to calculate the dispersive work for each RVE, the concentrations of all the elements in all the time steps were recorded for each analysis [156].

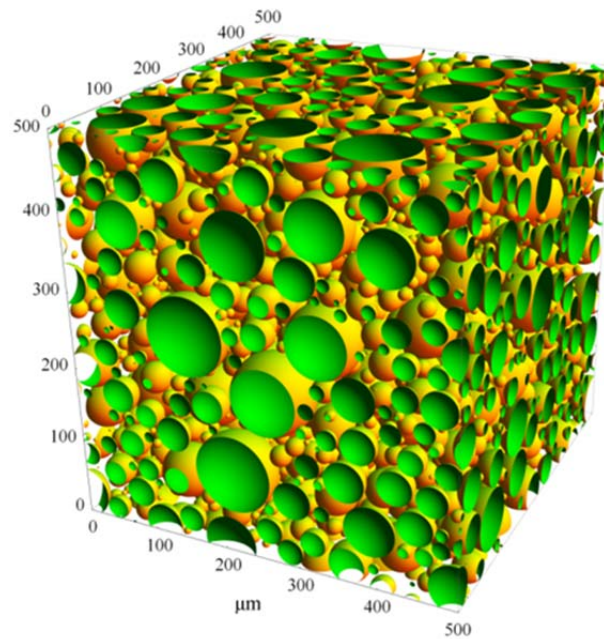


Figure 33. Simulated 3-D RVE of cement paste made from a coarse cement with w/c of 0.35, where cement particles are randomly dispersed within the paste.

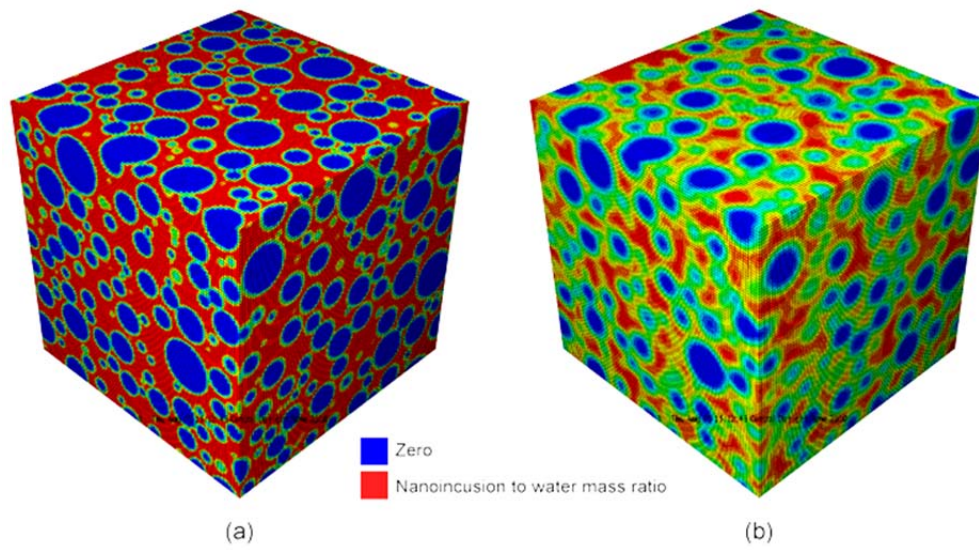


Figure 34. (a) Discretized RVE of cement paste incorporating nano-inclusions with w/c of 0.4. (b) The same RVE a few time steps after the start of mass diffusion finite element analysis.

5.3. Results and Discussion

As expected, dispersion is less uniform in cements with larger particles. This is shown in Figure 35. In this figure, the maximum dispersion values for nano-inclusions in a cement paste with w/c of 0.40 and nano-inclusion/c of 0.5% for the three cements with varying fineness are presented. The nano-inclusion dispersion corresponding to the fine cement is 0.988 while the dispersion corresponding to coarse cement is 0.945. However, these results show that geometry dependent clustering does not affect dispersion significantly in cementitious nanocomposites when the cement particles are randomly dispersed and the concentration of nano-inclusions is relatively low, as is the case in CNT-reinforced cement paste. This effect could be further reduced by using cements with much finer particles. However, using very fine cement causes practical complications in mixing and fabrication. In an earlier investigation cement was milled to reduce the average cement particle size to less than 1 μm [7]. Due to the extremely high surface area of the milled cement, the minimum w/c to produce a reasonably workable paste was very high (0.80),

even with a high concentration of superplasticizer. The high surface area also made the cement highly reactive causing a significant, rapid release of heat during mixing.

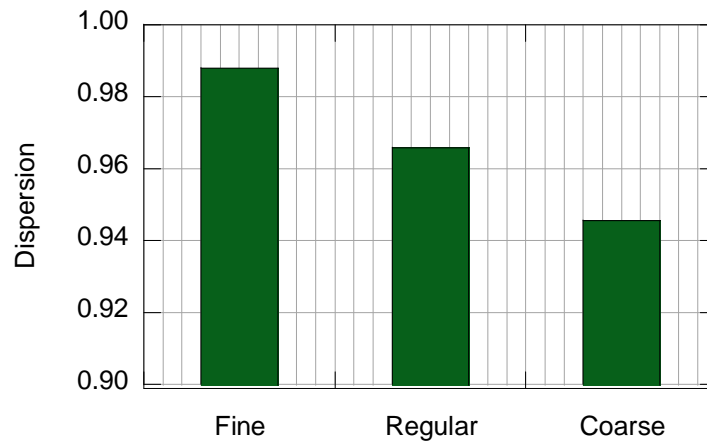


Figure 35. Maximum values of nanoinclusion dispersion for cements of varying fineness with w/c of 0.40 and nanoinclusion/c of 0.5% (typical ratios for producing CNT reinforced cement paste). As expected, the dispersion corresponding to coarse cement is the lowest due to the higher effect of geometry dependent clustering. These results show that the negative effect of geometry dependent clustering on dispersion of CNTs in cement paste is minimal.

Increasing the w/c is expected to improve the maximum theoretically achievable dispersion for a given nanoinclusion/c for two reasons. First, higher w/c yields a lower volume of cement within the RVE, which leads to less geometry-dependent clustering. Second, a higher w/c corresponds to a lower nanoinclusion to water ratio, which as explained by means of Figure 31 causes less geometry dependent clustering. The effect of w/c on the maximum theoretically achievable dispersion is shown in Figure 36a. As the range of practical w/c is narrow (0.35-0.45), the effect of w/c on the dispersion of nanoinclusions in cement paste is negligible. As demonstrated in Figure 31, increasing the nanoinclusion concentration boosts the effect of geometry dependent clustering. However, as shown in Figure 36b, this effect is insignificant for CNT-reinforced cement

pastes due to the existing limitation in the maximum amount of nanoinclusions that can be incorporated in cement paste while avoiding clumping (typically below 1.0% of the mass of cement).

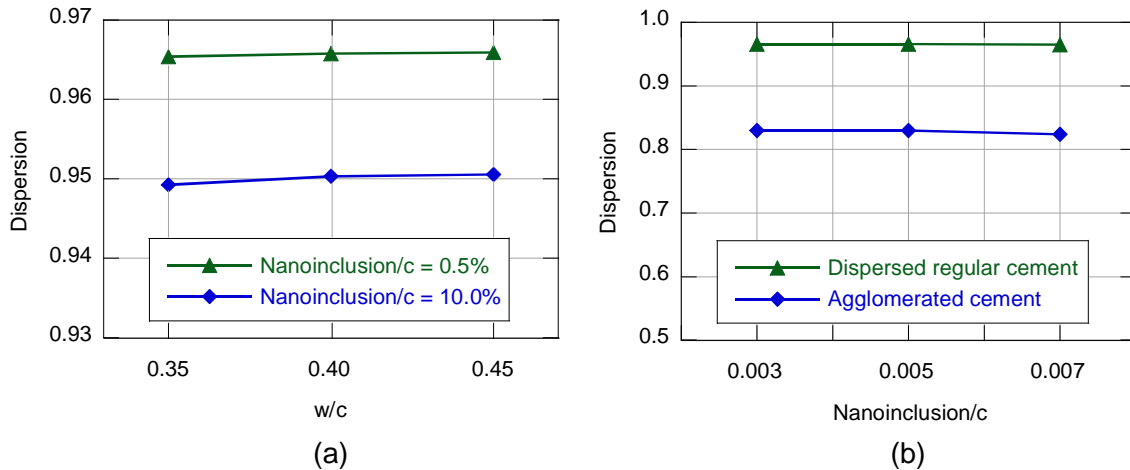


Figure 36. Calculated dispersion values for cement paste made from regular cement and with different parameters typically used for producing CNT reinforced cement paste. (a) Demonstrates the effect of w/c on dispersion for two different concentrations of nanoinclusions. (b) Shows the effect of nanoinclusion concentration on dispersion for regular and agglomerated cement with an average agglomeration size of 200 μm .

It is possible that future advances in cementitious nanotechnology will make it possible to produce materials with high concentrations of nanoinclusions, and as a result, a less uniform state of nanoinclusion dispersion. However, as shown in Figure 36a, increasing the nanoinclusion/c to 10% results in less than a 2% degradation in dispersion. Finally, it should be noted that cement particles agglomerate before and during cement paste and concrete mixing. The previously described simulations were all performed for the situation where the cement particles are fully disagglomerated and randomly dispersed within the paste. Assuming a paste made from agglomerated cement with an average clump size of 200 μm , dispersion would be approximately 13% less uniform compared to

its counterpart made from fully disagglomerated and randomly dispersed cement paste (Figure 36b).

Finally, one should be cautioned that the dispersion quality alone (as measured using the work method) does not control the constitutive properties of the composite material. While there is a unique dispersion value associated with each RVE, multiple RVEs may yield the same dispersion value. A single large cement particle may degrade the dispersion by the same amount as several smaller cement particles. However, it is well-known that a single, large flaw in a brittle matrix is more likely to propagate cracks than several, much smaller flaws. Thus, it may be necessary to consider additional measures with dispersion quality when predicting or modeling important composite constitutive properties.

5.4. Concluding Remarks

Using the novel method for quantifying the dispersion of discrete particles in a domain, the theoretical maximum dispersion of nanoinclusions in cement paste was quantified. Since the average size of cement particles are significantly larger than the spacing between nanoinclusions such as CNTs, the dispersion of nanoinclusions in cement paste is degraded due to geometry dependent clustering. Simulations showed that in the case of one of the most researched cementitious nanocomposites, namely CNT-reinforced cement paste, dispersion degradation due to geometry dependent clustering is negligible as long as the cement particles are fully disagglomerated and randomly dispersed within the paste. However, the results of the simulations indicate that the effect of geometry dependent clustering on dispersion can be significant if the cement particles are agglomerated. Therefore, ensuring a high level of dispersion of nanoparticles in cement paste requires simultaneously achieving a high level of dispersion of cement particles, but does not require the use of an ultra-fine cement.

6. UTILIZATION OF SILICA FUME TO STABILIZE THE DISPERSION OF CARBON NANOFILAMENTS IN CEMENT PASTE

In most such composite materials, the quality of the dispersion of the filaments strongly controls the composite constitutive properties. As shown in section 2, achieving a uniform distribution of CNT/Fs in a cement paste matrix is a major challenge due to the high van der Waal's attracting forces between the nanofilaments. Secondary nanoparticles such as clays have been used in the past to stabilize a uniform dispersion of CNT/Fs in polymeric nanocomposites. In the study presented in this chapter, the effect of using submicrometer silica (silica fume) powder on the dispersion and stability of CNFs in cement paste was investigated. The nominal diameter of silica fume particles was in the range of 0.1 to 0.3 micrometers. Specimens of CNF-incorporated cement paste with different concentrations of silica fume were produced and imaged by optical microscopy. Using a novel thermodynamic-based dispersion quantification method, the dispersion values of CNFs in the specimens were measured and compared. The results show that silica fume, if used in sufficient proportions, can largely prevent the agglomeration of, and thereby stabilize the distribution of, CNFs in fresh cement paste.

6.1. Introduction

Several studies, mostly in the past decade, have been carried out to develop methods for incorporating CNT/Fs in cementitious materials and investigating their constitutive properties [16-21, 147, 148, 157-159]. A summary of such efforts is presented in section 2. The studies have shown that CNT/Fs can improve properties such as tensile and compressive strength, although marginally in most cases. A likely reason for the marginal improvements is the typically poor dispersion of CNF/Ts in cement paste. The dispersion problem has been combated by methods like surface modification of the fibers and by using surfactants, usually in combination with ultrasonic processing of the nanofilaments in liquid solutions [40, 160-165]. Although different methods such as implanting or growing the fibers directly on non-

hydrated cement grains are being studied by some investigators, as explained in section 2, the most common method of producing CNT/F-incorporated cement paste is to first disperse the nanofilaments in water, typically by using surfactants and sonication, and then mix the aqueous dispersion with cement. Unfortunately, most of the effective surfactants are not compatible with cement hydration and their presence in cement paste results in a weak material, usually entrapping a notable amount of air [7]. Therefore, to avoid negative hydration and air entrapment issues, weaker surfactants known as water reducing admixtures or superplasticizers are used. These surfactants are typically polycarboxylate-based and are specifically made for cementitious materials. They are typically added to a fresh mix of cementitious material to disagglomerate the cement grains and disperse them, thereby reducing the amount of water required to produce a paste with a certain rheological property.

It has been shown that the established methods of incorporating CNT/Fs in cement paste (using superplasticizers and ultrasonic processing) do not maintain a sufficiently good dispersion of nanofilaments in cementitious materials and large volumes of the paste can remain absent of nanofilaments [7]. The reason, as will be shown, is that nanofilaments can move freely in fresh cement paste and van der Waals attracting forces will eventually cause the nanofilaments to migrate and reaggregate. It is not known yet why the carbon nanofilaments that can remain well-dispersed for days or even months in a water-superplasticizer solution reaggregate relatively rapidly when the solution is added to cement. However, it is definitely known that the reaggregation issue of carbon nanofilaments in the matrix of host material (sometimes even in polymeric nanocomposites [166]) does exist.

In this chapter, a novel, simple, and effective method for stabilizing the dispersion of CNT/Fs in cement paste is presented. In this method, silica fume is used to

immobilize and stabilize the nanofilaments already dispersed in cement paste and to prevent them from migrating towards each other and reagglomerating. The novel dispersion quantification method is used to compare the dispersion quality of CNFs in cement paste when it is made with different concentrations of silica fume and without silica fume. Although incorporating silica fume into cementitious composites might not be always desired, the novel method has considerable potential for implementation in the construction industry. The investigation presented here has been performed on CNFs due to their larger size and therefore the visibility of individual filaments through optical microscopy. The method is expected to be implementable for smaller nanoinclusions as well. In the next section, the novel method of dispersing carbon nanofilaments in cement paste will be presented followed by the quantitative comparison of CNF dispersion in specimens made with and without silica fume.

6.2. Dispersing carbon nanofilaments in cement paste using silica fume

The reason for the free movement and reagglomeration of CNFs in fresh cement paste is that most cement grains are much larger than CNFs. As a result, there are large volumes between cement grains that do not impose any restraint on the movement of nanofilaments. If the space between the cement grains can be filled by well-dispersed and stable nano particles, the movement of carbon nanofilaments will be confined. This concept has been implemented in the past to produce a stable dispersion of CNTs in polymeric materials. Secondary particles, such as clay, that have been used to improve electrical conductivity in polymer composites containing vapor grown carbon fibers [167] or carbon black [168] as the conductive filler, were also found to improve the dispersion of filaments. Liu and Grunlan used clay to improve the dispersion of carbon nanotubes in epoxy composites [169].

Silica fume is an amorphous sub-micrometer powder (with particles 100 to 150 times smaller than a grain of cement) used to enhance several properties of concrete such as compressive strength, bond strength, abrasion resistance [157, 170], and also to reduce permeability [159]. Mixture proportions for high-strength concrete typically contain 5 to 15 percent silica fume by mass of cement [160]. In this study, the use of silica fume as a secondary nanoparticulate additive for enhancing and stabilizing the dispersion of CNFs in cement paste is investigated. The method of producing CNF-incorporated cement paste using silica fume is presented in section 6.3. A novel dispersion quantification method (presented in the next section) will be used to compare the dispersion of CNFs in cement paste when the paste is made with and without silica fume.

It should be mentioned that silica fume has been used in the past in an effort to enhance the dispersion of CNFs in cement paste. Sanchez and Ince produced CNF-incorporated cement paste by dry-mixing as-received CNFs and then silica fume with cement followed by the addition of water [171]. They used CNFs with concentrations from 0.005% to 2% per mass of cement and also the silica fume to cement mass ratio of 10%. The results demonstrated the dispersing potential of silica fume for CNFs in cement pastes. Sanchez and Ince argued that the reason for the disagglomerating effect of silica fume is that their small size allowed them to work their way in between the individual CNFs during the dry mixing process, causing the CNFs to separate from one another as mixing occurred, resulting in the separation of some of the fibers. However, their findings showed that While CNFs were found to be dispersed throughout the pastes incorporating silica fume, a significant number of CNF clumps still remained disagglomerated.

6.3. Experiment

6.3.1. Materials and instruments

For the experiments presented in this chapter, undensified silica fume supplied by Norchem, Inc. was used. The silica fume powder consists of spherical particles that

average 0.1 to 0.3 micrometers in diameter with a surface area of 17 to 30 m^2/g . The CNFs used in this experiment were vapor grown [172, 173] and have a diameter between 60 to 150 nm, a length between 30 and 100 micrometer, and a specific surface area between 50-60 m^2/g . The fibers were provided by Applied Science Company under the commercial name Pyrograph PR-24 (PS). Type I portland cement was used. The surfactant utilized was a high range polycarboxylate-based superplasticizer provided by W.R. Grace with the commercial name ADVA Cast 575. Dispersions were made by ultrasonically processing the CNFs in a water-superplasticizer solution. A 20 kHz sonicator with a $\frac{1}{2}$ inch diameter titanium alloy probe was used at an amplitude setting of 40%. To produce high speed and high shear mixing, a 600W Oster BVCB07-Z blender was used for paste mixing at approximately 7500 RPM. Optical and electron microscopes were used to image CNFs in fresh and hardened cement pastes, respectively. For optical microscopy, a Zeiss Axiophot microscope was used in transmitted mode with 20x and 40x dry objective lenses and a 100x oil immersion objective lens. For electron microscopy, observations were performed by a JEOL JSM-7500F scanning electron microscope (SEM).

6.3.2. *Mix design, production and observation of CNF-incorporated cement paste*

Specimens with four different mixture designs were produced. Three of the mixtures contained silica fume (hereafter referred to as silica fume mixes) and the **control** mixture did not contain silica fume. It is known that the difficulty in achieving a good dispersion of nanoinclusions in any material is relative to the concentration of nanoinclusions. As a result, since the objective of the study is investigating the effectiveness of silica fume in maintaining a good dispersion, the relatively high CNF/cm mass ratio of 0.80 was used in all of the mixes (cm is the sum of cement and silica fume masses). This concentration of CNFs is by far larger than the typical concentrations of carbon nanofilaments used in the past to modify the constitutive properties of cementitious materials. The commonly used water to cementitious materials mass ratio (w/cm) of 0.40 was selected for all the

specimens. Based on preliminary investigations, the superplasticizer to cm mass ratio of 0.014 was used for all the mixtures to maintain the required workability. For the silica fume mixes, silica fume to cement ratios of 0.07, 0.13 and 0.20 were used to cover the typical concentrations used in the concrete construction industry and research. The complete mixture designs are presented in Table 4.

Table 4. Mixture proportions for the control and silica fume mixes. The proportions are presented as mass ratios.

Mix	w/c	Silica fume to cement ratio	CNF/cm*	Superplasticizer to cm* ratio
Control	0.40	0.00	0.80	0.014
SF_1	0.40	0.07	0.80	0.014
SF_2	0.40	0.13	0.80	0.014
SF_3	0.40	0.20	0.80	0.014

* cm = sum of cement and silica fume masses

To produce each specimen, first a water-superplasticizer solution was made. Then, CNFs were added to the solution and mixed with a manual stirrer. The solution then was transferred to a jacketed beaker (to maintain a constant room temperature) and was sonicated for 5 minutes. The dispersion was added to the blender that already contained the dry cement. For the silica fume mixes, the silica fume powder was slowly added while mixing was in progress. The total mixing time for all of the batches was 4 minutes.

For optical microscopy, a small droplet of the fully mixed paste was placed on a glass slide and subsequently covered with a transparent glass slip. Since the transmitted mode was used, it was important that the paste layer on the glass slide be as thin as possible so that a sufficient amount of light could be transmitted through the specimen. For this purpose, the glass slide was pressed firmly on the slide. The edges of the slip were sealed on the slide using nail polish to prevent the evaporation of water and drying of the

specimen during observation. Optical microscopy was performed within one hour after mixing. For SEM observation of the dispersion in the fully hardened cement paste specimens, beam specimens with a cross-section of 6 mm x 6 mm and length of 200 mm were cast. The beams were cured in a humidity room with 100% RH for 7 days. The beams were then broken and oven-dried for one day. The fractured surface was coated with 6 nm-thick Platinum/Palladium (80/20) layer to enhance surface conductivity for use in the SEM.

6.4. Results and discussion

The optical microscopy observation of the fresh control paste right after mixing showed that the CNFs were relatively well-dispersed and were freely moving in the water that surrounded cement particles. This is shown in Video 1. Approximately two hours after mixing, the movement of the fibers slowed down and more agglomerations formed (Video 2). After three hours, as shown in Figure 37, most of the CNFs were entangled and the movement of the remaining CNFs was confined, possibly due to the formation of hydration products and the beginning of setting.

As for the silica fume mixes, the effect of the presence of silica fume on dispersion was remarkable. It could be observed that the mobility of CNFs in fresh paste was related to the concentration of silica fume in the mix; the movement of CNFs reduced by increasing the concentration of silica fume. In fact in the SF-3 mix the CNFs barely moved and the dispersion of CNFs in the paste remained uniform. As expected, the silica fume particles prevented CNFs from moving such that the CNFs could hardly agglomerate. The optical microscopy images of silica fume paste SF-3 are shown in Figure 38. Due to the good dispersion of CNFs, a lens with higher magnification (100x) than used in Figure 37 was used to obtain images that were representative of the state of dispersion in the cement paste.

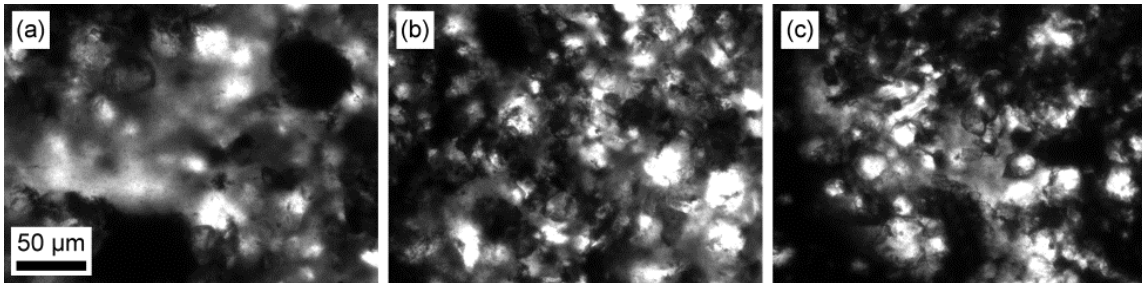


Figure 37. Optical microscopy images of fresh control paste three hours after mixing, acquired by a 20x objective lens. The images show that the CNFs are poorly dispersed and highly agglomerated. The scale bar applies to all three images.

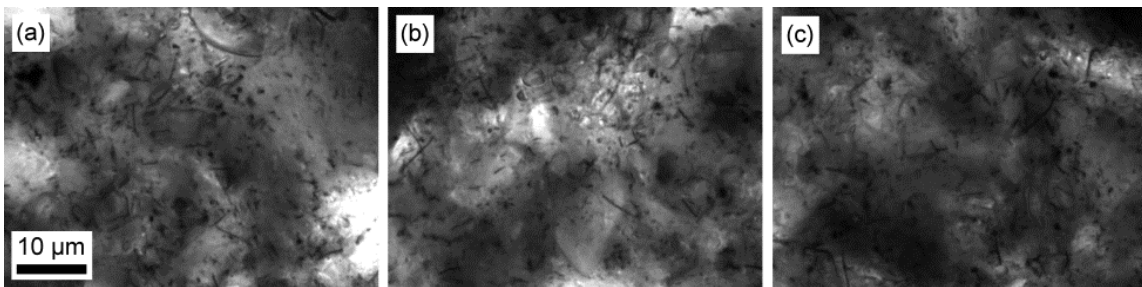


Figure 38. CNFs in the SF-3 mix three hours after mixing acquired by a 100x objective lens. The images show that the CNFs are well-dispersed. The scale bar applies to all three images.

SEM images of the fractured surfaces of hardened control and SF-3 pastes are presented in Figure 39 and Figure 40, respectively. Figure 39 shows the agglomeration of CNFs in the cement paste. During the SEM observation finding areas like the one shown in Figure 39a was difficult since a large portion of the fractured surface contained no or few fibers. However, in the case of specimen SF-3, the distribution of CNFs on the fractured surface of the hardened paste was relatively uniform Figure 40. The SEM observations indicate that the CNFs do not tend to reaggregate during the hydration process several days after initial mixing and fabrication.

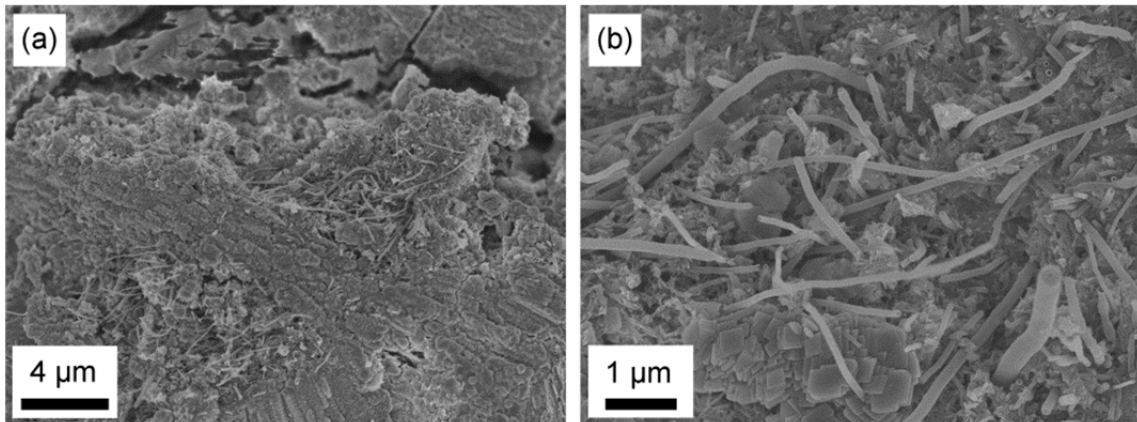


Figure 39. SEM images of the fractured surface of hardened control paste, indicating the poor dispersion of CNFs. (a) shows that a large portion of the paste does not contain CNFs. In this image CNFs are agglomerated in two different locations of the fractured surface. (b) is a closer look at the CNF agglomeration at the right side of image (a).

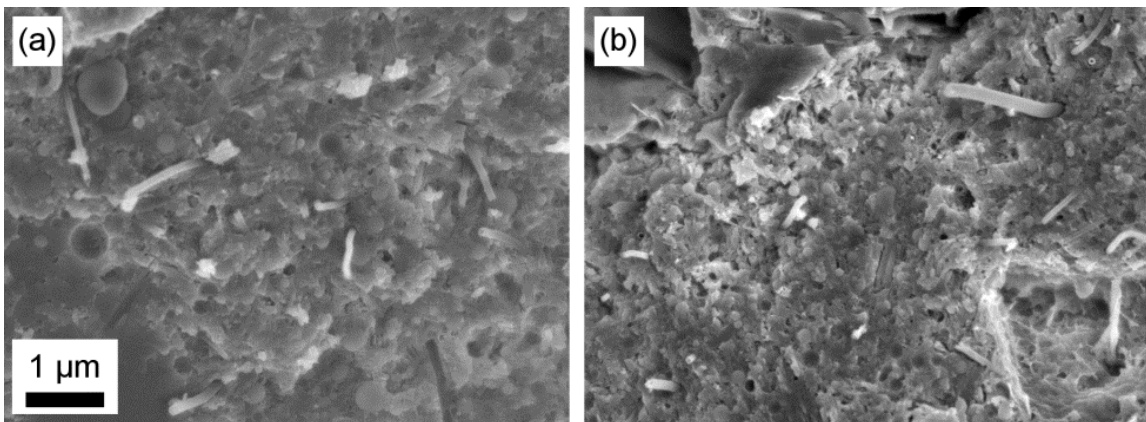


Figure 40. SEM images of fractured surface of hardened silica fume paste SF-3, indicating the uniform dispersion of CNFs. The scale bar applies to both images.

The results of the dispersion quantification by the work method is shown in Figure 41 for all the different mixtures. The average dispersion value for the control specimen (the three RVEs in Figure 37) is 0.69 while the dispersion for the silica fume paste SF-3 (the three RVEs in Figure 38) is 0.88, indicating an improvement of over 27 percent. The

dispersion values for SF-1 and SF-2 specimens are 0.78 and 0.83 respectively. This indicates a relatively linear correlation between the concentration of silica fume and improvement in dispersion.

Note that, as indicated in Figure 41, the standard deviations of the dispersion values for mixtures containing silica fume are lower than that of control specimens. This shows that, although the area of the images utilized for dispersion quantification of the silica fume mixes is smaller than that of the control mixture images, they better represent the state of dispersion, which indicates the more uniform dispersion of CNFs in silica fume specimens.

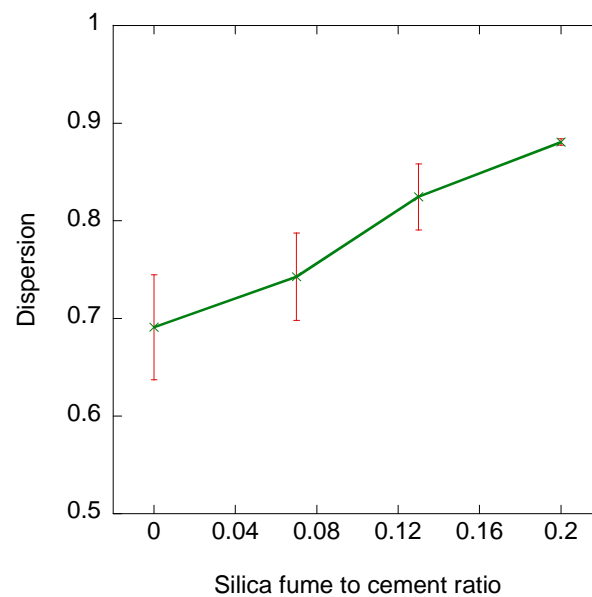


Figure 41. Dispersion of CNFs in cement pastes with different concentrations of silica fume. The error bars indicate one standard deviation either side of the mean.

6.5. Concluding remarks

It was shown that the sufficient use of silica fume can remarkably enhance the dispersion of CNFs in cement paste by acting as a stabilizing agent that prevents reagglomeration of CNFs. For silica fume to cement mass ratios up to 0.2, the quality of the stabilized CNF dispersion varies roughly linearly with silica fume content. The novel dispersion stabilization method is simple and practical, and can be readily implemented in the concrete construction industry due to the existing familiarity with silica fume as a concrete additive. The findings from this study should lead to further research correlating important CNF-cement composite constitutive properties to dispersion quality and silica fume dosage, and ultimately the determination of optimum silica fume concentration for different applications.

7. THE EFFECT OF CARBON NANOFIBERS ON THE MECHANICAL PROPERTIES OF HARDENED CEMENT PASTE

This chapter reports on an investigation in which CNFs have been utilized to make hardened cement past beams, which were tested in bending. The objective of this work is to show that despite the early findings of other investigators that usually indicate a marginal or even no improvement in mechanical properties due to the utilization of carbon nanofilaments, in certain conditions they can dramatically change the mechanical properties of cement paste. When cement paste with w/c of 0.4 was not cured for the first 24 hours after casting, a condition that commonly exists in structural and pavement construction, incorporation of CNFs with a concentration of 1.0 wt% of cement caused over 250% increase in the flexural strength. At the same curing condition, the incorporation of CNFs significantly reduced the formation of drying shrinkage cracks for high strength hardened cement paste produced either by the utilization of silica fume or low w/c.

7.1. Introduction

As mentioned in section 2 and section 3 CNF/Ts are of interest to the researchers of materials science due to their excellent characteristics and in particular their mechanical properties. CNTs have been the subject of many investigations in the past decade as reinforcement for several composite applications. Mechanically, CNTs exhibit elastic moduli of more than 1 TPa (1.5×10^8 psi) [9]. Their theoretical strength is 100 times that of steel, at only 1/6th the specific gravity [10]. Values as high as 60 GPa (8.7×10^6 psi) for ultimate strength and 6% for ultimate strain have been reported [11, 12]. Salvetat et al. reported an elastic strain capacity of 12%, which is 60 times higher than that of steel [9]. Recently, Ozkan et al. performed direct mechanical measurements on CNFs [15]. The CNFs that they investigated had a tensile strength between 2-5 GPa (2.9×10^5 - 7.3×10^5 psi) with an average modulus of elasticity of 300 GPa (4.4×10^7 psi). One of the concerns about the application of these nanofilaments is their current

relatively high price. However, due to ongoing advancement in the industrialization and mass production of these nanofilaments, their prices are decreasing rapidly [149].

The research on the effect of carbon nano fibers (CNFs) and nano tubes (CNTs) on the mechanical properties of cementitious materials is new and has a history spanning slightly more than a decade. These filaments are available in different sizes, shapes, dispersibilities, surface properties, mechanical properties, and structures. Moreover there are various methods for incorporating them in other materials. As a result, it is impossible to reach a general conclusion about their effect on the mechanical properties and behavior of any material in which they are incorporated. However, the outstanding properties of CNF/Ts support the idea that if these nanofilaments are selected and utilized optimally, they must be able to significantly change the mechanical properties of the material in which they are incorporated.

The early experiments on incorporating CNF/Ts in cementitious materials have not shown much enhancement in mechanical properties. When flexural or compressive strength is concerned, the majority of those experiments have resulted in improvements of not more than 50%; usually less than 25%. The amount of improvement in mechanical properties is not necessarily proportional to the concentration of CNF/Ts in cementitious matrix. In fact, beyond a certain concentration the dispersion of CNF/Ts in the matrix degenerates, and that often has a negative effect on the mechanical properties of the composite. The rest of this section briefly summarizes some of the important studies carried out in the past on the mechanical properties of CNF/T incorporated cement paste. More detailed information and references can be found in [7, 83, 147] . In the next sections, an experimental investigation will be presented, which indicates that through achieving a better dispersion of CNFs in cement paste, significant improvements in mechanical properties can be achieved.

Several methods have been developed for incorporating CNF/Ts in cementitious materials (see e.g. [7, 83, 147]). The most common and practical method consists of simply mixing cement, water, CNF/Ts and surfactants. Usually, the CNF/Ts are first dispersed in a solution of water and surfactant using ultrasonic processing, and then the resulted dispersion is added to and mixed with cement. The investigations summarized below have used this method.

Kowald used CNTs in cement paste with CNT/cement mass ratios in the range of 0.5 to 5.0% [33]. He tested the hardened specimens for compressive strength after 7, 14, and 28 days. Marginal improvements were observed in compressive strength and even a decrease in strength when the fiber dose was as high as 2.5% or more. Li et al. performed a set of experiments with CNTs in mortars with CNT/cement mass ratio of 0.5% and the water:cement:sand proportion of 0.45:1:1.5 [16]. The bending and compression tests showed that the addition of CNTs increased the compressive and flexural strength by 19% and 25% respectively. More references about the investigations performed on CNF/T-incorporated cementitious materials can be found in [7, 83]. Gay and Sanchez tested hardened cement paste specimens with different compositions and found that the addition of 0.2% CNFs per mass of cement resulted in increased splitting tensile strength of 22% in portland cement composites and 26% in cementitious composites that also contained silica fume [174]. Metaxa et al. [175], Shah [176] and Konsta et al. [177] showed that CNTs in cement matrix ($w/c = 0.5$) increased the flexural strength and the Young's modulus of plain cement paste by 25% and 50%, respectively. In another investigation, Konsta et al. reported that the flexural strength of the specimens reinforced with CNTs shows an increase of 30–40% over plain cement specimens [178]. Cwirzen et al. reported an increase of 50% in the compressive strength of hardened cement paste due to the use of CNTs with a concentration of 0.045% to the mass of cement [18].

Recently, an investigation was performed by Tyson et al. regarding the effect of CNF/Ts on the mechanical properties of hardened cement paste [147]. The results showed that utilizing CNFs with only a CNF/c mass ratio of 0.1% increased the flexural strength of hardened cement paste by over 80%, although the dispersion of CNFs in cement paste was not uniform. In light of the results from other investigations, this finding was remarkable, and motivated the experiments reported in this chapter.

Tyson et al., Kowald [33], and Konsta et al. [178] each found that after the CNF concentration exceeded a certain limit, CNFs became less effective in improving mechanical properties such as flexural strength. In fact, they observed a significant decline in flexural strength when the CNF to cement mass ratio (CNF/c) was increased from 0.1% to 0.2%; most probably due to the poor dispersion of CNFs. In this study, in order to enhance dispersion in comparison to that achieved in past studies, a larger dosage of superplasticizer and more prolonged ultrasonic processing and paste mixing were utilized. To reduce variability, beams with cross-sectional areas larger than those made by Tyson et al were tested. Bending tests were performed on the beams to measure flexural strength, Young's modulus, and toughness. In addition, the effect of CNFs on the shrinkage cracking of beams was observed.

This work also presents the results from an investigation for determining the effect of the dispersion quality of CNFs within a cementitious matrix on the mechanical properties of hardened cement paste. Although the results are not conclusive, they are important findings that provide useful information for future research. As mentioned earlier, in order to produce a CNF-incorporated cement paste an aqueous solution of CNF is mixed with cement. The CNFs are well-dispersed in the solution but after the solution is mixed with cement, the CNFs usually reaggregate and this results in a poor dispersion of CNFs in hardened cement paste [7]. Recently, Yazdanbakhsh and Grasley showed that incorporating silica fume in cement paste can physically restrain the CNFs and prevent the reagglomeration of CNFs in fresh cement to a great extent [179]. That is, the silica

fume helps to stabilize the dispersion. In this work, silica fume will be used to improve the dispersion of CNFs in hardened cement paste. Additionally, the effect of CNFs on the mechanical properties of cement paste with improved CNF dispersion will be investigated.

7.2. Experimental

7.2.1. Materials and Instruments

The CNF used in this experiment has a diameter between 60-150 nm, a length between 30-100 μm , and specific surface area of 50-60 m^2/g . The CNFs were provided by Applied Sciences Incorporated under the commercial name Pyrograph PR-24-XT-PS. The CNFs were used in two forms, non-milled and milled. Milling was performed by the manufacturer, through a ball-milling process. Ball-milling breaks the large clumps of CNFs and improves their dispersibility. The surfactant used for dispersing CNFs in water was a high range polycarboxylate-based water reducing admixture (superplasticizer) provided by W.R. Grace with the commercial name ADVA Cast 575. Type I portland cement was used for producing cement paste.

Dispersions were made by ultrasonically processing the CNFs in a water-superplasticizer solution. A 20 kHz sonicator with a $\frac{1}{2}$ inch diameter titanium alloy probe was used at an amplitude setting of 50%. To produce high speed and high shear mixing, a 600W Oster BVCB07-Z blender was used for mixing cement paste at approximately 7500 RPM. An optical microscope was used to image CNFs in aqueous dispersions and fresh cement paste using transmission mode. A scanning electron microscope (SEM) was used to observe the fractured surface of hardened cement paste. For optical microscopy, a Zeiss Axiophot microscope was used with 40x and 100x objectives lenses. For electron microscopy, observation was performed by a JEOL JSM-7500F scanning electron microscope. A Bose ElectroForce 3230-AT System was used for four-point bending tests. The tests were performed in the load-controlled mode and the load-deflection values were registered until fracture occurred. The loading rate of 5 N/sec was applied.

This rate was sufficiently slow so that it took at least few minutes for each beam to reach its ultimate strength, and the loading could be regarded as essentially static.

7.2.2. Mix proportions, preparation of specimens, and testing

The mix proportions are presented in Table 5. To observe the possible impact of w/c ratio on the effectiveness of CNFs in changing the mechanical properties, for the batches without silica fume, w/c ratios of 0.25 and 0.40 were investigated (batches 1, 2, 6, and 7). Silica fume to cement mass ratio of 0.20 was used in batches 8 and 9. In those batches the w/c ratio was 0.40. To maintain a consistent viscosity, the superplasticizer was used with the concentrations ranging from 0.7% to 1.7% to the mass of cement. The workability of the pastes was quantitatively controlled based on the amount of the power consumed by the blender during mixing, which was monitored using an electricity power (i.e. wattage) monitor. This method was implemented by first recording the power consumed for plain cement paste with w/c of 0.40, which had a desirable viscosity, and then using an amount of superplasticizer in other batches that resulted in the same or similar value of power consumption. Since superplasticizer should not be added to the paste during paste mixing and is required to be added to the aqueous solution to yield the best possible dispersion of CNTs in water during ultrasonic processing, a pilot experimental study was performed in which several batches of cement past were made with the compositions presented in Table 5 to determine the required amount of superplasticizer for each mix composition. It should be noted that all the batches had the same volume.

Table 5. Mix proportion of the cement paste batches. * The difference between batch 5 and other batches containing CNFs is that in batch 5 CNFs were directly added, in form of dry powder, to cement paste in the mixer, while in the other batches CNFs were first dispersed in a water-superplasticizer solution using ultrasonic processing.

Batch No.	CNF/c	w/c	SilicaFume/c	CNF type	Cast in 100% RH
1	0.00	0.40	0.00	-	No
2	1.00	0.40	0.00	milled	No
3	0.00	0.40	0.00	-	Yes
4	1.00	0.40	0.00	not milled	Yes
5*	1.00	0.40	0.00	not milled	Yes
6	0.00	0.25	0.00	-	No
7	1.00	0.25	0.00	milled	No
8	0.00	0.40	0.20	-	Yes
9	1.00	0.40	0.20	milled	No
10	1.00	0.40	0.20	not milled	Yes

As mentioned previously, in past studies found in the literature at some high level of CNF concentration the measured strength generally began to decline due to poor dispersion. In order to test the ability of the modified manufacturing process utilized in this project, CNF concentrations that would be expected to cause strength reductions utilizing past preparation techniques were considered. For this purpose, the CNF/cm mass ratio (cm indicates the sum of the weights of cement and silica fume, if any) of 1.0% was selected to be used in all the CNF-incorporated cement paste batches. Preliminary investigations showed that if higher concentrations were selected, CNFs were very difficult to disperse in the aqueous solution even by using large amounts of superplasticizer which intrinsically causes issues such as entrapping excessive air in the paste and slowing cement hydration.

To produce cement paste, first superplasticizer was mixed with water. Then CNFs were added to the solution and mixed with a manual stirrer for one minute. The mixture was

then sonicated for 10 minutes. The resulting aqueous dispersion was then added to the blender that contained cement and mixed for 10 minutes. For the batches with silica fume, the aqueous dispersion was added gradually to the paste in the blender during mixing; that made the mixing process easier and prevented the formation of dry clumps of cement/silica fume in the paste at the beginning of mixing. A similar procedure was used for making the batches with w/c ratio of 0.25; half of the cement was placed in the mixer before starting mixing, and the other half was added to the paste during mixing.

After mixing was completed, the paste was cast in PVC molds (Figure 42). Each mold had a square cross-section with the side length of 15.9 mm (0.625 inch) and length of 240 mm (9.5 in). To study the effect of CNFs on the early age shrinkage cracking, as indicated in Table 5, for some batches (1, 2, 6, 7, and 9), after casting the beams the mold was kept in the lab in the room temperature and relative humidity (RH) for 24 hours. After this 24 hour period, the beams were demolded and transferred to a humidity chamber with an RH of 100% and kept there until testing. The rest of the beams were cast in the humidity chamber and were kept in the RH of 100% until testing.



(a)

(b)

Figure 42. (a) PVC molds used for making hardened cement paste specimens. (b) Fresh cement paste cast in the molds.

For each batch, 8 beams were cast and 5 of them were tested so that the results could be averaged. More beams were tested when there were outliers (typically, beams with flexural strength of less than half of the average flexural strength value). The outliers were disregarded.

The beams were tested at the age of 45 days. This period was chosen for curing instead of 28 days to offset the retarding effect of superplasticizers on hydration since different concentrations of superplasticizer were utilized for producing different batches. The beams were removed from the humidity chamber, towel dried and tested after 30 minutes in four-point bending setup. The test setup is shown in Figure 43. The span between supports was 180 mm (7 in). The location of the supports and load points divided the beam span into three equal segments. The beams were tested in load-controlled mode and the values of applied load and beam mid-span deflection was recorded until the beam fractured. As mentioned earlier, load was applied with the rate of 5 N/sec.

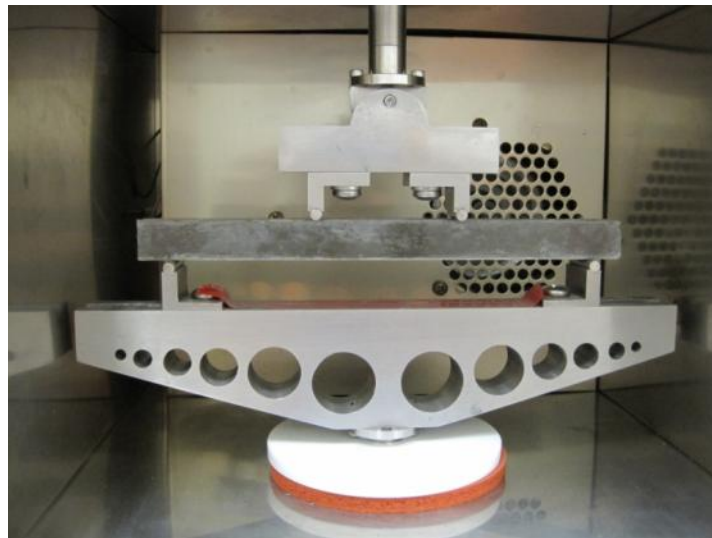


Figure 43. Four-point bending setup for testing hardened cement paste beam specimens.

7.2.3. Calculations

Three properties of each beam were measured: Flexural strength, Young's modulus, and resilience. Simple beam theory was utilized to calculate these properties. Flexural strength (or maximum tensile stress in the lower fiber of the beam under loading) is calculated by

$$\sigma_{\max} = \frac{F \cdot L}{b \cdot h^2} \quad (28)$$

where F is the applied force. ($F/2$ is applied by each of the two load points.), L is the beam span, and b and h are beam's width and height respectively. Young's modulus is calculated by

$$E = k \frac{F}{\delta}, \quad (29)$$

where δ is the displacement of beam's mid-span due to the application of F . $\frac{F}{\delta}$ is the slope of the elastic portion of load vs. deflection curve, and k is a constant value for beams of the same dimension and span. k is calculated by

$$k = \frac{23}{1296} \frac{L^3}{I}, \quad (30)$$

where L is the beam span, I is the beam's area moment of inertia ($I = \frac{1}{12}bh^3$). The tensile strain in the lower fiber of the beam under loading is calculated as follows:

$$\varepsilon = \frac{108}{23} \frac{\delta \cdot h}{L^2}, \quad (31)$$

Finally, resilience is measured by calculating the area under stress vs. strain curve.

7.3. Results and discussion

Stress vs. strain curves from testing four beams from one of the batches (batch 2) is shown in Figure 44. The curves from all the batches have some common features. They are not linear at the beginning of the loading, a phase known as “seating”. The reason is that the beam surfaces were not totally flat and some of the initial applied load was consumed to increase the contact area between the load points and the beam. The other common feature is the presence of outliers. As can be seen in Figure 44, the first beam failed at a much smaller load compared to the other beams. The main reason is the presence of relatively large air voids in a few of the tested beams. These air voids initiate and accelerate the propagation of cracks. The first beam from batch 2 is shown in Figure 45.

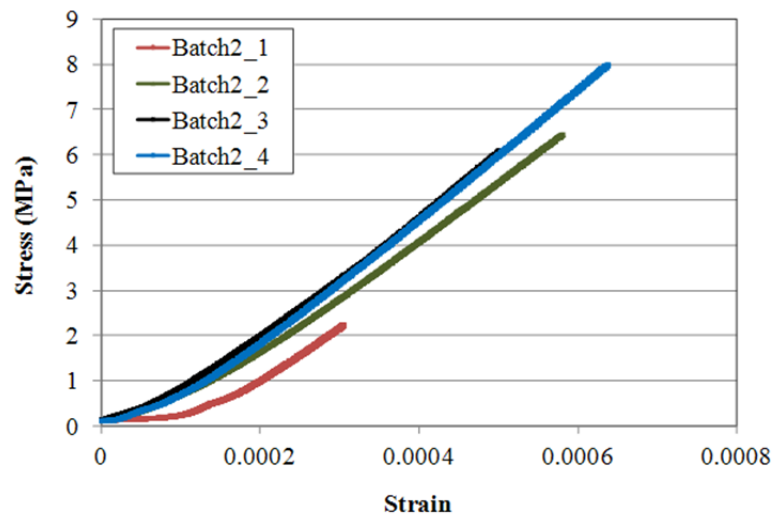


Figure 44. Stress vs. Strain curves for some of the beam specimens made from batch 2.

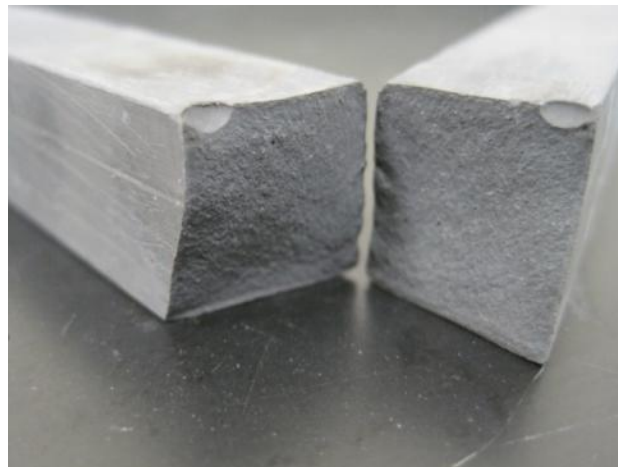


Figure 45. An image of the fracture surface of the first tested beam from batch 2. The beam broke at a large air void on the surface.

The average values of the mechanical properties (flexural strength, Young's modulus, and resilience) of the tested beams for each batch are presented in Table 6. The results show that CNFs are particularly effective in increasing these properties when the cement paste was proportioned to have normal strength ($w/c = 0.40$), and when the specimen was not moist cured in the first 24 hours (a situation that can occur frequently in concrete construction industry). In this condition, as the comparison of the results from batch 1 and batch 2 shows, the increase in strength due to the utilization of CNFs with the concentration of 1.0 wt% of cement was more than 250%. In addition, the increase in Young's modulus and resilience were 68% and 430% respectively.

When the batches with the same proportions as those of batch 1 and batch 2 were cast and cured in the RH of nearly 100%, the increases in mechanical properties due to the incorporation of CNF are significantly smaller. The comparison between batches 3 and 4 shows that the increase in strength due to the utilization of CNFs with the concentration of 1.0 wt% of cement was approximately 45%. There was no increase in Young's modulus, and the increase in resilience was approximately 120%.

The results from the high strength hardened cement pastes ($w/c = 0.25$) and the silica fume incorporated cement pastes show similar values of increase in mechanical properties due to the addition of CNFs with the concentration of 1.0 wt% of cement. In other words, CNFs are most effective when cement paste is normal strength and have not been moist cured in the first 24 hours. For example, for high strength concrete that was not cured in the first 24 hours the increase in strength due to the addition of CNFs with the concentration of 1.0 wt% of cement was 38%. As for the silica fume incorporated cement paste cast and cured in RH of 100%, this increase was 45%.

Table 6. Mechanical properties of the tested beams.

Batch No.	CNF/c	w/c	SF/c	CNF type	Cast in 100% RH	Flexural Strength, MPa	Young's Modulus, GPa	Resilience, MPa
1	0.00	0.40	0.00	-	No	1.91	7.76	0.00033
2	1.00	0.40	0.00	milled	No	6.83	13.06	0.00177
3	0.00	0.40	0.00	-	Yes	5.01	13.56	0.00097
4	1.00	0.40	0.00	not milled	Yes	7.30	13.08	0.00212
5	1.00	0.40	0.00	not milled	Yes	7.88	12.51	0.00247
6	0.00	0.25	0.00	-	No	9.87	18.06	0.00274
7	1.00	0.25	0.00	milled	No	13.62	20.60	0.00457
8	0.00	0.40	0.20	-	Yes	6.48	11.13	0.00198
9	1.00	0.40	0.20	milled	No	7.95	10.93	0.00236
10	1.00	0.40	0.20	not milled	Yes	9.45	12.00	0.00305

Observations of shrinkage cracking of the specimens 24 hours after casting provided a deeper insight into the contribution of CNFs to the mechanical properties and behavior of hardened cement paste. These observations show that when high strength cement paste ($w/c = 0.25$) and the silica fume incorporated cement paste are not moist cured in the first 24 hours, several large cracks form in the beam specimens, particularly in silica fume incorporated specimens. These cracks are usually so deep that they separate the beams into pieces while they are still in the mold. Figure 46 shows the image of high-strength cement paste ($w/c = 0.25$, without CNF) beam specimens 24 hours after casting (Batch 6). These beams were not cured during those 24 hours. Large cracks on most of the beams can be seen. Since most of the beams were fractured after 24 hours and could not be tested, an identical batch was made and more beams were produced. The cracking problem did not occur when batch 7 (having same proportions batch 6, except for incorporating CNFs) was produced in the same conditions. Few extremely shallow cracks were seen on the surface, and when the beams were tested the fracture did not even initiated from any of those cracks. As mentioned earlier, the testing showed that CNFs resulted in an increase of 38% in the flexural strength of high-strength cement paste. However in light of the mentioned observation the increase value is significantly more, because most of the beams were broken before demolding, which means that their flexural strength was zero.



Figure 46. Cement paste from batch 6 ($w/c = 0.25$, without silica fume and CNF) in the molds 24 hours after casting. The beams were not cured during this period and formed shrinkage cracks, some of them as deep as the beams, dividing the beams into pieces before demolding.

Figure 47 shows the image of uncured silica fume incorporated beams (without CNF) 24 hours after casting (same mix proportions as batch 8, but not cast and cured in RH of 100%). Multiple major cracks can be observed. The reason for the formation of large cracks in low water content and silica fume incorporated cement pastes is the presence of high shrinkage gradient. Both high cement content and silica fume reduce the pore size distribution of cement paste. As a result, the diffusivity of concrete decreases. After casting, the water on the top beams surface begins to evaporate. However, due to the very low diffusivity, the water from the lower depth of beam cannot migrate to the top surface and evaporate. Therefore, the top surface of the beam undergoes a remarkable degree of drying shrinkage while such shrinkage does not occur under that surface. That results in a significant shrinkage stress gradient that eventually results in formation of cracks that continue to deepen while the beam keeps shrinking.

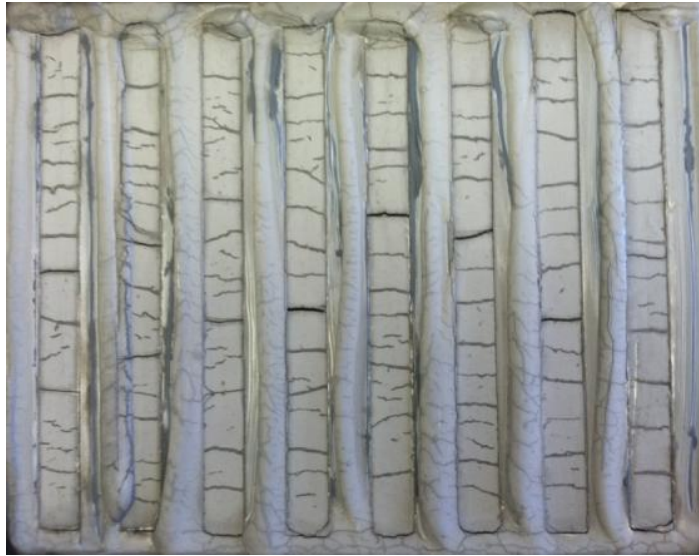


Figure 47. Cement paste ($w/c = 0.40$, with silica fume to cement ratio of 20 wt%, and without CNF) in the molds 24 hours after casting. The beams were not moist cured during this period and formed multiple deep shrinkage cracks. All of the beams were divided into pieces before demolding and therefore none of them could be tested in bending. Batch 8 was made with the same proportions but was casted and cured in a humidity chamber with $RH \approx 100\%$.



Figure 48. A beam made from Batch 9, 24 hours after casting and immediately after demolding. These beams have been produced in the same condition (no curing) and with the same mix proportions as those of the beams shown in Figure 47 ($w/c = 0.40$, with silica fume to cement ratio of 20 wt%). The only difference is that batch 9 contains CNF with the concentration of 1.0% of cement mass). There are very shallow shrinkage cracks at the surface. The beams did not break through any of those cracks during bending test.

7.4. Concluding remarks

An experimental testing program was performed to investigate the effect of CNFs on mechanical behavior and properties of hardened cement paste. The results showed that, in absence of curing in the first 24 hours after mixing the paste, the CNFs largely increase the flexural strength of hardened cement paste by over 250%. The effect of CNFs on mechanical properties of high strength concrete with either low w/c ratio or silica fume was not as large (less than 50% increase in strength). Although silica fume improves the dispersion quality of CNFs, it did not make the CNFs more effective in terms of increasing the strength.

It was shown that CNFs are very effective in preventing shrinkage cracks that occur in the absence of moist curing. Both the cement paste with a low w/c ratio and the cement paste containing silica fume have lower porosity and therefore lower diffusivity. That, in absence of moist curing, causes a large shrinkage gradient, and therefore stress gradient within the paste placed in molds, which eventually results in the formation of deep cracks. The observations showed that a concentration of 1.0 % by the mass of cement can successfully prevent the formation of such cracks. As a conclusion, it can be stated that, in absence of moist curing, CNFs are very beneficial additives in cement paste even when they are poorly dispersed. They greatly increase the strength of normal-strength hardened cement paste and they mitigate the issue of shrinkage cracking in high strength hardened cement paste.

The results of the testing program showed that improving dispersion by using silica fume does not increase the improvement of flexural strength due to the utilization of CNFs. As mentioned earlier, in this program the overall dispersion of CNFs in cement paste (even without the utilization of silica fume), was enhanced compared to the pastes produced and reported in the past. This improvement in dispersion was achieved by using higher concentrations of superplasticizer and longer period of ultrasonic processing. What can be concluded from these findings is that after the dispersion of CNFs reaches a certain

level, improving dispersion further will not affect flexural strength significantly. After that critical level of dispersion, other parameters, most likely the CNF-cementitious matrix interfacial bond, affect the flexural strength most strongly. This fact is schematically illustrated in Figure 49.

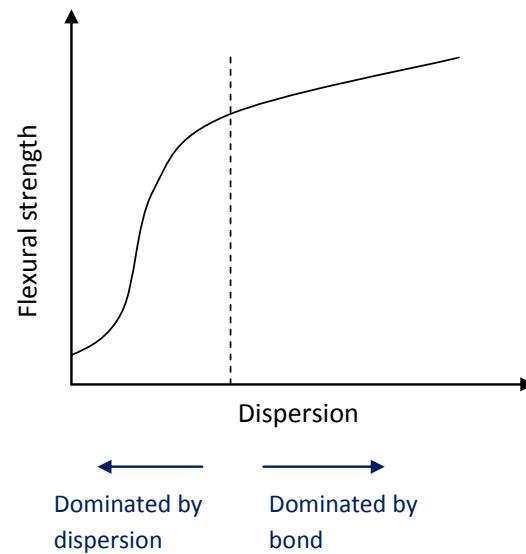


Figure 49. Schematic illustration of the sensitivity of flexural strength to dispersion.

8. SUMMARY AND CONCLUSIONS

In this project:

- The methods developed in the past for producing cementitious materials incorporating carbon nano filaments and enhancing the dispersion of those filaments were studied
- A novel method, incorporating the utilization of silica fume, for improving the dispersion of CNFs in cement paste was developed
- A novel and practical method for quantifying dispersion was devised
- The novel dispersion quantification method was implemented successfully to
 - measure the dispersion of carbon nano filaments in composites
 - investigate the effect of utilizing silica fume in cement paste
 - investigate the effect of geometric clustering in cementitious materials
- It was found that silica fume can enhance the dispersion of CNFs in cement paste significantly.
- It was found that the geometry dependent clustering caused by the size of cement particles is insignificant. However, clumped cement can degenerate the dispersion of nano inclusions significantly.
- It was found that CNFs, in drying conditions, and despite being poorly dispersed, can significantly improve the strength and crack resistance of hardened cement paste

The research presented in this work incorporated a comprehensive study of the past efforts on incorporating CNF/Ts in cementitious materials in order to improve the mechanical properties and behavior of these materials. The common method of incorporating these nanofilaments in cementitious materials was investigated in detail for the first time. This method consists of first dispersing the nanofilaments in a water-superplasticizer solution using ultrasonic processing and then adding the resulting

dispersion to cement in a mixer. The microscopic investigations showed that even when CNFs are well dispersed in the aqueous solution, they reaggregate after the solution is mixed with cement.

The quality of the dispersion of CNFs in a cementitious matrix dictates important properties of the hardened material. As a result it is important to have a reliable and bias-free means of dispersion quantification. During the initial period of this project, a novel thermodynamic-based dispersion quantification method was developed and used in the later stages of the project. For example, it was used to measure the effect of geometry dependent clustering (resulting from the relatively large size of cement particles in comparison to nanofilaments) on the dispersion of carbon nanofilaments in cement paste. The investigations showed that this effect is not significant for the typical concentrations of CNF, cement particle size, and w/c ratio.

A new method for improving and stabilizing the dispersion of CNFs in cement paste was developed. In this method, silica fume is incorporated into the paste. Silica fume restrains the movement of CNFs in fresh paste and prevents them from reagglomerating. The new dispersion quantification method showed that silica fume, when utilized in sufficient amount, can significantly improve the dispersion of CNFs in a hardened cementitious matrix.

Finally, an experimental investigation was performed to observe the effect of CNFs on the mechanical behavior and properties of hardened cement paste. The results showed that CNFs can have significant effects even when they are poorly dispersed within a cementitious matrix. For example, they greatly increase the flexural strength of normal-strength cement paste if it was not moist cured at the first 24 hours. In addition, CNFs can significantly reduce shrinkage cracking in high strength cement paste, or any type of cementitious material with low permeability. It was shown that although silica fume significantly improves dispersion, the resulted increased dispersion *does not* increase the

flexural strength improvement caused by the utilization of CNFs. Since results reported in the literature indicate that a severely degraded dispersion of CNFs *does* reduce the strength of cementitious materials in comparison to unreinforced material, it is apparent that there is some minimum level of dispersion necessary to notably improve strength using CNFs. Therefore, one can conclude that the level of dispersion obtained in the materials tested in this study – even when silica fume was not utilized to stabilize the dispersion – was above this minimum level. Above the minimum level of necessary dispersion, it seems as though other factors are more dominant in influencing strength than is dispersion. For example, the CNF-paste interfacial bond is another important parameter that affects the mechanical properties of cementitious materials and requires thorough investigation in the future.

The goal of the project was achieving a durable material with enhanced viscoelastic properties and high resistance to cracking through the utilization of nano inclusions; a material that can be used to build more durable concrete transportation infrastructure. The performed tasks were important steps towards achieving this goal; an advanced hardened cement paste was developed that is strong and resists shrinkage cracking quite well under certain levels of restraint. However, more research should be performed in the future to build on the findings of this project and produce cementitious materials ready for implementation in concrete transportation infrastructure. One of those areas of research is the interfacial bond between carbon nanofilaments and the cementitious matrix, the factors that affect it, and the methods that can be used to enhance/modify this bond in order to improve the properties and behavior of cementitious materials. Similar research should be performed on CNTs or the combination of both CNFs and CNTs, and investigate the possibility of achieving synergistic effects. And finally, carbon nanofilaments should be incorporated into concrete, rather than in only cement paste, and investigate the properties of the produced concrete by different mechanical tests, for strength, durability, and crack resistance. In fact, it is possible that strictly using the

methodologies described in this dissertation on concrete rather than cement paste might very well create a highly crack-resistant material.

REFERENCES

- [1] Mindess S, Young JF, Darwin D. Concrete. Second ed. Englewood Cliff, NJ: Prentice Hall; 2003.
- [2] Altoubat S, Yazdanbakhsh A, Rieder K-A. Shear behavior of macro-synthetic fiber-reinforced concrete beams without stirrups. *ACI Materials Journal* 2009; 106(4):381-9.
- [3] Altoubat S, Yazdanbakhsh A, Rieder K-A. Effect of synthetic macro-fibers on shear behavior of concrete beams. *ACI Special Publication* 2009; 248:41-52.
- [4] Altoubat S, Barakat S, Yazdanbakhsh A, Rieder K-A. Shear strength and ductility of beams reinforced with synthetic macro-fibers. *The Ninth International Symposium on Brittle Matrix Composites (BMC9)*. Warsaw, Poland 2009. p. 53-62.
- [5] Wang S, Li VC. Engineered cementitious composites with high-volume fly ash. *ACI Materials Journal* 2007; 104(3):233-41.
- [6] Wu H-C, Li VC. Stochastic process of multiple cracking in discontinuous random fiber reinforced brittle matrix composites. *International Journal of Damage Mechanics* 1995; 4(1):83-102.
- [7] Yazdanbakhsh A, Grasley Z, Tyson B, Abu Al-Rub R. Distribution of carbon nanofibers and nanotubes in cementitious composites. *Transportation Research Record: Journal of the Transportation Research Board* 2010; 2142(2):89-95.
- [8] Yazdanbakhsh A, Grasley Z, Tyson B, Abu Al-Rub R. Dispersion quantification of inclusions in composites. *Composites Part A: Applied Science and Manufacturing* 2011; 42:75-83.
- [9] Salvetat JP, Kuik AJ. Electronic and mechanical properties of carbon nanotubes. *Advanced Materials* 1997; 22:7-28.
- [10] Wong EW, Sheehan PE, Lieber CM. Nanobeam mechanics: Elasticity, strength, and toughness of nanorods and nanotubes. *Science* 1997; 277(5334):1971-5.

- [11] Yu M-F, Lourie O, Dyer MJ, Moloni K, Kelly TF, Ruoff RS. Strength and breaking mechanism of multiwalled carbon nanotubes under tensile load. *Science* 2000; 287(5453):637-40.
- [12] Walters DA, Ericson LM, Casavant MJ, Liu J, Colbert DT, Smith KA, et al. Elastic strain of freely suspended single-wall carbon nanotube ropes. *Applied Physics Letters* 1999; 74(25):3803-5.
- [13] Lourie O, Cox DM, Wagner HD. Buckling and collapse of embedded carbon nanotubes. *Physical Review Letters* 1998; 81(8):1638.
- [14] Yakobson B, Avouris P. Mechanical properties of carbon nanotubes. *Carbon Nanotubes* 2001; 80:287-327.
- [15] Ozkan T, Chen Q, Naraghi M, Chasiotis I. Mechanical and interface properties of carbon nanofibers for polymer nanocomposites. *The Technical Conference of the Society for the Advancement of Material and Process Engineering*. Nashville, TN 2008.
- [16] Li GY, Wang PM, Zhao X. Mechanical behavior and microstructure of cement composites incorporating surface-treated multi-walled carbon nanotubes. *Carbon* 2005; 43(6):1239-45.
- [17] Trettin R, Kowald T. Nanotubes für hochleistungsbetone (nanotubes for high-performance concretes). *Betonwerk und Fertigteil-Technik/Concrete Precasting Plant and Technology* 2005; 71(2):20-1.
- [18] Cwirzen A, Habermehl-Cwirzen K, Penttala V. Surface decoration of carbon nanotubes and mechanical properties of cement/carbon nanotube composites. *Advances in Cement Research* 2008; 20(2):65-73.
- [19] Xiupeng W, Jiandong Y, Yingjun W, Ling C. Reinforcement of calcium phosphate cement by bio-mineralized carbon nanotube. *Journal of the American Ceramic Society* 2007; 90(3):962-4.
- [20] Yakovlev G, Keriene J, Gailius A, Girniene I. Cement based foam concrete reinforced by carbon nanotubes. *Materials Science* 2006; 12(2):147-51.

- [21] Yakovlev G, Keriene Y, Krutikov V. Nanoreinforcement of foam concrete. Budapest, Hungary: ETH Honggerberg; 2006. p. 222-3.
- [22] Nadarajah A, Lawrence JG, Hughes TW. Development and commercialization of vapor grown carbon nanofibers: A review. *Key Engineering Materials* 2008; 380:193-206.
- [23] Girifalco LA, Hodak M, Lee RS. Carbon nanotubes, buckyballs, ropes, and a universal graphitic potential. *Physical Review B (Condensed Matter)* 2000; 62(19):13104-10.
- [24] Lourie O, Wagner HD. Transmission electron microscopy observations of fracture of single-wall carbon nanotubes under axial tension. *Applied Physics Letters* 1998; 73(24):3527-9.
- [25] Ajayan PM, Schadler LS, Giannaris C, Rubio A. Single-walled carbon nanotube-polymer composites: Strength and weakness. *Advanced Materials* 2000; 12(10):750-3.
- [26] Gogotsi Y, Naguib N, Libera JA. In situ chemical experiments in carbon nanotubes. *Chemical Physics Letters* 2002; 365(3-4):354-60.
- [27] Gogotsi Y, Libera JA, Guvenc-Yazicioglu A, Megaridis CM. In situ multiphase fluid experiments in hydrothermal carbon nanotubes. *Applied Physics Letters* 2001; 79(7):1021-3.
- [28] Yao N, Lordi V, Ma SXC, Dujardin E, Krishnan A, Treacy MMJ, et al. Structure and oxidation patterns of carbon nanotubes. *Journal of Materials Research* 1998; 13(9):2432-7.
- [29] Ebbesen TW, Hiura H, Bisher ME, Treacy MMJ, Shreeve-Keyer JL, Haushalter RC. Decoration of carbon nanotubes. *Advanced Materials* 1996; 8(2):155-7.
- [30] Joonwon Bae JJS-HY. Cure behavior of the liquid-crystalline epoxy/carbon nanotube system and the effect of surface treatment of carbon fillers on cure reaction. *Macromolecular Chemistry and Physics* 2002; 203(15):2196-204.

- [31] Eitan A, Jiang K, Dukes D, Andrews R, Schadler LS. Surface modification of multiwalled carbon nanotubes: Toward the tailoring of the interface in polymer composites. *Chemistry of Materials* 2003; 15(16):3198-201.
- [32] Timothy JM, John PL. *Applied sonochemistry : The uses of power ultrasound in chemistry and processing*: Weinheim : Wiley-VCH; 2002.
- [33] Kowald T. Influence of surface-modified carbon nanotubes on ultrahigh performance concrete. *International Symposium on Ultra High Performance Concrete*. 2004. p. 195-203.
- [34] Li GY, Wang PM, Zhao X. Pressure-sensitive properties and microstructure of carbon nanotube reinforced cement composites. *Cement and Concrete Composites* 2007; 29(5):377-82.
- [35] Moore VC, Strano MS, Haroz EH, Hauge RH, Smalley RE, Schmidt J, et al. Individually suspended single-walled carbon nanotubes in various surfactants. *Nano Letters* 2003; 3(10):1379-82.
- [36] Makar JM, Beaudoin JJ. Carbon nanotubes and their application in the construction industry. *1st International Symposium on Nanotechnology in Construction*. Paisley, Scotland 2004. p. 331-41.
- [37] Makar J, Margeson J, Luh J. Carbon nanotube/cement composites – early results and potential applications. *3rd International Conference on Construction Materials: Performance, Innovations and Structural Implications*. Vancouver, B.C. 2005.
- [38] Nasibulin AG, Shandakov SD, Nasibulina LI, Cwirzen A, Mudimela PR, Habermehl-Cwirzen K, et al. A novel cement-based hybrid material. *New Journal of Physics* 2009; 11.
- [39] Jiang L, Gao L, Sun J. Production of aqueous colloidal dispersions of carbon nanotubes. *Journal of Colloid and Interface Science* 2003; 260(1):89-94.
- [40] Yu J, Grossiord N, Koning CE, Loos J. Controlling the dispersion of multi-wall carbon nanotubes in aqueous surfactant solution. *Carbon* 2007; 45(3):618-23.

- [41] Kim JA, Seong DG, Kang TJ, Youn JR. Effects of surface modification on rheological and mechanical properties of cnt/epoxy composites. *Carbon* 2006; 44(10):1898-905.
- [42] Li S, Wang F, Wang Y, Wang J, Ma J, Xiao J. Effect of acid and teta modification on mechanical properties of mwents/epoxy composites. *Journal of Materials Science* 2008; 43(8):2653-8.
- [43] Bandyopadhyaya R, Nativ-Roth E, Regev O, Yerushalmi-Rozen R. Stabilization of individual carbon nanotubes in aqueous solutions. *Nano Letters* 2002; 2(1):25-8.
- [44] Bentz DP, Garboczi EJ, Haecker CJ, Jensen OM. Effects of cement particle size distribution on performance properties of portland cement-based materials. *Cement and Concrete Research* 1999; 29(10):1663-71.
- [45] Mehta PK. Durability - critical issues for the future. *Concrete International* 1997; 19(7):27-33.
- [46] Jang BZ, Chang YS. Assessment of particle size distribution and spatial dispersion of rubbery phase in a toughened plastic. *Particle size distribution*. Washington, DC: American Chemical Society; 1987. p. 30-45.
- [47] Matsuo M, Tsuey TW, Kwei TK. Crazing of polystyrene containing two rubber balls: A model for abs plastics. *Journal of Polymer Science Part A-2: Polymer Physics* 1972; 10(6):1085-95.
- [48] Donald AM, Kramer EJ. Craze initiation and growth in high-impact polystyrene. *Journal of Applied Polymer Science* 1982; 27(10):3729-41.
- [49] Clerici C, Gu X, Sung L-P, Forster AM, Ho DL, Stutzman P, et al. Effect of pigment dispersion on durability of a tio2 pigmented epoxy coating during outdoor exposure. *Service life prediction of polymeric materials* 2009. p. 475-92.
- [50] Hosseinpour D, Guthrie JT, Berg JC. The effect of additives on the quality of dispersion and physical properties of an automotive coating pigmented with tio2. *Journal of Adhesion Science and Technology* 2007; 21:141-51.

- [51] Woong JB, Luyi S, Jia L, Ehsan M, Abraham C, Hung-Jue S, et al. Effect of nanoplatelet dispersion on mechanical behavior of polymer nanocomposites. *Journal of Polymer Science Part B: Polymer Physics* 2007; 45(12):1459-69.
- [52] Hussain M, Oku Y, Nakahira A, Niihara K. Effects of wet ball-milling on particle dispersion and mechanical properties of particulate epoxy composites. *Materials Letters* 1996; 26(3):177-84.
- [53] Hamming LM, Qiao R, Messersmith PB, Catherine Brinson L. Effects of dispersion and interfacial modification on the macroscale properties of tio2 polymer-matrix nanocomposites. *Composites Science and Technology* 2009; 69(11-12):1880-6.
- [54] Pu Z, Mark JE, Jethmalani JM, Ford WT. Effects of dispersion and aggregation of silica in the reinforcement of poly(methyl acrylate) elastomers. *Chemistry of Materials* 1997; 9(11):2442-7.
- [55] Karen S, Pierre GL, Johanne D. The effect of clay dispersion on the properties of lldpe/ldpe-g-mah/montmorillonite nanocomposites. *Polymer Engineering & Science* 2008; 48(12):2459-73.
- [56] Prasad VVB, Bhat BVR, Mahajan YR, Ramakrishnan P. Structure-property correlation in discontinuously reinforced aluminium matrix composites as a function of relative particle size ratio. *Materials Science and Engineering A* 2002; 337(1-2):179-86.
- [57] Bhanu Prasad VV, Bhat BVR, Ramakrishnan P, Mahajan YR. Clustering probability maps for private metal matrix composites. *Scripta Materialia* 2000; 43(9):835-40.
- [58] Lewandowski JJ, Liu C, In WHH. Powder metallurgy composites. In: Kumar P, Vedula K, editors. Warrendale, PA 1988. p. 117.
- [59] Slipenyuk A, Kuprin V, Milman Y, Spowart JE, Miracle DB. The effect of matrix to reinforcement particle size ratio (psr) on the microstructure and mechanical properties of a p/m processed alumn/sicp mmc. *Materials Science and Engineering A* 2004; 381(1-2):165-70.

- [60] Akkaya Y, Shah SP, Ankenman B. Effect of fiber dispersion on multiple cracking of cement composites. *Journal of Engineering Mechanics* 2001; 127(4):311-6.
- [61] Akkaya Y, Picka J, Shah SP. Spatial distribution of aligned short fibers in cement composites. *Journal of Materials in Civil Engineering* 2000; 12(3):272-9.
- [62] Rapoport JR, Shah SR. Cast-in-place cellulose fiber-reinforced cement paste, mortar, and concrete. *ACI Materials Journal* 2005; 102(5):299-306.
- [63] Sun L, Gibson RF, Gordaninejad F, Suhr J. Energy absorption capability of nanocomposites: A review. *Composites Science and Technology* 2009; 69(14):2392-409.
- [64] Ma RZ, Wu J, Wei BQ, Liang J, Wu DH. Processing and properties of carbon nanotubes–nano-sic ceramic. *Journal of Materials Science* 1998; 33(21):5243-6.
- [65] Peigney A, Laurent C, Flahaut E, Rousset A. Carbon nanotubes in novel ceramic matrix nanocomposites. *Ceramics International* 2000; 26(6):677-83.
- [66] Estili M, Kawasaki A, Sakamoto H, Mekuchi Y, Kuno M, Tsukada T. The homogeneous dispersion of surfactantless, slightly disordered, crystalline, multiwalled carbon nanotubes in [alpha]-alumina ceramics for structural reinforcement. *Acta Materialia* 2008; 56(15):4070-9.
- [67] Balázsi, Kónya Z, Wéber F, Biró LP, Arató P. Preparation and characterization of carbon nanotube reinforced silicon nitride composites. *Materials Science and Engineering: C* 2003; 23(6-8):1133-7.
- [68] Weisenberger M, Andrews R, Rantell T. Carbon nanotube polymer composites: Recent developments in mechanical properties. *Physical properties of polymers handbook* 2007. p. 585-98.
- [69] Wei L, Zheng-Ying L, Ming-Bo Y. Preparation of carbon black/polypropylene nanocomposite with low percolation threshold using mild blending method. *Journal of Applied Polymer Science* 2009; 115(5):2629-34.
- [70] Tjong SC. Carbon nanotube reinforced composites, metal and ceramic matrices. Weinheim: Wiley-VCH Verlag GmbH & Co. KGaA; 2009.

- [71] O'Connell MJ, Bachilo SM, Huffman CB, Moore VC, Strano MS, Haroz EH, et al. Band gap fluorescence from individual single-walled carbon nanotubes. *Science* 2002; 297(5581):593-6.
- [72] Chirila V, Marginean G, Brandl W. Effect of the oxygen plasma treatment parameters on the carbon nanotubes surface properties. *Surface and Coatings Technology* 2005; 200(1-4):548-51.
- [73] Brandl W, Marginean G. Functionalisation of the carbon nanofibres by plasma treatment. *Thin Solid Films* 2004; 447-448:181-6.
- [74] He P, Gao Y, Lian J, Wang L, Qian D, Zhao J, et al. Surface modification and ultrasonication effect on the mechanical properties of carbon nanofiber/polycarbonate composites. *Composites Part A: Applied Science and Manufacturing* 2006; 37(9):1270-5.
- [75] Wang J, Fang Z, Gu A, Xu L, Liu F. Effect of amino-functionalization of multi-walled carbon nanotubes on the dispersion with epoxy resin matrix. *Journal of Applied Polymer Science* 2006; 100(1):97-104.
- [76] Pyrz R. Quantitative description of the microstructure of composites. Part i: Morphology of unidirectional composite systems. *Composites Science and Technology* 1994; 50(2):197-208.
- [77] Pyrz R. Correlation of microstructure variability and local stress field in two-phase materials. *Materials Science and Engineering: A* 1994; 177(1-2):253-9.
- [78] Brockenbrough JR, Hunt Jr WH, Richmond O. A reinforced material model using actual microstructural geometry. *Scripta Metallurgica et Materialia* 1992; 27(4):385-90.
- [79] Ghosh S, Nowak Z, Lee K. Tessellation-based computational methods for the characterization and analysis of heterogeneous microstructures. *Composites Science and Technology* 1997; 57(9-10):1187-210.
- [80] Ghosh S, Nowak Z, Lee K. Quantitative characterization and modeling of composite microstructures by voronoi cells. *Acta Materialia* 1997; 45(6):2215-34.

- [81] Esawi AMK, El Borady MA. Carbon nanotube-reinforced aluminium strips. *Composites Science and Technology* 2008; 68(2):486-92.
- [82] Estili M, Takagi K, Kawasaki A. Multiwalled carbon nanotubes as a unique agent to fabricate nanostructure-controlled functionally graded alumina ceramics. *Scripta Materialia* 2008; 59(7):703-5.
- [83] Yazdanbakhsh A, Grasley Z, Tyson B, Abu Al-Rub R. Carbon nanofibers and nanotubes in cementitious materials: Some issues on dispersion and interfacial bond. *ACI Special Publication* 2009; SP 267-3:21-34.
- [84] Peng Z, Kong LX, Li S-D, Chen Y, Huang MF. Self-assembled natural rubber/silica nanocomposites: Its preparation and characterization. *Composites Science and Technology* 2007; 67(15-16):3130-9.
- [85] Bartlett MS. *The statistical analysis of spatial patterns*. London: Chapman & Hall; 1976.
- [86] Daley DJ, Milne RK. *The theory of point processes: A bibliography*. *International Statistical Review* 1973; 41(183).
- [87] Diggle PJ. On parameter estimation and goodness-of-fit testing for spatial point patterns. *Biometrics* 1979; 35(1):87-101.
- [88] Hanisch KH, Stoyan D. Stereological estimation of the radial-distribution function of centers of spheres. *Journal of Microscopy-Oxford* 1981; 122(MAY):131-41.
- [89] Ripley BD. Modelling spatial patterns. *Journal of the Royal Statistical Society Series B (Methodological)* 1977; 39(2):172-212.
- [90] Ripley BD. Tests of 'randomness' for spatial point patterns. *Journal of the Royal Statistical Society Series B (Methodological)* 1979; 41(3):368-74.
- [91] Schwarz H. *Quantitative kennzeichnung der anordnung und form von bild- und gefugebestandteilen*: University of Stuttgart; 1980.
- [92] Uhl VW, Gray JB, Eds. *Mixing: Theory and practice*. New York: Academic Press; 1986.

- [93] Fan LT, Chen Y-m, Lai FS. Recent developments in solids mixing. *Powder Technology* 1990; 61(3):255-87.
- [94] Williams JC. Mixing and segregation of powders. In: Rhodes MJ, editor. *Principles of powder technology*. New York: John Wiley & Sons; 1990.
- [95] Poux M, Fayolle P, Bertrand J, Bridoux D, Bousquet J. Powder mixing: Some practical rules applied to agitated systems. *Powder Technology* 1991; 68(3):213-34.
- [96] Harnby N, Edwards MF, Nienow AW. *Mixing in the process industries* Butterworth Heinemann: Oxford; 1992.
- [97] Kaye BH. *Powder mixing*. London: Chapman and Hall; 1996.
- [98] Rhodes MJ. *Introduction to particle technology*. New York: John Wiley & Sons; 1998.
- [99] Schwarz H. The characterization of the arrangement of feature centroids in planes and volumes. *Journal of microscopy - Oxford* 1983; 129(Feb):155-69.
- [100] Russ JC. *Computer-assisted microscopy, the measurement and analysis of images*. New York: Plenum Press; 1990.
- [101] Brian HK, Garry GC. Computer aided image analysis procedures for characterizing the stochastic structure of chaotically assembled pigmented coatings. *Particle and Particle Systems Characterization* 1992; 9(1-4):157-70.
- [102] Diggle PJ. *Statistical analysis of spatial point patterns*. San Diego: Academic; 1983.
- [103] Clark PJ, Evans FC. Distance to nearest neighbor as a measure of spatial relationships in populations. *Ecology* 1954; 35(4):445-53.
- [104] Gleason HA. Some applications of the quadrat method. *Bulletin of the Torrey Botanical Club* 1920; 47(1):21-33.
- [105] Svedberg T. Ett bidrag till de statistiska metodernas användning inom vaxtbiologien (in swedish). *Svensk Bot Tidskr* 1922; 16:1-8 (in Swedish).
- [106] Curtis JT, McIntosh RP. The interrelations of certain analytic and synthetic phytosociological characters. *Ecology* 1950; 31(3):434-55.

- [107] Viktorov SV. A study of the distribution and dispersion of plants by aerial photographs. (in russian). The Society of Natural Sciences Bulletin, Moscow (Biology Section) 1947; 52(4):71-8.
- [108] Cottam G, Curtis JT. A method for making rapid surveys of woodlands by means of pairs of randomly selected trees. Ecology 1949; 30(1):101-4.
- [109] Dice LR. Measure of the spacing between individuals within a population. Contributions from the laboratory of vertebrate biology, University of Michigan, 1952; 55:1-23.
- [110] Skellam JG. Studies in statistical ecology: I. Spatial pattern. Biometrika 1952; 39(3/4):346-62.
- [111] Baddeley A, Gregori P, Mateu J, Stoica R, (Editors) DS. Case studies in spatial point process modeling: Springer; 2006.
- [112] Soneira RM. Is there evidence for a spatially homogeneous population of field galaxies. Astrophysical journal 1977; 211(1):1-15.
- [113] Peebles PJE, Groth EJ. Statistical analysis of catalogs of extragalactic objects. The Astrophysical Journal 1975; 196(1):7-20.
- [114] Sidaner A, Bailleux O, Chabrier J-J. Measuring the spatial dispersion of evolutionary search processes: Application to walksat. Artificial evolution, lecture notes in computer science: Springer; 2002. p. 77-87.
- [115] Binglin L, Torquato S. Local volume fraction fluctuations in heterogeneous media. The Journal of Chemical Physics 1990; 93(5):3452-9.
- [116] Tjong SC, Tam KF. Mechanical and thermal expansion behavior of hipped aluminum-tib2 composites. Materials Chemistry and Physics 2006; 97(1):91-7.
- [117] Luo ZP, Koo JH. Quantitative study of the dispersion degree in carbon nanofiber/polymer and carbon nanotube/polymer nanocomposites. Materials Letters 2008; 62(20):3493-6.
- [118] Bakshi SR, Batista RG, Agarwal A. Quantification of carbon nanotube distribution and property correlation in nanocomposites. Composites Part A: Applied Science and Manufacturing 2009; 40(8):1311-8.

- [119] Gurland J. In: DeHoff RT, Rhine FN, editors. Quantitative microscopy. New York: McGraw-Hill; 1968.
- [120] Ripley BD. Spatial statistics. Hoboken, NJ: Wiley; 1981.
- [121] Ripley BD. Statistical inference for spatial processes. London: Cambridge University Press; 1988.
- [122] Cressie NAC. Statistics for spatial data, revised ed. New York: Wiley; 1993.
- [123] Stoyan D, Kendall WS, Mecke J. Stochastic geometry and its applications. 2nd ed. New York: Wiley; 1995.
- [124] Spitzig WA, Kelly JF, Richmond O. Quantitative characterization of second-phase populations. *Metallography* 1985; 18(3):235-61.
- [125] Wray PJ, Richmond O, Morrison HL. Use of the dirichlet tessellation for characterizing and modeling nonregular dispersions of second-phase particles. *Metallography* 1983; 16(1):39-58.
- [126] Tyson B. Carbon nanotubes and nanofiber reinforcement for improving the flexural strength and fracture toughness of portland cement paste. Texas A&M University, College Station 2010.
- [127] Rahaman MN. Mixing and packing of powders. *Ceramic processing*. Boca Raton: Taylor & Francis Group; 2007. p. 253-77.
- [128] Lawler EL. Combinatorial optimization: Networks and matroids. New York: Holt, Rinehart and Winston; 1976.
- [129] Papadimitriou CH, Steiglitz K. Combinatorial optimization, algorithms and complexity. Mineola, New York: Dover Publishing, Inc.; 1998.
- [130] Kuhn HW. The hungarian method for the assignment problem. *Naval Research Logistics* 1955; 2(1-2):83-97.
- [131] Munkres J. Algorithms for the assignment and transportation problems. *Journal of the Society for Industrial and Applied Mathematics* 1957; 5(1):32-8.
- [132] Kusy RP. Influence of particle size ratio on the continuity of aggregates. *Journal of Applied Physics* 1977; 48(12):5301-5.

- [133] Zhao L-D, Zhang B-P, Liu W-S, Li J-F. Effect of mixed grain sizes on thermoelectric performance of Bi_2Te_3 compound. *Journal of Applied Physics* 2009; 105(2):023704-6.
- [134] Pan Y, Li L, Chan SH, Zhao J. Correlation between dispersion state and electrical conductivity of mwents/pp composites prepared by melt blending. *Composites Part A: Applied Science and Manufacturing* 2010; 41(3):419-26.
- [135] Yazdanbakhsh A, Grasley Z, Tyson B, Abu Al-Rub RK. Dispersion quantification of inclusions in composites. *Composites Part A: Applied Science and Manufacturing* 2011; 42(1):75-83.
- [136] Yazdanbakhsh A, Grasley Z, Tyson B, Abu Al-Rub R. Carbon nanofibers and nanotubes in cementitious materials: Some issues on dispersion and interfacial bond. *ACI SP* 2009; 267:21-34.
- [137] Yazdanbakhsh A, Grasley Z, Tyson B, Abu Al-Rub R. Distribution of carbon nanofibers and nanotubes in cementitious composites. *Transportation Research Record: Journal of the Transportation Research Board* 2010; 2142:89-95.
- [138] Hartley PA, Parfitt GD, Pollack LB. The role of the van der waals force in the agglomeration of powders containing submicron particles. *Powder Technology* 1985; 42(1):35-46.
- [139] Kuhn HW. The hungarian method for the assignment problem. *Naval Research Logistics Quarterly* 1955; 2(1-2):83-97.
- [140] Jacobsen J. As flat as possible. *SIAM Review* 2007; 49(3):491-507.
- [141] Douglas J, Gunn JE. A general formulation of alternating direction methods. *Numerische Mathematik* 1964; 6(1):428-53.
- [142] Gunn JE. On the two-stage iterative method of douglas for mildly nonlinear elliptic difference equations. *Numerische Mathematik* 1964; 6(1):243-9.
- [143] Gunn JE. The numerical solution of $\nabla \cdot a(\nabla u) = f$ by a semi-explicit alternating-direction iterative technique. *Numerische Mathematik* 1964; 6(1):181-4.
- [144] Wang TY, Chen CCP. Thermal-adi: A linear-time chip-level dynamic thermal simulation algorithm based on alternating-direction-implicit (adi) method.

- Sonoma, CA, United states: Association for Computing Machinery; 2001. p. 238-43.
- [145] Shah SP, Konsta-Gdoutos MS, Metaxa ZS, Mondal P. Nanoscale modification of cementitious materials. In: Bittnar Z, Bartos PJM, Němeček J, Šmilauer V, Zeman J, editors. *Nanotechnology in construction 3*: Springer Berlin Heidelberg; 2009. p. 125-30.
- [146] Chung D. Cement-matrix structural nanocomposites. *Metals and Materials International* 2004; 10(1):55-67.
- [147] Tyson B, Al-Rub RA, Yazdanbakhsh A, Grasley Z. Carbon nanotubes and carbon nanofibers for enhancing the mechanical properties of nanocomposite cementitious materials. *Journal of Materials in Civil Engineering* 2011; 23(7):1028-35.
- [148] Raki L, Beaudoin J, Alizadeh R, Makar J, Sato T. Cement and concrete nanoscience and nanotechnology. *Materials* 2010; 3(2):918-42.
- [149] Welch CR, Marcuson WF, Adiguzel I. Will supermolecules and supercomputers lead to super construction materials? *ASCE Civil Engineering Magazine*. 2009. p. 42-53.
- [150] Bentz DP. Blending different fineness cements to engineer the properties of cement-based materials. *Magazine of Concrete Research*; 62(5):327-38.
- [151] Han BG. A self-sensing carbon nanotube/cement composite for traffic monitoring. *Nanotechnology* 2009; 20(44).
- [152] Gao D, Sturm M, Mo YL. Electrical resistance of carbon-nanofiber concrete. *Smart Materials and Structures* 2009; 18(9).
- [153] Yu X, Kwon E. A carbon nanotube/cement composite with piezoresistive properties. *Smart Materials and Structures* 2009; 18(5).
- [154] Collins PG, Avouris P. Nanotubes for electronics. *Scientific American* 2000; 283(6):62.

- [155] Bentz DP, Garboczi EJ, Snyder KA. A hard core/soft shell microstructural model for studying percolation and transport in three-dimensional composite media. NISTIR 6265, US Department of Commerce, January. 1999.
- [156] Grasley Z, Yazdanbakhsh A. Quantifying the dispersion of discrete inclusions using continuum theory. *Composites Part A: Applied Science and Manufacturing* 2011; 42(12):2043-50.
- [157] Fu X, Chung DDL. Submicron-diameter-carbon-filament cement-matrix composites. *Carbon* 1998; 36(4):459-62.
- [158] Chung DDL. Comparison of submicron-diameter carbon filaments and conventional carbon fibers as fillers in composite materials. *Carbon* 2001; 39(8):1119-25.
- [159] Ormsby R, McNally T, Mitchell C, Halley P, Martin D, Nicholson T, et al. Effect of mwcnt addition on the thermal and rheological properties of polymethyl methacrylate bone cement. *Carbon*; 49(9):2893-904.
- [160] Zhao J, Shi D, Lian J. Small angle light scattering study of improved dispersion of carbon nanofibers in water by plasma treatment. *Carbon* 2009; 47(10):2329-36.
- [161] Azoubel S, Magdassi S. The formation of carbon nanotube dispersions by high pressure homogenization and their rapid characterization by analytical centrifuge. *Carbon* 2010; 48(12):3346-52.
- [162] Nadler M, Mahrholz T, Riedel U, Schilde C, Kwade A. Preparation of colloidal carbon nanotube dispersions and their characterisation using a disc centrifuge. *Carbon* 2008; 46(11):1384-92.
- [163] Bai Y, Song Park I, Jeong Lee S, Sung Bae T, Watari F, Uo M, et al. Aqueous dispersion of surfactant-modified multiwalled carbon nanotubes and their application as an antibacterial agent. *Carbon* 2011; 49(11):3663-71.
- [164] Leinonen H, Pettersson M, Lajunen M. Water-soluble carbon nanotubes through sugar azide functionalization. *Carbon* 2011; 49(4):1299-304.

- [165] Sobkowicz MJ, Dorgan JR, Gneshin KW, Herring AM, McKinnon JT. Controlled dispersion of carbon nanospheres through surface functionalization. *Carbon* 2009; 47(3):622-8.
- [166] Ma P-C, Mo S-Y, Tang B-Z, Kim J-K. Dispersion, interfacial interaction and re-agglomeration of functionalized carbon nanotubes in epoxy composites. *Carbon* 2010; 48(6):1824-34.
- [167] Kotaki M, Wang K, Toh ML, Chen L, Wong SY, He C. Electrically conductive epoxy/clay/vapor grown carbon fiber hybrids. *Macromolecules* 2006; 39(3):908-11.
- [168] Feller JF, Bruzard S, Grohens Y. Influence of clay nanofiller on electrical and rheological properties of conductive polymer composite. *Materials Letters* 2004; 58(5):739-45.
- [169] Liu L, Grunlan JC. Clay assisted dispersion of carbon nanotubes in conductive epoxy nanocomposites. *Advanced Functional Materials* 2007; 17(14):2343-8.
- [170] Luo S, Liu T, Wang B. Comparison of ultrasonication and microfluidization for high throughput and large-scale processing of swent dispersions. *Carbon* 2010; 48(10):2992-4.
- [171] Sanchez F, Ince C. Microstructure and macroscopic properties of hybrid carbon nanofiber/silica fume cement composites. *Composites Science and Technology* 2009; 69(7-8):1310-8.
- [172] Suresh GA. *Processing and properties of nanocomposites*. First ed. Singapore: World Scientific Publishing Co. Pte. Ltd.; 2007.
- [173] Baker RTK. *Synthesis, properties and applications of graphite nanofibers*. WTEC Workshop Report on R&D Status and Trends in Nanoparticles, Nanostructured Materials, and Nanodevices in the United States. 1997.
- [174] Gay C, Sanchez F. Performance of carbon nanofiber-cement composites with a high-range water reducer. *Transportation Research Record* 2010; (2142):109-13.

- [175] Metaxa ZS, Konsta-Gdoutos MS, Shah SP. Carbon nanotubes reinforced concrete. 267 SP ed. New Orleans, LA, United states: American Concrete Institute; 2009. p. 11-20.
- [176] Shah SP. Nanoscale modification of cementitious materials. Nanotechnology in construction 3, Proceedings 2009:125-30.
- [177] Konsta-Gdoutos MS, Metaxa ZS, Shah SP. Highly dispersed carbon nanotube reinforced cement based materials. Cement and Concrete Research; 40(7):1052-9.
- [178] Konsta-Gdoutos MS, Metaxa ZS, Shah SP. Multi-scale mechanical and fracture characteristics and early-age strain capacity of high performance carbon nanotube/cement nanocomposites. Cement and Concrete Composites; 32(2):110-5.
- [179] Yazdanbakhsh A, Grasley Z. Utilization of silica fume to stabilize the dispersion of carbon nanofilaments in cement paste. Carbon 2011; (under review).